Abiotic Influences on Free-Living Microbial Communities in Hydrothermal Vent Ecosystems

Abiotic Influences on Free-Living Microbial Communities in Hydrothermal Vent Ecosystems

a dissertation presented

by

Heather Craig Olins

to

The Department of Organismic and Evolutionary Biology

in partial fulfillment of the requirements
for the degree of
Doctor of Philosophy
in the subject of
Biology

Harvard University
Cambridge, Massachusetts

April 2016

Dissertation advisor: Peter R. Girguis Heather Craig Olins

Abiotic Influences on Free-Living Microbial Communities in Hydrothermal Vent Ecosystems

Abstract

Hydrothermal vent ecosystems are defined by steep thermal and chemical gradients. Chemosynthetic microorganisms are the primary producers in these systems, utilizing the available chemical energy to support substantial animal biomass. The variety of chemical substrates provided by hydrothermal fluid and surrounding seawater enables a metabolically diverse community of microbes. However, our understanding of how abiotic factors such as temperature, geochemistry, and mineral substrate influence the activity of these microbes is limited. The overarching goal of this dissertation is to examine the influence of these abiotic factors on free-living microbial community composition, structure, and function. In this work I first examined the influence of temperature on primary productivity by using radio isotopic tracer studies to measure rates of carbon fixation by epi- and endolithic microbial communities from vent chimney sulfides. I show evidence that these communities fix more carbon at low temperatures, underscoring the importance of low temperature habitats in these environments commonly characterized by high temperature. I then utilized *in situ* RNA preservation to examine community-wide microbial activity in low temperature vent fluids throughout a vent field. These data show two distinct activity profiles that cross-cut canonical habitat descriptions, and highlight the importance of the intra-field waters among the discrete vents as regions of high primary

productivity bearing similarity in microbial activity to plumes emanating from high temperature chimneys. Finally, I designed novel colonization devices to examine the influence of mineral substrate on microbial community composition, structure, and succession. Mineralogy influenced certain taxa. I also identified potential early and late successional taxa. The combination of metabolic rate measurements, metatranscriptomics, and colonization experiments presented here, all with co-registered geochemistry, underscore the substantial heterogeneity of these systems and offer insights into the relative strengths of the abiotic forces that help to govern these ecosystems.

Assessing the Influence of Abiotic Factors on Microbial Communities at Hydrothermal Vent Ecosystems

Table of Contents

Acknowledgements

There are many people without whom I would have given up on myself a long time ago. My advisor, Peter Girguis, took a chance on me - a student who knew nothing about microbiology before starting in his lab. I am incredibly lucky to have found an advisor who genuinely cares for the people in his lab, and whose pep talks always seem to make the world less ominous and my data more exciting. Pete has helped me find my confidence as a scientist, and see the value of "wrench science" when my tendency is for "duct tape science". I am incredibly grateful for the value he always placed on my ideas, and for his willingness to speak openly and truly listen to my opinions on a wide variety of topics. I am also very grateful to my committee members Andrew Knoll and Colleen Cavanaugh for their considerable support and thoughtful, detailed, feedback over the years.

The Girguis Lab and OEB have been home to a huge number of incredible scientists, colleagues, and friends throughout the seven years I have been a part of them. Despite "Girgoyles" coming and going, the lab has always had a wonderful collegial and fun-loving atmosphere, and has always felt like home. I don't know what I would have done without the amazing problem solving, morale boosting, and general awesomeness of Jennifer Delaney, Stephanie Hillsgrove, and Charles Vidoudez. Post-docs Mark Nielsen and Daniel Rogers were important mentors who shared their expertise and advice generously, and whose presence made lab more fun. Kiana Frank gave me a personal crash course in microbiology and taught me how to "cruise" when I joined the lab, for which I will be eternally grateful. Kiana, Roxanne Beinart, and Dipti Nayak have each taught me a huge amount of nitty gritty science, provided more support than they will ever know, and most importantly become friends who feel like sisters. I am grateful for the wonderful

camaraderie and support of OEB grad students Jon Sanders, Didem Sarikaya, Leonora Bittleston, Shane Campbell-Staton, and Ambika Kamath, you have inspired me to be a better scientist and a more conscientious person.

I have benefited from the knowledge and talents of a long list of co-authors, collaborators, and scientists who gave their advice freely: Kiana Frank, Daniel Rogers, Charles Vidoudez, Christina Preston, Bill Ussler, Chris Scholin, Amy Gartman, Xiaofei Guan, Colleen Hansel, Anne Pearson, Deb Kelley, Frank Stewart, and Aude Picard. Additionally, this work wold have been impossible without the talented and accommodating crews of the R/V Atlantis, HOV Alvin, R/V Western Flyer, and ROV Doc Rickets.

I am incredibly lucky to have a wonderful group of friends and family beyond Harvard who have supported me over the years. Nina Lanza, Alison Cristiello, Rachel Fineman, and Kate Piper have provided inspiration, perspective, and much needed laughs. My extended family of Donna, Carl, and Jeff Albro, and Leah Sawyer have been incredibly supportive over these challenging last few months, stepping up whenever I needed anything. My siblings Jake, Shura, and Matt Olins have all inspired me in different ways, and their confidence in me has helped me have confidence in myself. My husband and true partner in life Donald Albro has kept me laughing throughout everything, and knows how to take care of me when I don't know I need care.

Finally, my biggest fans over the decades, my parents Elizabeth Craig-Olins and Andrew Olins have made me who I am today. My father instilled in me a reverence for knowledge, reason, and education, while my mother inspired my passion and wonder for the natural world. I do not have the words to adequately express my gratitude for their unending support and love.

Chapter 1

Introduction

Why study microbial communities at hydrothermal vents?

The vast majority of life on Earth depends on sunlight, either directly or indirectly, for its energy. Even in the dark deep sea, most organisms are dependent on energy that drifts down from the sunlit surface water in the form of dead or decaying organic matter. Hydrothermal vents, on the other hand, represent an ecosystem that relies on a completely different energy source - chemicals from within the Earth - and microbes that can perform chemosynthesis to exploit that energy. While many vent organisms are still dependent on oxygen initially generated through photosynthesis, this chemical energy source distinguishes deep sea hydrothermal vents as unique. Ultimately, our understanding of biology is incomplete without understanding such a distinct system of ecosystem support. The microbial communities investigated in this dissertation are relevant far beyond the deep sea, and are important for a diverse set of reasons including a better understanding of global biogeochemical cycles, the global search for valuable mineral and biological resources, exploration of the origin of life on Earth, and even the search for life beyond Earth.

As awareness of global climate change grows, so does the importance of understanding Earth's biogeochemical cycles. A volume of water equal to that of Earth's global ocean cycles through the mid-ocean ridge system every 70,000-200,000 years (Wheat *et al.*, 2003; Johnson and Pruis, 2003). As such, hydrothermal vents (where this fluid re-enters the ocean) are a global phenomenon and exert influence over certain aspects of global ocean chemistry. In particular, the global iron cycle is strongly influenced by mid ocean ridge hydrothermal venting from which iron is transported thousands of kilometers and accounts for a substantial fraction of total dissolved iron (Resing *et al.*,

2015). Additionally, global hydrothermal circulation is the primary control of marine magnesium and sulfate concentrations (McDuff and Edmond, 1982; Mottl and Wheat, 1994). While it is known that hydrothermal vents influence global marine geochemistry, the contributing influence of microorganisms and their metabolism on vent geochemistry (and therefore global ocean chemistry) remains an open question.

In addition to dissolved chemicals, hydrothermal vents produce a variety of minerals and metal ores. There is huge and growing global need for minerals such as copper, zinc, lead, gold, and silver used in much of modern technology. As terrestrial sources of these minerals continue to be depleted and technology for drilling in the deep sea continues to improve, the mining of seafloor massive sulfide deposits (SMSs), which underlie many hydrothermal vent fields, becomes increasingly economically favorable (Boschen *et al.*, 2013). It is impossible to analyze the ecological impact of such mining when many of the vent habitats under discussion for mining are so poorly characterized. While mining is not currently under discussion for the Juan de Fuca Ridge (JdFR) investigated in this work, the JdFR does sit atop a SMS analogous to those likely to be mined in the near future. The more we know about the ecology of these areas, and more specifically about the role that mineralogy plays in microbial activity and therefore local geochemistry, the better prepared we will be to make decisions about mining that may help to minimize ecological damage and loss of biodiversity.

In addition to mineral resources, hydrothermal vents are a potential source of valuable biological resources. Organisms, especially microorganisms, adapted to life in "extreme" environments generally have physiological adaptations that enable them to thrive where most organisms cannot. Unique biological adaptations to heat, toxic

chemicals, or pressure could theoretically be of use to industry or medicine. For example, a thermally stable DNA polymerase was first isolated from a Yellowstone hot spring bacterium named *Thermus aquatics* called Taq Polymerase and now is used in countless molecular biology labs, increasing the efficiency of the PCR reaction. Organismal adaptations to heat in particular may prove useful in a warming world. Additionally, the combination of seawater and hydrothermal fluid and the resulting minerals create a huge menu of potential electron donors (e.g., Fe^{2+}, $S_2O_3^{2-}$, S^0, H_2, H_2S, $S_4O_6^{2-}$, various organic substrates) and acceptors (e.g., O_2, NO_3^-, S^0, CO_2, SO_4^{2-}, $S_2O_3^{2-}$, SO_3^{2-}, Fe^{3+-}, Mn^{4+}) that microbes can take metabolic advantage of (Sievert and Vetriani, 2012), resulting in truly remarkable metabolic diversity. The more organisms that are described and studied from these environments, the more likely we are to discover new compounds that could benefit society in a variety of ways. While this work does not attempt to culture new microbes, the insights gleaned here about microbial physiology may be relevant to those who attempt to cultivate these often difficult to culture organisms.

Hydrothermal vents represent analogs for environments present on early earth, and may, therefore, contain organisms that can offer clues about life on early earth, its evolution, and perhaps even the origin of life itself. Many of the most evolutionarily ancient organisms on this planet, are thought to be hyperthermophiles (organisms that thrive above 60°C) and therefore likely evolved in hot environments such as hydrothermal vents. Additionally the vent chimney structures themselves may have played a role in the early evolution of life (Burcar *et al.*, 2015). Whether or not life evolved at vents, the metabolic diversity present in hydrothermal vent microbes is remarkable and, therefore represents a fascinating evolutionary story. If life did, in fact, evolve in hydrothermal vents, than extant

vent species might offer clues to the early evolution of life on Earth. Regardless of whether or not life evolved at hydrothermal vents, the chemosynthetic metabolisms that did evolve there may represent ancient metabolisms that may offer insight to early evolution.

Hydrothermal vents also represent an analogue for ecosystems potentially conducive to life on other bodies in our solar system (e.g. Europa). Any planetary body known to have liquid and volcanic activity could, in theory, support life via chemosynthesis. For example, Europa's potential liquid water and tectonic activity, could support Earth-like microbial metabolism (Kargel, 2000), while Titan's liquid methane and cryovolcanism could, theoretically, support methanogenic life via hydrogen and acetylene consumption (McKay and Smith, 2005). Better understanding microbial activity at vents on this planet can help us refine and target our search for life beyond Earth. The Deep Environmental Sample Processor (D-ESP) used in Chapter 3 of this work was funded by NASA with the long-term goal of producing a molecular biology lab hypothetically capable of detecting DNA-based life in oceans on other planetary bodies (such as Europa) in our solar system.

What are we ultimately trying to learn?

Hydrothermal vent environments have a great deal to offer to both scientists and broader society; however we still lack a thorough understanding of vent ecology. We have a general sense of which organisms are present, but what they are doing, and how they are influenced by their physical environment are not well understood. These are questions of great importance in the microbial ecology of any environment, but perhaps nowhere more so than an environment characterized by such steep geochemical gradients and dynamic physical forces. The underlying tectonic processes at vents result in the mixing of heated,

chemically reduced (anoxic), hydrothermal fluid with cold, chemically oxidized (aerobic), seawater. This mixing creates dramatic thermal and chemical gradients over centimeter-long spatial scales. Additionally, biofilm formation as well as chimney porosity and permeability likely create geochemical heterogeneity on much smaller spatial scales - scales that are microbially relevant, but very difficult to measure. Our macro-scale sampling of microbial environments makes it challenging to interpret geochemical correlations (or lack thereof) with microbial communities and their activity. Temporal variability further confounds the search for causal relationships between environment and biology. From daily shifts in mixing due to overlying tidal pressure to decade-long lifetime of many vent structures, life in these habitats must have evolved to deal with constantly changing conditions. All of this heterogeneity makes it challenging to understand the processes that govern the ecology of these systems.

There are a variety of distinct habitats at mid-ocean ridge, hydrothermal environments. The subsurface crustal aquifer, the chimney structures, the buoyant dispersing plume, diffuse low-temperature vents, and even the intra-field space surrounding distinct vents all have distinct physical and chemical attributes that set them apart. As such, they are often studied in isolation. However, studying individual habitats may prevent us from seeing them as the truly interconnected regions that they are. Many of the same microbes are found throughout these different habitats, and we have yet to truly understand what governs their distribution and activity.

The list of unanswered questions about microbial eco-physiology at vents is far longer than the list of answered questions, but some of the most fundamental are geared towards a better understanding of community composition and structure. Much of the

early work investigating vent microbial communities took place within chimney walls. There were documented patterns of distribution among different groups of microbes, but to this day many questions remain about the forces structuring those patterns. How do chemistry, temperature, and mineral substrate influence microbial community composition, structure, and succession? Because these factors can co-vary, and because minerals themselves can be sources or sinks for electrons – making them potentially related to energy metabolism, I was interested in the role of mineralogy in selecting the community and potentially influencing microbial metabolism within vent chimneys. Chapter 4 of this dissertation describes a novel colonization sampler specifically designed to assess the influence of mineral substrate on these communities.

Chemosynthetic primary productivity (autotrophy) drives this entire ecosystem, the influence of environmental factors on rates of activity are not well understood. What influences rates of primary productivity among free-living microbes at vents? Where is it fastest and slowest? What is the distribution of different carbon fixation pathways among the active vent microbial communities? At the outset of this work, rates of carbon fixation had only been made in a handful of chimney rocks (Wirsen *et al.*, 1993; Polz *et al.*, 1998; Bonch-Osmolovskaya *et al.*, 2011). I was interested in the influence of temperature on rates of carbon fixation (or primary productivity) within a sulfide chimney walls. Chapter 2 of this dissertation (Olins *et al.*, 2013) represents the first systematic attempt at documenting rates of primary productivity, and how they vary with temperature, in hydrothermal vent chimney walls.

Another set of unanswered questions about hydrothermal vent microbes centers around better understanding broader microbial activity across the thermal and chemical

gradient that defines low temperature diffuse venting. What are microbes doing in low temperature hydrothermal vent fluid, and how is their activity related to geochemistry? Where do vent-endemic communities dominate activity and where do seawater-derived communities dominate? How are these communities distributed, and how is their distribution related to geochemistry? After realizing the importance of low temperature primary productivity (described in Chapter 2), I was interested in the activity profile of whole communities in different low temperature hydrothermal fluid environments. Chapter 3 of this dissertation represents the first systematic survey of microbial activity with co-registered geochemistry across a diffuse flow vent field including the intra-field habitat of fluids between diffuse flows.

What did I do to address these questions?

Chemosynthetic primary production carried out by free-living and symbiotic microorganisms supports the astounding biomass that characterizes hydrothermal vent ecosystems. The work presented within this dissertation is aimed at better understanding chemosynthetic primary production at hydrothermal vents. I address how environmental variables, such as geochemistry and mineralogy, influence microbial metabolism in vent ecosystems by directly measuring rates (Chapter 2), investigating total microbial activity (Chapter 3), and examining the role of solid-state mineral substrates as colonization surfaces and as electron donors and acceptors (Chapter 4),

The work presented in chapter two furthers our understanding of factors that govern primary productivity in vent chimneys. Temperature significantly influenced rates of primary productivity likely due to the distribution of biomass throughout the vent

chimney wall, with highest biomass concentrated in/on the outer layer (Harmsen *et al.*, 1997; Takai *et al.*, 2001; Schrenk *et al.*, 2003). Here, the highest rates of primary productivity were observed at the lowest temperature, 4°C - the temperature, roughly, of the ambient seawater, which suggests that low temperature environments may play a significant role in fixing carbon in these ecosystems

Given the vast extent of low temperature vent environments (Rona and Trivett, 1992; Baker *et al.*, 1993; Wankel *et al.*, 2011; Bemis *et al.*, 2012), the activities of organisms within these environments are potentially more important to global primary productivity than the high temperature environments (as Chapter 2 implies). Chapter three examines the correlation between microbial activity and geochemistry in low temperature diffuse flow vents. It also describes the extent to which the subsurface vent-associated and seawater-derived microbial communities are active throughout a vent field characterized by low temperature diffuse flow venting. This chapter highlights the heterogeneity of diffuse flow active communities. It also underscores that the relationship between geochemistry and microbial activity is not a simple, direct one by providing evidence that ecological niches are not defined purely by ambient geochemistry. Most importantly, this work identifies the intra-field habitat as one that has received very little research attention, but appears to support substantial microbial primary productivity similar to that which occurs in buoyant plumes from high temperature vent structures, making it potentially highly relevant to global cycles of iron, sulfur, carbon, and possibly other elements

Finally, in chapter four I return to rock/mineral associated communities and examine the influence of mineral substrate on microbial community structure and succession. Microbial community composition within hydrothermal vent chimney walls as

been shown to differ between distinct mineral layers (Schrenk *et al.*, 2003; Kormas *et al.*, 2006). Because mineralogy is determined by chemistry and temperature at the time of precipitation, it is impossible to disentangle the influence of mineralogy, temperature, chemistry, and time on these communities and it is therefore unclear whether or not the minerals themselves are influencing the community composition of the microbes that colonize them. To attempt to disentangle these influences and ask what role mineral substrate plays in microbial community composition, structure and succession, we designed novel colonization samplers called In Situ Mineral Associated Colonization Sampler (ISMACS). ISMACS incubate minerals separately in (hopefully) identical thermal and chemical conditions and record temperature of the fluids throughout the incubation. This work again highlights the substantial heterogeneity characteristic of these dynamic environments concluding that mineralogy is not the primary force structuring diffuse flow mineral-associated communities. In this chapter I identify microbial taxa that seem to be influenced by mineral substrate, as well as potential early and late successional taxa in diffuse flow environments, providing ecological hypotheses to be more rigorously tested in the future. I also identify an association between Deltaproteobacteria and substrate consisting of different minerals in close proximity, potentially reflecting a metabolic advantage of extracellular electron transfer between different minerals.

This dissertation examines hydrothermal vent microbial communities from an interdisciplinary geological, chemical, ecological, molecular, and physiological perspective. This approach is possible by the use of a diverse set of tools including radiotracer rate experiments, mineralogical and stable isotope analysis, metatranscriptomics, seafloor *in situ* sample preservation, *in situ* mass spectrometry, shipboard and lab-based geochemical

analyses, novel collection and incubation devices, and DNA and RNA sequencing. The conclusions described within help to disentangle some of the complex interconnectedness of physical and biological forces inherent to such a dynamic, heterogeneous environment.

References

Baker, E.T., Massoth, G.J., and Walker, S.L. (1993) A method for quantitatively estimating diffuse and discrete hydrothermal discharge. *Earth and planetary science letters* **118**: 235–249.

Bemis, K., Lowell, R., and Farough, A. (2012) Diffuse Flow On and Around Hydrothermal Vents at Mid-Ocean Ridges. *oceanog* **25**: 182–191.

Bonch-Osmolovskaya, E.A., Perevalova, A.A., Kolganova, T.V., Rusanov, I.I., Jeanthon, C., and Pimenov, N.V. (2011) Activity and Distribution of Thermophilic Prokaryotes in Hydrothermal Fluid, Sulfidic Structures, and Sheaths of Alvinellids (East Pacific Rise, 13 N). *Applied and Environmental Microbiology* **77**: 2803–2806.

Boschen, R.E., Rowden, A.A., Clark, M.R., and Gardner, J.P.A. (2013) Mining of deep-sea seafloor massive sulfides: A review of the deposits, their benthic communities, impacts from mining, regulatory frameworks and management strategies. *Ocean & Coastal Management* **84**: 54–67.

Burcar, B.T., Barge, L.M., Trail, D., Watson, E.B., Russell, M.J., and McGown, L.B. (2015) RNA Oligomerization in Laboratory Analogues of Alkaline Hydrothermal Vent Systems. *Astrobiology* **15**: 509–522.

Harmsen, H., Prieur, D., and Jeanthon, C. (1997) Distribution of microorganisms in deep-sea hydrothermal vent chimneys investigated by whole-cell hybridization and enrichment culture of thermophilic subpopulations. *Applied and Environmental Microbiology* **63**: 2876–2883.

Johnson, H.P. and Pruis, M.J. (2003) Fluxes of fluid and heat from the oceanic crustal reservoir. *Earth and planetary science letters* **216**: 565–574.

Kargel, J. (2000) Europa's Crust and Ocean: Origin, Composition, and the Prospects for Life. *Icarus* **148**: 226–265.

Kormas, K.A., Tivey, M.K., Damm, Von, K., and Teske, A. (2006) Bacterial and archaeal phylotypes associated with distinct mineralogical layers of a white smoker spire from a deep-sea hydrothermal vent site (9oN, East Pacific Rise). *Environmental Microbiology* **8**: 909–920.

McDuff, R.E. and Edmond, J.M. (1982) On the fate of sulfate during hydrothermal circulation at mid-ocean ridges. *Earth and planetary science letters* **57**: 117–132.

McKay, C.P. and Smith, H.D. (2005) Possibilities for methanogenic life in liquid methane on the surface of Titan. *Icarus* **178**: 274–276.

Mottl, M.J. and Wheat, C.G. (1994) Hydrothermal circulation through mid-ocean ridge flanks: Fluxes of heat and magnesium. *Geochimica et Cosmochimica Acta* **58**: 2225–2237.

Olins, H.C., Rogers, D.R., Frank, K.L., Vidoudez, C., and Girguis, P.R. (2013) Assessing the

influence of physical, geochemical and biological factors on anaerobic microbial primary productivity within hydrothermal vent chimneys. *Geobiology* 279–293.
Polz, M.F., Robinson, J.J., Cavanaugh, C.M., and Van Dover, C.L. (1998) Trophic ecology of massive shrimp aggregations at a Mid-Atlantic Ridge hydrothermal vent site. *Limnology and Oceanography* **43**: 1631–1638.
Resing, J.A., Sedwick, P.N., German, C.R., Jenkins, W.J., Moffett, J.W., Sohst, B.M., and Tagliabue, A. (2015) Basin-scale transport of hydrothermal dissolved metals across the South Pacific Ocean. *Nature* **523**: 200–203.
Rona, P. and Trivett, D. (1992) Discrete and diffuse heat transfer atashes vent field, Axial Volcano, Juan de Fuca Ridge. 567–571.
Schrenk, M.O., Kelley, D.S., Delaney, J.R., and Baross, J.A. (2003) Incidence and Diversity of Microorganisms within the Walls of an Active Deep-Sea Sulfide Chimney. *Applied and Environmental Microbiology* **69**: 3580–3592.
Sievert, S. and Vetriani, C. (2012) Chemoautotrophy at Deep-Sea Vents: Past, Present, and Future. *oceanog* **25**: 218–233.
Takai, K., Komatsu, T., Inagaki, F., and Horikoshi, K. (2001) Distribution of Archaea in a Black Smoker Chimney Structure. *Applied and Environmental Microbiology* **67**: 3618–3629.
Wankel, S.D., Germanovich, L.N., Lilley, M.D., Genc, G., DiPerna, C.J., Bradley, A.S., et al. (2011) Influence of subsurface biosphere on geochemical fluxes from diffuse hydrothermal fluids. *Nature Geosci* **4**: 1–8.
Wheat, C.G., McManus, J., Mottl, M.J., and Giambalvo, E. (2003) Oceanic phosphorus imbalance: Magnitude of the mid-ocean ridge flank hydrothermal sink. *Geophys. Res. Lett.* **30**: 1–4.
Wirsen, C.O., Jannasch, H.W., and Molyneaux, S.J. (1993) Chemosynthetic microbial activity at Mid-Atlantic Ridge hydrothermal vent sites. *Journal of Geophysical Research: Solid Earth* **98**: 9693–9703.

Chapter 2

Assessing the influence of physical, geochemical and biological factors
on anaerobic microbial primary productivity within hydrothermal vent chimneys

(as published in the journal Geobiology)

Geobiology

Geobiology (2013), **11**, 279–293 DOI: 10.1111/gbi.12034

Assessing the influence of physical, geochemical and biological factors on anaerobic microbial primary productivity within hydrothermal vent chimneys

H. C. OLINS, D. R. ROGERS, K. L. FRANK, C. VIDOUDEZ AND P. R. GIRGUIS

Department of Organismic and Evolutionary Biology, Harvard University, Cambridge, MA, USA

ABSTRACT

Chemosynthetic primary production supports hydrothermal vent ecosystems, but the extent of that productivity and its governing factors have not been well constrained. To better understand anaerobic primary production within massive vent deposits, we conducted a series of incubations at 4, 25, 50 and 90 °C using aggregates recovered from hydrothermal vent structures. We documented *in situ* geochemistry, measured autochthonous organic carbon stable isotope ratios and assessed microbial community composition and functional gene abundances in three hydrothermal vent chimney structures from Middle Valley on the Juan de Fuca Ridge. Carbon fixation rates were greatest at lower temperatures and were comparable among chimneys. Stable isotope ratios of autochthonous organic carbon were consistent with the Calvin–Benson–Bassham cycle being the predominant mode of carbon fixation for all three chimneys. Chimneys exhibited marked differences in vent fluid geochemistry and microbial community composition, with structures being differentially dominated by gamma (γ) or epsilon (ε) proteobacteria. Similarly, qPCR analyses of functional genes representing different carbon fixation pathways showed striking differences in gene abundance among chimney structures. Carbon fixation rates showed no obvious correlation with observed *in situ* vent fluid geochemistry, community composition or functional gene abundance. Together, these data reveal that (i) net anaerobic carbon fixation rates among these chimneys are elevated at lower temperatures, (ii) clear differences in community composition and gene abundance exist among chimney structures, and (iii) tremendous spatial heterogeneity within these environments likely confounds efforts to relate the observed rates to *in situ* microbial and geochemical factors. We also posit that microbes typically thought to be mesophiles are likely active and growing at cooler temperatures, and that their activity at these temperatures comprises the majority of endolithic anaerobic primary production in hydrothermal vent chimneys.

Received 2 October 2012; accepted 25 February 2013

Corresponding author. P. R. Girguis. Tel.: +(617) 496 8328; fax: +(617) 495 8848; e-mail: pgiruis@oeb.harvard.edu

INTRODUCTION

The substantial animal and microbial biomass evident at deep-sea hydrothermal vents is a result of chemolithoautotrophic primary productivity, whereby bacteria and archaea generate energy from the oxidation of inorganic compounds to 'fix' inorganic carbon (as reviewed in Sievert & Vetriani, 2012). Numerous studies have documented the diversity and distribution of epi- and endolithic microbial communities within deep-sea hydrothermal vents (Reysenbach *et al.*, 2000; Reysenbach, 2002; Hoek *et al.*, 2003; Schrenk *et al.*, 2003; Kormas *et al.*, 2006; Nakagawa & Takai, 2008; Pagé *et al.*, 2008; Opatkiewicz *et al.*, 2009; Flores *et al.*, 2011), and many cultivated representatives of these communities are known to be chemolithoautotrophs (Takai *et al.*, 2003, 2006, 2009; Inagaki *et al.*, 2004; Reysenbach *et al.*, 2006). Recent work has shown a relationship between vent fluid composition and microbial community composition that might also influence microbial metabolism, including the mode and rate of carbon fixation (Inskeep *et al.*, 2010; Flores *et al.*, 2011, 2012). However, this supposition has not been tested using native microbial communities at near *in situ* conditions.

Thermodynamic and bioenergetic models predict sufficient chemical energy in vent fluids globally to support the production of 10^{10}–10^{13} g of microbial biomass annually

(McCollom & Shock, 1997; Bach & Edwards, 2003). Studies have shown that chemolithoautotrophic communities, both free-living and symbiotic, support substantial densities of macrofauna ranging from <1 kg m^{-2} (Juan de Fuca tubeworms fields; Sarrazin & Jumiper, 1999) to 70 kg m^{-2} (Mid-Atlantic Ridge mussel beds; Gebruk *et al.*, 2000), which exceeds estimates of the average biomass in the Brazilian Amazon forest (9–23 kg m^{-2}; Houghton *et al.*, 2001). At vents, chemolithoautotrophic microbes support carbon fixation by oxidizing reduced chemicals with a variety of electron acceptors ranging from oxygen to carbon dioxide. Consequently, chemolithoautotrophs occupy the full range of aerobic to anaerobic habitats that result from the dynamic mixing of reduced hydrothermal fluid and oxygenated seawater. Many vent chemolithoautotrophs are facultative, fixing carbon under aerobic or anaerobic conditions (e.g. *Salinisphera hydrothermalis*; Crespo-Medina *et al.*, 2009), but it is not known how their rates of carbon fixation vary under different geochemical regimes. To date, however, studies have empirically examined rates of carbon fixation by chemolithoautotrophic symbioses (Felbeck, 1985; Fisher *et al.*, 1989; Childress *et al.*, 1991; Scott *et al.*, 1994; Scott & Cavanaugh, 2007), as well as in a variety of hydrothermal plume fluids (Table S1; Campbell *et al.*, 2006; Chase *et al.*, 1985; Kato *et al.*, 2012; Mandernack & Tebo, 1999; Minic & Thongbam, 2011; Nakagawa & Takai, 2008; Perner *et al.*, 2007; Sievert *et al.*, 2008; Sievert & Vetriani, 2012; Sorokin, 1994; Tuttle, 1985; Wirsen *et al.*, 1986, 1993). Fewer studies have determined carbon fixation rates in hydrothermally influenced sediments (summarized in Das *et al.*, 2011), microbial mats (Nelson *et al.*, 1989; Wirsen *et al.*, 1993) or vent chimneys. To our knowledge, four studies have examined carbon fixation in hydrothermal vent chimney deposits (Wirsen *et al.*, 1993; Polz *et al.*, 1998; Eberhard *et al.*, 1995; Bonch-Osmolovskaya *et al.*, 2011; Table S1), although none have compared rates of primary productivity across a range of temperatures and multiple structures, or from habitats with varying geochemical and temperature regimes. Although it is known that habitable regions within chimney structures can be anaerobic (Tivey, 1995; McCollom & Shock, 1997; Schrenk *et al.*, 2003), no previous study of free-living microbial communities, to our knowledge, has examined the environmental factors and molecular mechanisms that might influence anaerobic carbon fixation rates at hydrothermal vents.

In addition, little is known about the distribution of biochemical pathways used to fix carbon within anaerobic habitats at hydrothermal vents. There are six known biochemical pathways by which autotrophic organisms reduce inorganic carbon to organic carbon, three of which are likely to play important roles at vents (the other three pathways have, to date, only been found in specific taxa and are still poorly understood, so they are not considered here). Differences in the energy requirements and oxygen and temperature sensitivity of these pathways likely result in varied favourability at different physico-chemical conditions (Hügler & Sievert, 2011).

Briefly, the Calvin–Benson–Bassham (CBB) cycle is found in many prokaryotes, including free-living and symbiotic γ-proteobacteria (Berg, 2011). It is also the primary carbon fixation pathway among cyanobacteria, algae and plants and is therefore responsible for the majority of global primary productivity. Ribulose-1,5-biphosphate carboxylase/oxygenase (RuBisCO) and the gene encoding for this enzyme are markers for the CBB cycle. RuBisCO is more oxygen tolerant than the key enzymes of the other carbon fixation pathways, conferring a significant advantage in oxic to suboxic environments. However, in the environment, the distribution of RuBisCO may be limited by the requirement of substantial activation energy as well as an apparent thermal stability up to only approximately 75 °C (Berg, 2011). The reductive tricarboxylic acid (rTCA) cycle is typically observed in ε-proteobacteria (known to be abundant in hydrothermal vent microbial communities; Hügler & Sievert, 2011; Campbell & Cary, 2004; Campbell *et al.*, 2006). Based on gene abundance, it has been suggested that microbes using the rTCA cycle are the dominant contributors to vent primary productivity (Campbell & Cary, 2004; Sievert *et al.*, 2008), although other studies suggest that microbes using the CBB cycle might be dominant (Wang *et al.*, 2009). ATP citrate lyase (encoded by the *acl* gene), the key marker for the rTCA cycle, is more oxygen sensitive than RuBisCO (Hügler & Sievert, 2011) and may require less activation energy in highly reducing environments. Finally, the Wood–Ljungdahl (WL; also known as the reductive acetyl-CoA) pathway is found in archaeal methanogens and is thought to be the most thermal tolerant of the carbon fixation pathways (Berg, 2011). It putatively requires the least amount of activation energy in reducing environments, and it has been primarily detected in strictly anaerobic organisms, likely due to highly oxygen-sensitive enzymes. At present, molecular targets that are specific to this pathway are lacking; therefore, the methyl coenzyme-M reductase (*mcr*) gene can be utilized as a proxy for this pathway (Luton *et al.*, 2002).

One long-standing question is how the nature and magnitude of primary production varies within these dynamic hydrothermal environments where steep thermal and geochemical gradients are common. Here, we examine anaerobic primary productivity in three massive hydrothermal deposits in the Middle Valley vent field along the Juan de Fuca Ridge (Fig. 1) through a series of radiotracer incubations (conducted over a range of temperatures), *in situ* geochemical analyses and molecular biological assessments of diversity as well as phylogenetic and functional gene abundances. Because vent deposits can consist of a range of minerals and precipitates, not all of which are sulphides,

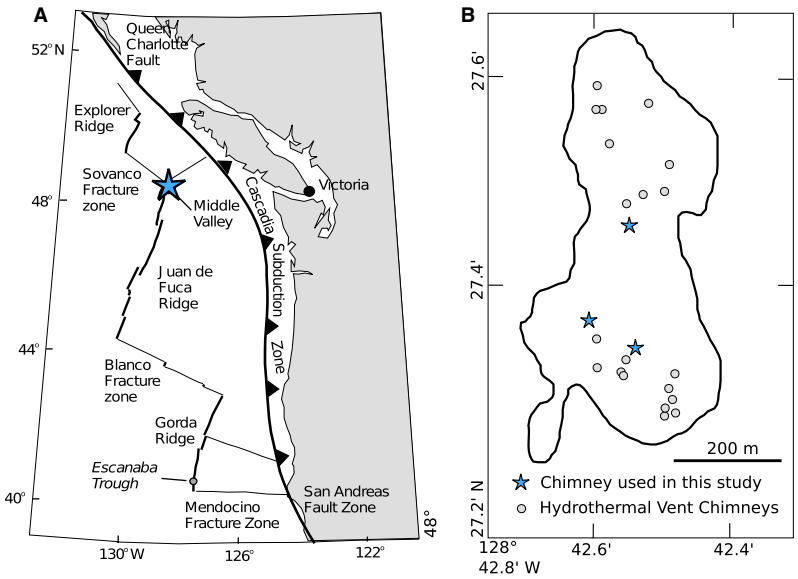

Fig. 1 (A) Location of Middle Valley on the Juan de Fuca Ridge (From Bjerkgård *et al.*, 2000). (B) Map of hydrothermal vent chimneys at Middle Valley's Area of Active Venting (AAV; after Stein & Fisher, 2001). Chimneys sampled in this study are marked with blue stars.

we refer to these structures throughout as 'chimneys'. We hypothesized that carbon fixation rates would be highest at the intermediate temperatures, in which both vent-derived reductants and seawater-derived oxidants would be sufficiently available, and consequently where biomass would be highest. We further posited that the distribution of genes representing these different pathways of carbon fixation would exhibit an *in situ* distribution consistent with the conditions in which they are most favoured.

METHODS

Sample collection

Middle Valley is a sedimented hydrothermal system located on the northern Juan de Fuca Ridge (Fig. 1A) and characterized by a diversity of chimneys with varying temperatures, as well as varying and elevated concentrations of volatile reductants such as hydrogen (Cruse & Seewald, 2006). Samples and experiments presented here were collected and conducted during the *RV Atlantis* expedition AT 15–67 in July of 2010. Samples were collected using the *DSV Alvin* (dive number 4625; 7/18/2010) from Dead Dog (48° 27.365′ N, 128° 42.584′ W, depth 2405 m), Chowder Hill (48° 27.328′ N, 128° 42.550′ W, depth 2398 m) and Needles (48° 27.466′ N, 128° 42.546′ W, depth 2412 m) chimneys (Fig. 1B). Prior to collection, temperature was recorded using the onboard resistance temperature detector (RTD) probe from an associated vigorously flowing chimney orifice. Temperatures were logged both verbally (by the science observer) and digitally, and the highest observed value is reported. An *in situ* mass spectrometer (ISMS; configured and calibrated as described by Wankel *et al.*, 2010) was used to analyse dissolved volatiles in both the vigorously venting fluid and ambient seawater. After temperature and geochemical measurements, we recovered the samples of hydrothermal vent chimney from which these measurements were made. Samples were placed into thermally insulated collection boxes using the submersible's manipulator and brought to the surface. Animals were removed from the chimney surfaces, and samples were broken into smaller chunks using sterilized chisels and stored in gastight glass jars in filter-sterilized (0.2 μm) anaerobic, sulphidic (approximately 2 mM) seawater. In the case of the Needles chimney, a conspicuous darker mineral stratum was subsampled and treated separately from the remainder of the Needles sample. These are referred to as Needles-grey and Needles-white, respectively. Samples were stored at approximately 4°C until experiments were carried out 3 days later.

^{14}C-INORGANIC CARBON INCUBATIONS

Samples of hydrothermal chimney were homogenized under a nitrogen atmosphere in a commercial blender ('Xtreme' model, Waring Inc.) with media consisting of 1:1 proportions of filter-sterilized (0.35 μm) bottom seawater collected outside the vent field using 20-L Niskin bottles and sulphate-free artificial seawater (1.9 g L^{-1} KCl, 4.8 g L^{-1} $CaCl_2x2H_2O$, 23.3 g L^{-1} NaCl). The medium was made anaerobic by sparging with nitrogen gas and made sulphidic by the addition of pre-weighed sodium sulphide flakes. The final media also contained 2 mM sulphide, 14 mM sulphate and 18 μM nitrate and was adjusted to pH 6.5 using 1 M HCl.

In an anaerobic glove bag, Balch tubes were filled with approximately 15 mL of homogenized slurry and sealed with blue butyl rubber stoppers. Sealed tubes were placed

in water baths at 25, 50 and 90 °C or refrigerated at 4 °C. All samples were allowed to acclimate to temperature for 2 h prior to addition of 2.5 μCi ^{14}C-bicarbonate label via syringe and needle. Kill controls were attempted by the addition of 1 mL of 1 M NaOH. Note that kill controls proved to be ineffective, and accordingly, we used the t_0 time points and non-labelled subsamples to best estimate carbon fixation rates as described later. All incubations were terminated with the addition of 1 mL glacial acetic acid (to volatilize DIC) and frozen upside down (to reduce the risk of DIC loss through the stopper) until analysis. Initial (t_0) time points were terminated immediately after the addition of label, and experimental tubes were terminated after 72 h. Experimental samples from each chimney were run in triplicate at each temperature. However, one biological replicate was lost from both the Dead Dog and Needles-white samples that were incubated at 25 °C.

Upon thawing frozen samples, the volumes of sediment and seawater were recorded from each tube to normalize rate measurements. Solid sample volumes ranged from 2.26 to 10.08 mL, while the liquid phase ranged from 15.01 to 27.42 mL. The thawed samples were transferred to 15-mL Falcon tubes and acidified to pH 4.0 using HCl in order to convert DIC to $CO_{2(g)}$. The samples were mixed and allowed to degas overnight. The mineral and aqueous phases were separated by centrifugation (500g for 5 min) in a Clinical 50 Centrifuge (VWR, Inc., Radnor, PA, USA). The mineral phase was acidified again with 2 mL of 10% HCl and equilibrated overnight. Mineral phases were washed three times with deionized water. The final supernatant was decanted and analysed for DI^{14}C. Three or six weighed subsamples (0.08–1.3 g wet weight) of the mineral phase from each sample were dried overnight, rehydrated with 1 mL of DI water and 20 mL of EcoScint™ A scintillation cocktail (National Diagnostics, Atlanta, GA, USA) and shaken to resuspend the sample immediately prior to analysis on a LS 600IC liquid scintillation counter (Beckman, Inc., Brea, CA, USA). Counts lower than 30 counts per minute (cpm) were considered below detection. Sealed ^{14}C standards (Perkin Elmer, Inc., Waltham, MA, USA) were run alongside experimental samples, and efficiency throughout analysis was observed to be 87% (SD = 3.41%).

Subsamples of sulphide slurry from both Dead Dog and Needles-white without any added ^{14}C inorganic carbon were analysed as a control for non-specific activity, as well as to determine the lower limits of detection. Some samples had reads up to 30 cpm g^{-1} of chimney material (with an average of 17) due to a small amount of naturally occurring radioactivity. Accordingly, carbon fixation rates from any experimental subsamples with values below 30 cpm g^{-1} were considered below background levels and therefore below detection limits. Although this lowers our analytical sensitivity, it prevents artificial inflation of the calculated carbon fixation rates.

To determine the quenching factor of the hydrothermal deposits, a quench curve was run with non-labelled sample from Needles chimney. Similar masses of non-labelled chimney material were spiked with different activities of ^{14}C-sucrose, ranging from 5×10^{-1} to 5×10^{-7} μCi. Independently, different chimney masses were spiked with a constant activity of ^{14}C-sucrose (0.01 μCi). No quenching was detected with any of the Middle Valley samples in the mass range corresponding to the mass subsampled; however, quenching was apparent with greater masses of material.

Determination of carbon fixation rates

Rates of carbon fixation were calculated as follows:

$$\mathrm{CFX_{rate}} = \frac{(A_{tn} - A_{t0}) * [\mathrm{DIC}]}{A_{\mathrm{total}} * t} \quad (1)$$

where A_{tn} = measured activity of the sample at time n (in μCi/g, average of three or six subsamples); A_{t0} = activity of samples frozen immediately after adding label and shaking, which was close to zero in all cases; DIC = total dissolved inorganic carbon of the media (in mmol bicarbonate); A_{total} = total activity added to experimental incubation tube (μCi); t = incubation time in days.

Total dissolved inorganic carbon (DIC) in the media was quantified from sterile gastight samples using a gas chromatography mass–spectrometry (GCMS) system (Agilent Headspace Sampler 7697A, GC System 7890A with inert XL MSD with triple axis detector 5975C; Agilent Technologies, Santa Clara, CA, USA). Samples were run alongside a set of standards, and DIC concentration was interpolated from the linear fit to the calibration curve (R^2 = 0.996).

Nitrate concentrations in the media were also determined post-cruise from NaOH-preserved samples of media using NitraVer® Nitrate Powder Pillows (Hach, Inc., Loveland, CO, USA) according to the manufacturer's instructions, with the following exception: one packet was added to 500 μL sample plus 500 μL deionized (DI) water instead of 10 mL of sample. Samples were run alongside a set of standards made in 3.5% salt solution and were quantified using a Spectramax Plus384 XS Absorbance Microplate Reader (Molecular Devices, Inc., Sunnyvale, CA, USA) at 540 nm. Nitrate concentration was interpolated from the linear fit to the calibration curve (R^2 = 0.994).

Characterization of volatiles in vent effluent and bottom seawater

An *in situ* mass spectrometer was used to quantify CO_2, CH_4 and H_2S concentrations in the high-temperature vent fluid, as well as in nearby background seawater during the dives where the sulphide deposits were collected (Wankel *et al.*, 2010, 2011). The instrument was configured, operated and calibrated as previously described (Wankel *et al.*,

2011). High-temperature samples were recovered by using a wand with a gastight titanium heat exchanger, which reduced the vent effluent temperatures to that of the ambient bottom seawater prior to *in situ* analyses.

Stable isotope analysis of endogenous organic carbon

Stable isotope analysis of the endogenous organic carbon in the chimney deposits was carried out by the University of New Hampshire Stable Isotope Lab using an ECS4010 Elemental Analyzer (Costech, Inc., Valencia, CA, USA) interfaced with a DeltaPlus XP Mass Spectrometer (Thermo Fisher Scientific, Inc., Waltham, MA, USA). Mineral samples, frozen at sea immediately upon collection, were prepared by crushing the samples with a mortar and pestle, rinsing and acidifying (10% HCl) for one hour and then rinsing a final time in deionized water.

Scanning electron microscopy and energy dispersive X-ray spectroscopy

Powder from the same samples used for stable isotope analysis (prepared as previously, but without the acid rinse) was analysed for bulk elemental chemistry using an Evo50 scanning electron microscope (SEM; Zeiss, Inc., Thornwood, NY, USA) with an energy dispersive X-ray spectroscopy (EDAX) detector. Elemental peaks were recorded at 10 kV from each sample of individual mineral grains, as well as entire fields of view.

X-ray diffraction analysis

Mineral composition was confirmed through X-ray diffraction (XRD) analysis of the same samples used for SEM analysis by Margaret Tivey at the Woods Hole Oceanographic Institution. Samples were scanned from 3° to 75° 2θ using copper (PW3123/00 curved Cu monochromator) X-radiation at 30 mA and 40 kV. The Macdiff software package (http://www.geol-pal.uni-frankfurt.de/Staff/Homepages/Petschick/MacDiff/MacDiffInfoE.html) was used to identify minerals from the peak output.

DNA extractions

DNA was extracted following a modified protocol of Santelli *et al.* (2008). Chimney samples were crushed with a sterile mortar and pestle (to ca. ≥ 1 mm diameter) and divided into aliquots of approximately 0.5 g (up to 1.0 g). Samples were washed with 0.1 N HCl and rinsed twice with 50 mM EDTA and 10 mM Tris (pH 8.0). The samples were then added to a PowerSoil™ bead-beating tube (MoBio Laboratories, Inc., Carlsbad, CA, USA). The mixture was incubated at 70 °C for 10 min, after which 200 ng of poly-A (polyadenylic acid) was added to the solution. The cells were disrupted by bead beating (twice) in a FastPrep24 bead beater (MP Biomedicals, Santa Ana, CA, USA) at 6.5 Nm s^{-1} for 60 s, followed by three cycles of freeze–thaw disruption. The supernatant was then treated according to the manufacturer's protocols. Prior to elution, the filter and 100 μL TE were heated to 50 °C for 5 min to improve yield. Three aliquots per sample were extracted in parallel, and DNA was pooled post-extraction. DNA was quantified using the Qubit™ fluorometer according to the manufacturer's instructions (Life Technologies, Inc., Grand Island, NY, USA).

Quantitative PCR

Quantitative PCR (qPCR) was used to enumerate bacterial and archaeal 16S rRNA genes, as well as key genes involved in specific carbon fixation pathways. RuBisCO form II (*cbbM* gene) was chosen to represent the CBB cycle, because it has been found in higher abundance than form I in vent environments (Elsaied & Naganuma, 2001; Elsaied *et al.*, 2007; Wang *et al.*, 2009). Moreover, attempts to amplify RuBisCO form I from these samples were unsuccessful. ATP citrate lyase (*aclB* gene) was used to represent the rTCA cycle and methyl coenzyme-M reductase (*mcrA* gene), which is indicative of methanogens at vents (Ver Eecke *et al.*, 2012), was used to represent the archaeal WL pathway.

For assay development, genes of interest were amplified from known culture strains (Table S2) and cloned using the StrataClone vector (Agilent Technologies, Inc.) according to the manufacturer's instructions. The resulting plasmids were extracted using the Qiaprep™ Spin Miniprep Kit (Qiagen, Inc., Germantown, MD, USA), linearized by EcoRV digestion (Fermentas, Inc.), purified using a Qiaquick PCR cleanup column (Qiagen, Inc.) and quantified with Quant-iT PicoGreen™ assay (Life Technologies, Inc.) on a Spectramax Gemini XS fluorometer (Molecular Devices, Inc.). Each pool was serially diluted to concentrations ranging from 10^8 to 10^1 copies μL^{-1}.

Assays were performed using the PerfeCTa® SYBR® Green FastMix®, Low ROX™ (Quanta Biosciences, Inc., Gaithersburg, MD, USA; primers and annealing temperatures specified in Table S2). Cycling conditions were as follows: 10 min at 94 °C, followed by 40 cycles of 30 s at 94 °C, 60 s at the annealing temperature (Table S2) and 60 s at 72 °C. Fluorescence was measured after 10 s at 80 °C. Dissociation curves were calculated across a temperature range of 55–95 °C. C_t for each well was calculated using the manufacturer's software. All reactions were performed on a Stratagene™ Mx3005P QPCR system (Agilent Technologies, Inc.).

Sequencing and phylogenetic analysis

Extracted DNA was sequenced using 454 FLX (Roche, Inc., San Francisco, CA, USA) with Titanium™ reagents (Dowd *et al.*, 2008) and established bacterial and archaeal primers (Table S2). Data were analysed with Mothur (Schloss

et al., 2009). Sequences were trimmed and quality checked, aligned to the SILVA-compatible alignment database reference alignment, analysed for chimeras (via chimera.uchime command), classified according to the Greengenes99 database and clustered into OTUs at the 97% identity level. Shannon and Simpson diversity indices and Chao estimates were calculated using Mothur, which generated a random subsample of sequences from each library to yield equally sized samples (n = 1709 for bacteria, n = 338 for archaea) for beta diversity calculations. Abundant OTUs not successfully classified with the Mothur pipeline were identified using Basic Local Alignment Search Tool (BLAST; Altschul *et al.*, 1990) using randomly selected (by mother) representative sequences that were blasted manually.

Sequence accession numbers

The 16S rRNA sequences reported in this study have been submitted to NCBI's Sequence Read Archive (SRA) under the accession numbers SRX154514 through SRX154519.

RESULTS

Chimney morphology, geochemistry and temperature

The three chimneys used in this study differed markedly in shape, size and fluid chemistry (Table 1). Needles chimney was a small, skinny spire approximately 50 cm tall and 30 cm wide at the base. The sample collected from Needles was roughly 10 cm wide and was sectioned as previously mentioned. Dead Dog chimney was approximately 40 cm tall with a much larger orifice and was about 20 cm wide at the point of collection. Chowder Hill chimney, in contrast, consisted of two tall, thin spires, each with a height between 5 and 9 m. The width of these spires varied between 10 and 40 cm. Maximum recorded venting fluid temperature for both Dead Dog and Chowder Hill was 261 °C. At Needles, the maximum recorded vent temperature was 123 °C, but the mineralogical composition of that chimney (primarily anhydrite, which dissolves below approximately 150 °C) implies that the structure was experiencing temperatures of at least 150 °C prior to sampling.

Table 1 Geochemical characteristics of the chimneys used in this study

	Needles	Dead Dog	Chowder Hill
Size estimation*	50 cm tall, 30 cm base, 10 cm spire	40 cm tall, 20 cm wide	5–9 m tall, 10–40 cm wide
Depth (m)†	2412	2405	2398
Max recorded temp. °C‡	123	260.95	261.04
CH_4 [mM]§**	3.55	7.58	13.6
CO_2 [mM]§¶**	4.04	10.13	17.07
Estimated pH††	5.98	5.642	6.057
pH compensated CO_2 [mM]**	8.096	14.521	37.686
Excess CO_2‡‡	2.381	4.271	11.084
$\delta^{13}C$ ratio (permil)§§	−25.04 ± 0.24	−26.35 ± 0.68	-25.39 ± 0.18
Bulk Mineralogy¶¶	Anhydrite	Anhydrite	Anhydrite

*Based on laser sights recorded in DSV Alvin dive video.†From Alvin Frame Grabber.‡Recorded by the Alvin temperature probe.§Data from ISMS, mean of 10 highest measurements at site.¶Values are not pH compensated. **Values are the mean of 10 highest values per site.††This is an estimate of pH based on Butterfield *et al.*, 1994; 1990 data.‡‡Excess CO_2 values are relative to 3.4 mM measured in nearby bottom water.§§Mean of four replicate measurements ± SD of crushed, acid and DI water washed samples.¶¶Based on Ames *et al.*, 1993 and confirmed with SEM–EDX analysis.

Carbon fixation rates

The average carbon fixation rates per sample reported here spanned three orders of magnitude (Fig. 2, Table 2).

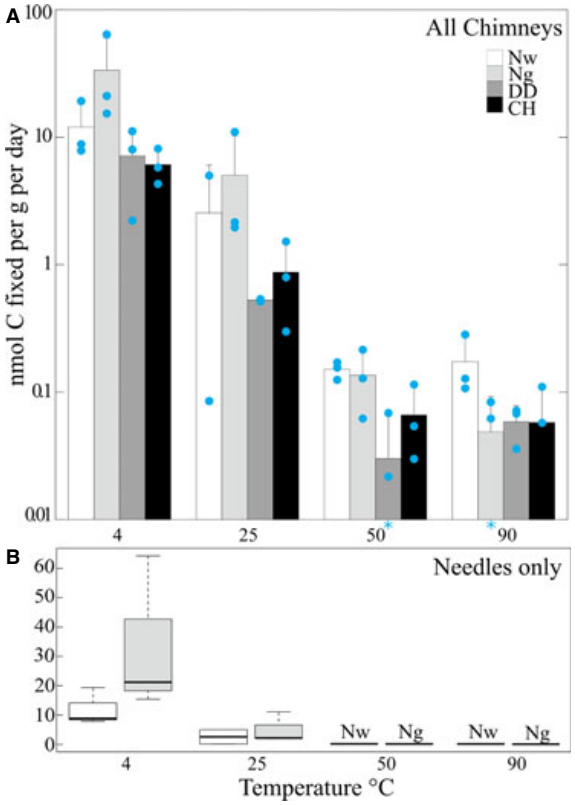

Fig. 2 $H^{14}CO_3^-$ incorporation measured in slurries of hydrothermal deposit material and media designed to mimic diffuse hydrothermal fluid (2 mM sulphide, 14 mM sulphate, pH 6.5) conducted shipboard at four temperatures. (A) Rates measured from all chimney samples across a 4–90°C temperature gradient. Note the log scale. (B) Rates measured from the two Needles subsamples across a 4–90 °C temperature gradient (data also shown in panel a). Bars represent the mean ± SD of the average value per experimental treatment. N = 3 for each treatment, except in DD and Nw at 25 °C, in which N = 2. Blue dots represent the average of three replicate analyses for each biological replicate. Abbreviations: Nw, Needles-white (white); Ng, Needles-grey (light grey); DD, Dead Dog (dark grey); CH, Chowder Hill (black). Asterisks represent rate values below detection level.

Table 2 Measured rates of anaerobic carbon fixation reported in nmol C fixed per g chimney per day.

Temperature °C	Needles-white	Needles-grey	Dead Dog	Chowder Hill
4	12.02	33.63	7.15	6.1
25	2.55*	5.06	0.53*	0.87
50	0.15	0.14	0.03	0.07
90	0.17	0.05	0.06	0.06

Values represent the average of three samples, each of which was measured in triplicate (except where noted). These values correspond to those presented in Fig. 2.*These treatments are represented by only two samples, due to breakage.

These rates varied significantly as a function of incubation temperature within the Needles-grey, Chowder Hill and Dead Dog samples, with higher rates observed at cooler thermal regimes (Kruskal–Wallis rank-sum test, *P*-values = 0.022, 0.025 and 0.036, respectively). Carbon fixation rates within the Needles-white sample were not significantly different between temperatures (*P*-value = 0.11). All four chimney samples showed the highest rates at 4 °C, followed by 25 °C (Fig. 2, Table 2; no significant difference was found between rates at 50 and 90 °C; Wilcoxon's rank-sum test *P*-value = 0.60). Despite the similarity between rates at 50 and 90 °C, rates were significantly different across the four experimental temperatures (Kruskal–Wallis rank-sum test, *P*-values < 0.05) for all samples except Needles-white (*P*-value = 0.11). Rates were also significantly different between temperatures when all chimneys were pooled into one data set (*P*-value = 1.52×10^{-7}).

The range of carbon fixation rates also varied by chimney. In Chowder Hill, the average rates per sample spanned two orders of magnitude, while in Needles-grey, they spanned approximately three orders of magnitude. The highest observed carbon fixation rate was 64.0 nmol $C{\cdot}g^{-1}{\cdot}d^{-1}$, measured in Needles-grey at 4 °C. Two samples (Needles-grey, 90 °C and Dead Dog, 50 °C) showed no detectable carbon fixation. The lowest detectable rates were 0.006 nmol $C{\cdot}g^{-1}{\cdot}d^{-1}$, observed in Chowder Hill samples at 90 °C. Within-tube replicates also exhibited heterogeneity, with carbon fixation rates varying by up to 12 nmol $C{\cdot}g^{-1}{\cdot}d^{-1}$ among subsamples from the same experimental tube. The average difference between the lowest and highest subsample from the same homogenized sample was 1.4 nmol $C{\cdot}g^{-1}{\cdot}d^{-1}$.

Volatile geochemistry via *in situ* mass spectrometry

Statistically significant differences in methane and carbon dioxide (Table 1) as well as sulfide (Frank *et al.*, 2013) were observed among the three sites (one-way analysis of means, *P*-value – 2.2×10^{-16}). Consistent with lower fluid temperature, Needles vent fluid had lower concentrations of both CO_2 and CH_4 than the two higher temperature chimneys. Because inorganic carbon speciates between H_2CO_3*, HCO_3^- and CO_3^{2-} as a function of pH, data are presented both without pH correction and with pH compensation according to previous published values from the same locations (our *in situ* pH electrode failed during deployment; Table 1).

Stable carbon isotope ratios of autochthonous organic matter

Stable isotope analysis revealed $\delta^{13}C$ values of autochthonous organic matter of −25.04 for Needles, −26.35 for Dead Dog and −25.39 for Chowder Hill (average of four replicates, SD = 0.24; Table 1). Although the differences between chimneys were small, they were statistically significant (ANOVA, *P*-value = 0.005).

Mineralogy

Scanning electron microscope (SEM) with EDAX and XRD of all four hydrothermal samples revealed that the structures were dominated by anhydrite, consistent with previous mineralogical analyses of samples from Dead Dog and Chowder Hill (Ames *et al.*, 1993). These authors concluded that active chimneys in Middle Valley are predominantly (>40%) anhydrite, contain minor (1–5%) amounts of gypsum, pyrrhotite, and clay, minor to trace (<1%) amounts of sphalerite and chalcopyrite, and trace amounts of pyrite, isocubanite, galena, arsenopyrite, barite and chlorite. There were no obvious differences in mineralogy samples, despite the obvious visual difference between the white and grey sections of Needles.

Functional and taxonomic gene abundances

The DNA yields varied by chimney, with the highest yield from Needles, followed by Chowder Hill, and then Dead Dog (4603.2, 2467.5 and 1896.6 ng DNA g^{-1} chimney material, respectively).

For all three chimneys, the number of archaeal 16S rRNA gene copies exceeded bacterial 16S rRNA genes by 1–2 orders of magnitude (Fig. 3A). The number of copies of the archaeal 16S rRNA gene per gram of material ranged from 9.6×10^5 (Dead Dog) to 5.9×10^8 (Needles), while bacterial 16S gene copy number ranged from 5.9×10^4 (Dead Dog) to 2.2×10^6 (Needles).

The abundance of genes selected as proxies for carbon fixation also varied by chimney (Fig. 3B). The genes *cbbM* (RuBisCO form II, representing the CBB cycle), *aclB* (ATP citrate lyase, representing the rTCA cycle), *and mcrA* (methyl coenzyme-M reductase, representing the archaeal WL pathway) were detected in all vent samples (Fig. 3B). *cbbM* and *aclB* gene copy numbers were within an order of magnitude of each another within each chimney. In all cases,

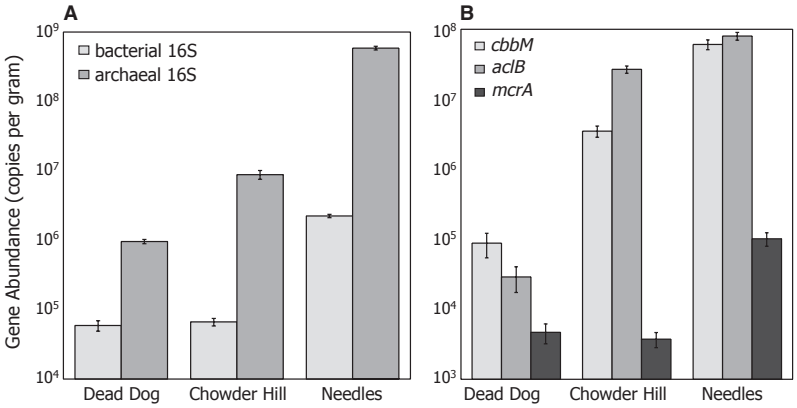

Fig. 3 (A) Bacterial and archaeal 16S rRNA gene abundances at three hydrothermal chimneys. DNA was not extracted from Needles-grey and Needles-white separately due to limited sample size. (B) Abundance of gene markers representing the major carbon fixation pathways thought to be important at hydrothermal vents. *cbbM*, CBB cycle; *aclB*, rTCA cycle; *mcrA*, methanogens/WL pathway. Gene abundances are standardized to gram of chimney material from which DNA was extracted. Data represent the mean ± SD of three replicate qPCR runs per assay.

mcrA was 1–3 orders of magnitude lower in abundance than *cbbM* or *aclB*. *cbbM* genes dominated in Dead Dog, *aclB* genes dominated in Chowder Hill and *cbbM* and *aclB* genes were roughly equivalent in Needles (Fig. 3B). Note that because RuBisCO form II was chosen to represent the CBB cycle (see Methods), this may be an underrepresentation of total RuBisCO abundance in these samples. Needles chimney contained the highest abundances (normalized to either mass of material extracted or DNA yield) of all three genes. Needles and Chowder Hill showed the same pattern of abundance, namely *aclB* > *cbbM* > *mcrA*. Dead Dog exhibited a different pattern of *cbbM* > *aclB* > *mcrA*. The difference in abundance of *aclB* genes between Needles and Chowder Hill was within one order of magnitude, as was the difference in *mcrA* genes between Dead Dog and Chowder Hill. All other differences were greater than an order of magnitude among chimneys.

Microbial community composition

Pyrotag sequencing revealed strikingly different community compositions among the sites (Fig. 4). The Dead Dog bacterial sequence library was dominated by sequences classified as ε-proteobacteria (49% of all bacterial sequences), with 7% of sequences classified as γ-proteobacteria. In contrast, Chowder Hill and Needles libraries were dominated by sequences classified as γ-proteobacteria (50 and 41% of all bacterial sequences, respectively). 27% and 0.6% of the bacterial sequences recovered from Chowder Hill and Needles, respectively, were classified as ε-proteobacteria.

The most abundant bacterial OTU in Needles (16% of bacterial sequences) was allied to *Thermodesulfovibrio*, a group of thermophilic sulphate reducers that belong to the Nitrospirae clade and are thought to use the rTCA pathway (Hügler & Sievert, 2011). The most abundant bacterial OTU from Dead Dog (11% of bacterial sequences) was allied to *Sulfurimonas paralvinellae*, an ε-proteobacteria that is also thought to use the rTCA cycle (Takai *et al.*, 2006). Finally, the most abundant bacterial OTU from Chowder Hill (27% of bacterial sequences) was allied to ε-proteobacteria from the sulphur-oxidizing taxa *Sulfuricurvales* ('hydrothermal_eubacterium_PVB_OTU_6'). The archaeal libraries were also distinct between Dead Dog and

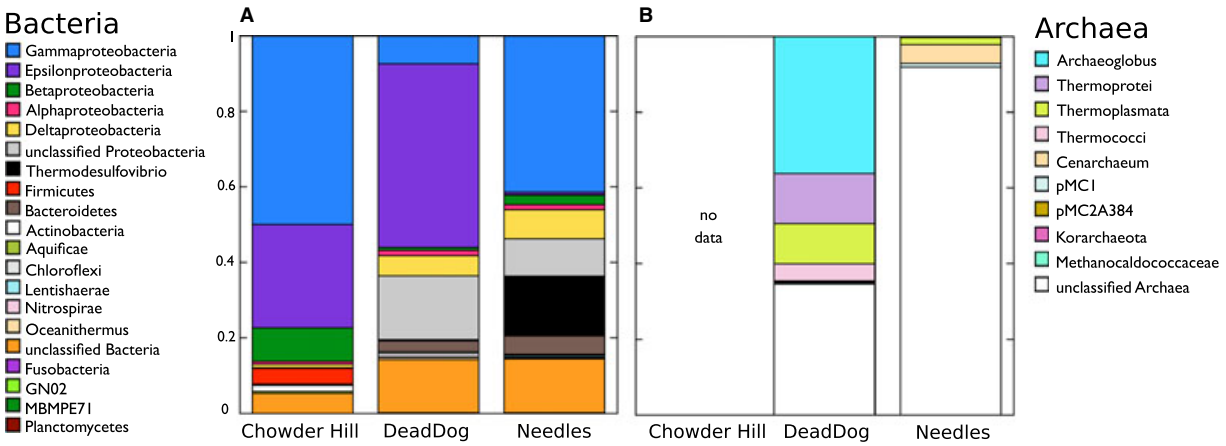

Fig. 4 Taxonomic distribution of (A) bacterial and (B) archaeal 16S rRNA gene sequences from 454 pyrosequencing. Values are the proportion of total sequences (n = 1709 for bacteria and 338 for archaea). Sequencing was unsuccessful for Chowder Hill archaea.

Needles, with no shared OTUs. Archaeal sequencing was unsuccessful for Chowder Hill samples. Thirty-six per cent of Dead Dog archaeal sequences were allied to *Archaeoglobus*, 35% were unclassified archaeal sequences, 12% were Thermoprotei sequences, 6% were *Aciduliprofundaceae* sequences and 4% were *Thermococci* sequences. Needles, on the other hand, had 92% unclassified sequences and 5% *Cenarchaeum* (46 OTUs). It should be noted that commonly used archaeal primers have been shown to be inadequate in capturing the diversity of deep subsurface and hydrothermal sediments (Teske & Sørensen, 2008) and can exhibit cross-reactivity with bacteria, limiting their utility in characterizing hydrothermal vent chimney communities.

The number of identified OTUs and the Chao OTU estimate (Table S3) show that Needles was the most diverse structure, followed by Dead Dog and then Chowder Hill. There was also variation in the representation of rare taxa among the libraries. OTUs with fewer than 10 sequences represented 92%, 79% and 50% of the bacterial library from Needles, Dead Dog and Chowder Hill, respectively, and 28% and 9% of the archaeal library from Needles and Dead Dog, respectively. Shannon and Simpson's diversity indices, in contrast, indicate that Dead Dog was more diverse than Needles, likely because these indices are less sensitive to the presence of rare taxa (Table S3).

DISCUSSION

The abundance of biomass at hydrothermal vents is one of their most striking features. While the vast abyssal plane ecosystems are largely dependent on allochthonous carbon from the overlying water column, hydrothermal vent communities exploit the geochemical gradients driven by the interaction of cold, oxidized bottom water with the hot reduced crust to produce autochthonous carbon, supporting enormous, if localized, biomass. Through tracer incubations and co-registered geochemical/molecular biological analyses, we observed surprising patterns in anaerobic carbon fixation within hydrothermal and a striking degree of heterogeneity that prohibited relating the *in situ* geochemistry and quantitative molecular surveys to the observed rates. The paragraphs below discuss these observations in greater detail and further explore the relevance of anaerobic carbon fixation to local and global productivity.

Carbon Fixation Rates

The carbon fixation rates measured at Middle Valley (0.03 –33.63 nmol $C{\cdot}g^{-1}{\cdot}day^{-1}$) are comparable to those from the few previous studies at hydrothermal vent chimneys (summarized in Table S1; Bonch-Osmolovskaya *et al.*, 2011; Eberhard *et al.*, 1995; Polz *et al.*, 1998; Wirsen *et al.*, 1993), although direct comparisons are challenging due to differences in reported rate units and experimental design. Previously reported rate estimates from the surface scrapings of vent chimneys were higher than rates from subsurface scrapings (a maximum of 1292 nmol $C{\cdot}mL^{-1}$ $slurry{\cdot}day^{-1}$ versus 10.5 nmol $C{\cdot}g^{-1}{\cdot}day^{-1}$; to facilitate comparison, we assumed 2.9 g per cm^3 for the bulk chimney material; Eberhard *et al.*, 1995; Polz *et al.*, 1998; Wirsen *et al.*, 1993; Bonch-Osmolovskaya *et al.*, 2011). Note that subsurface scrapings were only incubated at high temperature. If we assume that 1 g of chimney deposit is comparable to 1 mL of diffuse vent fluid, our highest rates are between 1 and 2 orders of magnitude higher than many of the published rates from hydrothermal fluid (most range from 0.01 to 0.5 nmol $C{\cdot}ml^{-1}{\cdot}day^{-1}$; Table S1; Chase *et al.*, 1985; Mandernack & Tebo, 1999; Tuttle, 1985; Tuttle *et al.*, 1983; Wirsen *et al.*, 1986, 1993). This is notable considering that cell density within chimney deposits is often lower than within hydrothermal plumes (Edwards *et al.*, 2003; Schrenk *et al.*, 2003; Takai *et al.*, 2004; Zhou *et al.*, 2009), suggesting that rates may be much higher on a per cell basis within these deposits.

While an increase in temperature is generally thought to increase microbial metabolic rates (reviewed in Nedwell, 1999), here we measured a decrease in rate with increasing temperature. The inverse relationship reported here may be explained by the observation that hydrothermal vent microbial communities are denser within and upon the outer layers than deeper within the chimney structure (Harmsen *et al.*, 1997; Takai *et al.*, 2001; Schrenk *et al.*, 2003). This relationship between carbon fixation rates and temperature was also observed by Wirsen *et al.* (1993). The dense outer-layer communities are likely adapted to life at temperatures near that of ambient seawater (approximately 4 °C). Given our sampling regime, in which we homogenized chimney material to facilitate replication for statistical analyses, we posit that microbes adapted to life at cooler temperatures dominated these samples – both in abundance and activity.

Microbial community composition

This work includes, to our knowledge, the first investigation of *in situ* microbial communities in hydrothermal chimneys from Middle Valley. Microbial community composition has been described for many hydrothermal vent sites, including those along the Juan de Fuca Ridge (Huber *et al.*, 2002, 2003, 2006a,b, 2007; Cowen, 2003; Schrenk *et al.*, 2003; Nakagawa *et al.*, 2006; Sogin *et al.*, 2006; Opatkiewicz *et al.*, 2009; Zhou *et al.*, 2009; Orcutt *et al.*, 2011). However, the Middle Valley chimneys are quite different in mineralogy, as they are primarily composed of anhydrite rather than sulphide minerals. Additionally, while hydrothermal vent chimneys (including those of the Juan de Fuca Ridge) have been described as dominated

by ε-proteobacteria (Zhou *et al.*, 2009; Opatkiewicz *et al.*; Flores *et al.*, 2011; Reysenbach *et al.*, 2000), our community diversity assessments suggest that chimneys can also be dominated by γ-proteobacteria, and that chimneys in the same vent field can have dramatically different representations of these major bacterial taxa.

These data further suggest that organisms canonically described as meso- or thermophilic may be active at cooler temperatures. It is known from both ecological surveys and laboratory studies of cultivated vent microbes that many ε- and γ-proteobacteria appear to be present in cooler habitats and are metabolically active at lower temperatures. As one example, Perner *et al.* (2007) showed that low-temperature (approximately 5 °C) diffuse-flow venting fluids from the Mid-Atlantic Ridge were dominated by ε-proteobacteria, lacked thermophiles and hyperthermophiles and contained a diversity of rTCA as well as RuBisCO (form II) genes. Moreover, vent isolates such as the ε-proteobacteria *Sulfurimonas paralvinellae* (Takai *et al.*, 2006) and the γ-proteobacteria *Thiomicrospira crunogena* (Jannasch *et al.*, 1985; Wirsen *et al.*, 1998) are known to be active and grow at temperatures down to 4 °C (although their realized optimal growth in the laboratory setting is approximately 30 °C). Similarly, members of the ε-proteobacterial genus *Arcobacter* are known to thrive at cold seeps at ambient seawater temperatures (Wirsen *et al.*, 2002; Perner *et al.*, 2007). The presence of phylogenetically allied ribotypes in our samples to these organisms known to be successful at cool temperatures suggests a potential within our microbial community for growth and activity at cooler temperatures. Two abundant OTUs from Needles and one from Dead Dog were identified as most closely related to *Thiomicrospira* strains, and four OTUs from Dead Dog were similarly identified as *S. paralvinellae*. One abundant OTU from Needles was identified as *Arcobacteraceae*. If these are indeed dominant *in situ*, γ-proteobacteria at Needles chimney may be moderate psychrophiles and responsible for the majority of primary productivity, while ε- and γ-proteobacteria may be responsible for the majority of carbon fixation at Dead Dog and Chowder Hill. Given the qualitative nature of PCR-based 16S libraries, additional analyses are required to establish that these ribotypes are in fact dominant and active *in situ*.

Functional gene abundance

Quantitative assessments of gene abundance captured site-to-site variation in genomic composition (and hence functional potential) of hydrothermal chimney microbial communities from Middle Valley, revealing that both γ- and ε-proteobacteria can dominate these chimney communities. They further reveal site-to-site variation in the abundance (although not necessarily expression) of genes representing the aforementioned three carbon fixation pathways. Most importantly, however, these analyses demonstrate that, despite comparable carbon fixation rates across structures, there are marked, large-scale differences in the phylotypic abundance and gene representation. The similarities in rates among these different communities underscore that direct measurements of microbial activity, and not phylotype abundance or diversity, are the best metric of primary productivity.

Contrary to our initial hypotheses, we did not find any correlation between carbon fixation rates and patterns of abundance of genes related to different carbon fixation pathways. We examined this through qPCR of genes representing the CBB and rTCA cycles and the WL pathway (*cbbM, aclB* and *mcrA*, respectively). These processes are likely responsible for the majority of primary production within vent ecosystems and may occur at different locations within the vent deposits based on their specific energy requirements and the oxygen tolerance of key enzymes (reviewed in Bar-Even *et al.*, 2012; Berg, 2011; Berg *et al.*, 2010; Hügler & Sievert, 2011). The genes *cbbM, aclB* and *mcrA* were detected in all vent samples (Fig. 3). *cbbM* and *aclB* gene copy numbers were within an order of magnitude of one another in each chimney, but *mcrA* was 1–3 orders of magnitude lower in abundance. However, abundances of *mcrA* are on the same order of magnitude as those reported recently from vent fluids elsewhere along the Juan de Fuca Ridge (Ver Eecke *et al.*, 2012).

We provide two potential explanations for the apparent lack of correlation among these factors. First, these habitats exhibit tremendous biological and geochemical heterogeneity, and very little is known about how these communities vary at small spatial scales (Perner *et al.*, 2012). Vent fluid and seawater chemical reactions result in a large degree of mineralogical heterogeneity (Tivey, 2007), which may support or stimulate microbial heterogeneity (in terms of community composition or activity) at the mineral grain scale. Indeed, there is some evidence that microbial communities at hydrothermal vents are influenced significantly by mineral substrate (Edwards *et al.*, 2003; Suzuki *et al.*, 2004; Kormas *et al.*, 2006; Toner *et al.*, 2012). Sample heterogeneity is also evident in the data presented here, as we observed variation in rates among subsamples from seemingly homogenized material. The second possible explanation is the difference between metabolic potential (examined via DNA) and metabolic activity, which may or may not be reflected in the DNA-based picture of these communities. Further work is needed to investigate the differences between the total community and the active community in this and other systems.

Isotopic evidence of carbon fixation pathways

Stable carbon isotope ratios of the total autocthonous organic carbon (TOC) within each structure can be used

to constrain the reaction pathways and hence the activity of the primary producers. Because the CBB cycle, rTCA cycle and WL pathway have different isotopic fractionations, this approach enables us consider their relative contributions to biomass and, hence, primary productivity. $\delta^{13}C$ values of total organic carbon ($\delta^{13}C_{TOC}$) from all native chimney samples were approximately −25‰ (Table 1). If we assume that *in situ* carbon fixation is occurring primarily in water with a DIC composition somewhere between that of background seawater from the Juan de Fuca Ridge (−1.40‰; Walker *et al.*, 2008) and hydrothermal plumes within the habitable range (approximately 60 °C) from actively venting structures along the Juan de Fuca Ridge (roughly −6% to −7‰; Proskurowski *et al.*, 2004; Walker *et al.*, 2008), then the apparent fractionation in these samples was approximately −24 to −18‰, which is consistent with biomass generated primarily via the CBB cycle. Biomass generated by the CBB cycle has generally been observed to have delta values in the range of −18 to −29‰ depending on the form of RuBisCO (−11% to −30‰ for Form I and −18% to 23‰ for form II; Boller *et al.*, 2011; House *et al.*, 2003; Pearson, 2010). Delta values for RuBisCO-generated biomass are generally, though not always, more negative than those for biomass generated using the rTCA cycle (−2 to −13‰; Fuchs, 1989; House *et al.*, 2003; Pearson, 2010) and substantially more positive than values expected for biomass generated by the WL pathway (−34 to −40‰; Fuchs, 1989; House *et al.*, 2003; Pearson, 2010).

The observed $\delta^{13}C_{TOC}$ represents a composite of all carbon fixation processes (both anaerobic and aerobic) at vents and could be explained by various contributions from the rTCA cycle, WL pathway and CBB cycle. Future studies should specifically aim to identify the fractional contributions of these different modes of carbon fixation to vent productivity in carefully subsampled sections of chimneys representing inner, middle and outer zones, as well as the role of oxygen in regulating the distribution and magnitude of carbon fixation in chimneys and other vent habitats. Previous gene abundance data indicate that hydrothermal vent environments may be dominated by both the CBB cycle (Wang *et al.*, 2009) and the rTCA cycle (Campbell & Cary, 2004; Sievert *et al.*, 2008). However, our data seem to be consistent with a dominance of the CBB cycle over the rTCA cycle in contributing to net primary productivity in these environments.

It should also be noted that these sulphide-amended anaerobic incubations would not support carbon fixation by aerobic or microaerophilic chemolithoautotrophs and consequently only represent a fraction of the community engaged in chemolithoautotrophy. In these incubations, the most abundant electron donors were sulphide in the medium, reduced sulphur compounds present in the initial sample and ammonium or acetate present initially or produced during the incubation. Potential electron acceptors included nitrate (18 μM) and sulphate (14 mM) from the media, and possibly elemental sulphur and iron (III) present in the inoculum. Although there are many anaerobic energy metabolisms known to be coupled to carbon fixation at hydrothermal vents (e.g. Fe^{2+}-oxidation, S-oxidation, H_2-oxidation, methanogenesis, sulphate reduction; reviewed in Fisher *et al.*, 2007; Orcutt *et al.*, 2011), we suggest that the majority of the observed carbon fixation is attributable to microbially mediated sulphide oxidation using nitrate as an oxidant. This would be consistent with the high representation of γ- and ε-proteobacterial sulphur oxidizers in these samples (i.e. OTUs related to *Sulfurimonas*). Future studies should examine the contribution of aerobic and microaerophilic carbon fixation to net primary productivity.

Implications

The similarities in the rates presented here to those from previous studies of fluids or hydrothermal deposit material provided an opportunity to make first-order estimates of primary productivity in hydrothermal chimneys at mid-ocean ridge systems. Given that carbon fixation rates are comparable with hydrothermal chimneys along the East Pacific Rise (Tuttle, 1985; Wirsen *et al.*, 1986; Bonch-Osmolovskaya *et al.*, 2011; Sievert & Vetriani, 2012), the Mid-Atlantic Ridge (Wirsen *et al.*, 1993; Eberhard *et al.*, 1995; Polz *et al.*, 1998) and the Juan de Fuca Ridge (Chase *et al.*, 1985), we assumed that these samples accurately represent the actively venting chimneys at Middle Valley and used these rates and other metrics to develop a first-order estimate of the extent of carbon fixation attributable to active deep-sea hydrothermal chimney deposits. At 4 °C, anaerobic carbon fixation rates, extrapolated annually, ranged from 26.80 to 147.53 μg C per year per gram of chimney material.

We assumed a total mass of venting chimneys of 2,480,000 g for Middle Valley's Area of Active Venting (AAV; 800 × 350 m) based on chimney volume estimates from our dive videos, published documentation of the number of active chimneys at AAV (Ames *et al.*, 1993) and the assumption of chimney density of 2.9 g/cm^{-3} (which is the density of both anhydrite and ocean crust). From this, we estimated the amount of carbon fixed annually at AAV to range from 66.26 to 365.36 g. When the 90 °C rates were used for this estimation, we arrived at 0.53–1.88 g C fixed annually. Regardless, the maximum annual estimate of anaerobic primary productivity within actively venting hydrothermal vent chimneys was three orders of magnitude lower than estimates of annual primary productivity in surface waters of the Pacific Ocean when normalized per metre squared (0.0002 and 0.1 g C · m^{-1} · $year^{-1}$ for AAV and Pacific Ocean, respectively;

Behrenfeld & Falkowski, 1997), and a diminutive fraction of the estimated $10^{10} - 10^{13}$ g of global microbial biomass that could be produced annually from the energy found in vent fluids (McCollom & Shock, 1997; Bach & Edwards, 2003). It has been estimated that there are 500 to 5000 hydrothermal vent fields globally (Hannington *et al.*, 2011), but before further extrapolation, additional rate measurements are needed that better represent the variety of habitats at vent fields, especially from cooler hydrothermal environments such as diffuse-flow areas, hydrothermal sediments and extinct chimneys or rubble.

CONCLUSIONS

Data from tracer incubation, molecular and natural abundance stable isotopic data sets presented here demonstrate the potential role of anaerobic carbon fixation the net productivity at hydrothermal vents along the Juan de Fuca ridge. The similarity in patterns of carbon fixation rates, as well as the $\delta^{13}C_{TOC}$ across all chimneys suggests that similar processes of carbon fixation (in terms of both pathway and rate) are active under *in situ* conditions. It therefore seems likely that all these chimneys harbour a particular physico-chemical niche, that is, cooler regimes replete with nitrate, wherein functionally comparable (but phylogenetically distinct) microbial taxa are responsible for the majority of primary productivity. However, as seen in these data, DNA-based surveys of microbial density, distribution and functional potential might not correlate with activity and, if used as a proxy, may misrepresent rates of carbon fixation. While these data did not capture the precise drivers of primary productivity, they are compelling because they indicate that geographically close, geochemically distinct structures show similar patterns in activity despite different microbial communities. These data underscore the fact that hydrothermal vents are highly heterogeneous environments with respect to both geochemistry and microbiology and underscore the importance of matching the resolution of geochemical measurements with the scale of microbial measurements to better discern the factor(s) governing primary production.

AUTHOR CONTRIBUTIONS

HCO, KLF and PRG designed the carbon fixation experiments. PRG collected the samples. HCO and KLF carried out the shipboard experiments. HCO analysed the carbon fixation experiments. DRR performed the DNA extractions and qPCR assays. HCO and KLF performed the bioinformatics analyses. CV and PRG collected and analysed the *in situ* geochemical data. HCO analysed the data. HCO, DRR, PRG and KLF assisted with analytical design and data interpretation. HCO and PRG wrote the manuscript with input from all co-authors.

ACKNOWLEDGEMENTS

We are grateful for the expert assistance of the *R/V Atlantis* crew and the pilots and team of the *DSV Alvin* for enabling the collections of hydrothermal chimney samples used in our experiments. We also thank Dr. Kathleen Scott, Dr. Margaret Tivey and Mr. Andrew Ouimette for providing assistance with various technical aspects of the experiments and sample processing and/or data interpretation. This material is based upon work supported by the National Science Foundation (NSF OCE-0838107 and NSF OCE-1061934 to P. R. Girguis and a Graduate Research Fellowship under Grant No. DGE-1144152 to H. C. Olins), as well as the National Aeronautic and Space Administration (NASA-ASTEP NN X09AB78G to C. Scholin and P. R. Girguis and NASA-AST EP NNX07AV51G to A. Knoll and P. R. Girguis). The authors have no conflicts of interest to declare.

REFERENCES

Altschul SF, Gish W, Miller W, Myers EW, Lipman DJ (1990) Basic local alignment search tool. *Journal of molecular biology* **215**, 403–410.

Ames D, Franklin J, Hannington M (1993) Mineralogy and geochemistry of active and Inactive chimneys and massive sulfide, Middle Valley, northern Juan-De-Fuca Ridge - an evolving hydrothermal system. *Canadian Mineralogist* **31**, 997–1024.

Bach W, Edwards K (2003) Iron and sulfide oxidation within the basaltic ocean crust: implications for chemolithoautotrophic microbial biomass production. *Geochimica Et Cosmochimica Acta* **67**, 3871–3887.

Bar-Even A, Noor E, Milo R (2012) A survey of carbon fixation pathways through a quantitative lens. *Journal of Experimental Botany* **63**, 2325–2342.

Behrenfeld M, Falkowski P (1997) Photosynthetic rates derived from satellite-based chlorophyll concentration. *Limnology and Oceanography* **42**, 1–20.

Berg IA (2011) Ecological aspects of the distribution of different autotrophic CO_2 fixation pathways. *Applied And Environmental Microbiology* **77**, 1925–1936.

Berg IA, Kockelkorn D, Ramos-Vera WH, Say RF, Zarzycki J, Hügler M, Alber BE, Fuchs G (2010) Autotrophic carbon fixation in archaea. *Nature Reviews Microbiology* **8**, 447–460.

Bjerkgård T, Cousens B, Franklin J (2000) The Middle Valley sulfide deposits, northern Juan de Fuca Ridge: radiogenic isotope systematics. *Economic Geology and the Bulletin of the Society of Economic Geologists* **95**, 1473–1488.

Boller AJ, Thomas PJ, Cavanaugh CM, Scott KM (2011) Low stable carbon isotope fractionation by coccolithophore RubisCO. *Geochimica Et Cosmochimica Acta* **75**, 7200–7207.

Bonch-Osmolovskaya EA, Perevalova AA, Kolganova TV, Rusanov II, Jeanthon C, Pimenov NV (2011) Activity and distribution of thermophilic prokaryotes in hydrothermal fluid, sulfidic structures, and sheaths of alvinellids (East Pacific Rise, 13 N). *Applied And Environmental Microbiology* **77**, 2803–2806.

Butterfield D, Massoth G, McDuff R, Lupton J, Lilley M (1990) Geochemistry of hydrothermal fluids from axial seamount hydrothermal emissions study vent field, juan de fuca ridge: subseafloor boiling and subsequent fluid-rock interaction.

Journal of Geophysical Research-Solid Earth and Planets **95**, 12895–12921.
Butterfield DA, McDuff RE, Franklin J, Wheat CG (1994) Geochemistry of hydrothermal vent fluids from Middle Valley, Juan de Fuca Ridge. *Proceedings of the Ocean Drilling Program, Scientific Results* **139**, 395–410.
Campbell BJ, Cary SC (2004) Abundance of reverse tricarboxylic acid cycle genes in free-living microorganisms at deep-sea hydrothermal vents. *Applied and Environmental Microbiology* **70**, 6282–6289.
Campbell BJ, Engel AS, Porter ML, Takai K (2006) The versatile ε-proteobacteria: key players in sulphidic habitats. *Nature Reviews Microbiology* **4**, 458–468.
Chase RL, Delaney JR, Karsten JL, Johnson HP, Juniper SK, Lupton JE, Scott SD, Tunnicliffe V, Hammond SR, McDuff RE (1985) Hydrothermal vents on an axis seamount of the Juan de Fuca ridge. *Nature* **313**, 212–214.
Childress J, Fisher C, Favuzzi J, Sanders N (1991) Sulfide and carbon-dioxide uptake by the hydrothermal vent clam, calyptogena-magnifica, and its chemoautotrophic symbionts. *Physiological Zoology* **64**, 1444–1470.
Cowen JP (2003) Fluids from aging ocean crust that support microbial life. *Science* **299**, 120–123.
Crespo-Medina M, Chatziefthimiou A, Cruz-Matos R, Perez-Rodriguez I, Barkay T, Lutz RA, Starovoytov V, Vetriani, (2009) *Salinisphaera hydrothermalis* sp. nov., a mesophilic, halotolerant, facultatively autotrophic, thiosulfate-oxidizing gammaproteobacterium from deep-sea hydrothermal vents, and emended description of the genus Salinisphaera. *International Journal of Systematic and Evolutionary Microbiology* **59**, 1497–1503.
Cruse A, Seewald J (2006) Geochemistry of low-molecular weight hydrocarbons in hydrothermal fluids from Middle Valley, northern Juan de Fuca Ridge. *Geochimica Et Cosmochimica Acta* **70**, 2073–2092.
Das A, Sujith PP, Mourya BS, Biche SU, LokaBharathi PA (2011) Chemosynthetic activity prevails in deep-sea sediments of the Central Indian Basin. *Extremophiles* **15**, 177–189.
Dowd SE, Sun Y, Secor PR, Rhoads DD, Wolcott BM, James GA, Wolcott RD (2008) Survey of bacterial diversity in chronic wounds using Pyrosequencing, DGGE, and full ribosome shotgun sequencing. *BMC Microbiology* **8**, 43.
Eberhard C, Wirsen C, Jannasch H (1995) Oxidation of polymetal sulfides by chemolithoautotrophic bacteria from deep-sea hydrothermal vents. *Geomicrobiology Journal* **13**, 145–164.
Edwards K, McCollom T, Konishi H, Buseck P (2003) Seafloor bioalteration of sulfide minerals: results from in situ incubation studies. *Geochimica et Cosmochimica Acta* **67**, 2843–2856.
Elsaied H, Naganuma T (2001) Phylogenetic diversity of ribulose-1,5-bisphosphate carboxylase/oxygenase large-subunit genes from deep-sea microorganisms. *Applied Environmental Microbiology* **67**, 1751–1765.
Elsaied HE, Kimura H, Naganuma T (2007) Composition of archaeal, bacterial eukaryal RuBisCO genotypes in three Western Pacific arc hydrothermal vent systems. *Extremophiles* **11**, 191–202.
Felbeck H (1985) CO_2 fixation in the hydrothermal vent tube worm Riftia-pachyptila (Jones). *Physiological Zoology* **58**, 272–281.
Fisher C, Childress J, Minnich E (1989) Autotrophic carbon fixation by the chemoautotrophic symbionts of Riftia-pachyptila. *Biological Bulletin* **177**, 372–385.
Fisher CR, Takai K, Bris NL (2007) Hydrothermal vent ecosystems. *Oceanography* **20**, 14–23.
Flores GE, Campbell JH, Kirshtein JD, Meneghin J, Podar M, Steinberg JI, Seewald JS, Tivey MK, Voytex MA, Yang ZK, Reysenbach A-L (2011) Microbial community structure of hydrothermal deposits from geochemically different vent fields along the Mid-Atlantic Ridge. *Environmental Microbiology* **13**, 2158–2171.
Flores G, Shakya M, Meneghin J, Yang ZK, Seewald JS, Wheat CG, Podar M, Reysenbach A-L (2012) Inter-field variability in the microbial communities of hydrothermal vent deposits from a back-arc basin. *Geobiology* **10**, 333–346.
Frank K, Rogers D, Olins H, Vidoudez C, Girguis P (2013). Characterizing the distribution and rates of microbial sulfate reduction at middle valley. *ISME Journal*. doi: 10.1038/ismej.2013.17. in press.
Fuchs G (1989) Alternative pathways of autotrophic CO_2 fixation. In *Autotrophic Bacteria* (eds Schlegel H., Bowien B.). Science Tech Publishers, Madison, WI, USA, pp. 365–382.
Gebruk A, Chevaldonne P, Shank T, Vrijenhoek R (2000) Deep-sea hydrothermal vent communities of the Logatchev area (14 45′N, Mid-Atlantic Ridge): diverse biotopes and high biomass. *Journal of The Marine Biological Association of the United Kingdom* **80**, 383–393.
Hannington M, Jamieson J, Monecke T, Petersen S, Beaulieu S (2011) The abundance of seafloor massive sulfide deposits. *Geology* **39**, 1155–1158.
Harmsen H, Prieur D, Jeanthon C (1997) Distribution of microorganisms in deep-sea hydrothermal vent chimneys investigated by whole-cell hybridization and enrichment culture of thermophilic subpopulations. *Applied And Environmental Microbiology* **63**, 2876–2883.
Hoek J, Banta A, Hubler F, Reysenbach A-L (2003) Microbial diversity of a sulphide spire located in the Edmond deep-sea hydrothermal vent field on the Central Indian Ridge. *Geobiology* **1**, 119–127.
Houghton R, Lawrence K, Hackler J, Brown S (2001) The spatial distribution of forest biomass in the Brazilian Amazon: a comparison of estimates. *Global Change Biology* **7**, 731–746.
House C, Schopf J, Stetter K (2003) Carbon isotopic fractionation by Archaeans and other thermophilic prokaryotes. *Organic Geochemistry* **34**, 345–356.
Huber JA, Butterfield DA, Baross JA (2002) Temporal changes in archaeal diversity and chemistry in a mid-ocean ridge subseafloor habitat. *Applied and Environmental Microbiology* **68**, 1585–1594.
Huber JA, Butterfield DA, Baross JA (2003) Bacterial diversity in a subseafloor habitat following a deep-sea volcanic eruption. *FEMS Microbiology Ecology* **43**, 393–409.
Huber JA, Butterfield DA, Baross JA (2006a) Diversity and distribution of subseafloor Thermococcales populations in diffuse hydrothermal vents at an active deep-sea volcano in the northeast Pacific Ocean. *Journal of Geophysical Research*, **111**, 1–13.
Huber JA, Johnson HP, Butterfield DA, Baross JA (2006b) Microbial life in ridge flank crustal fluids. *Environmental Microbiology* **8**, 88–99.
Huber JA, Welch DBM, Morrison HG, Huse SM, Neal PR, Butterfield DA, Sogin ML (2007) Microbial population structures in the deep marine biosphere. *Science* **318**, 97–100.
Hügler M, Sievert SM (2011) Beyond the calvin cycle: autotrophic carbon fixation in the ocean. *Annual Review of Marine Science* **3**, 261–289.
Inagaki F, Takai K, Nealson K, Horikoshi K (2004) Sulfurovum lithotrophicum gen. nov., sp. nov., a novel sulfur-oxidizing chemolithoautotroph within the -Proteobacteria isolated from Okinawa Trough hydrothermal sediments. *International Journal of Systematic and Evolutionary Microbiology* **54**, 1477–1482.

Inskeep , W. P. , Rusch , D. B. , Jay , Z. J. , Herrgard , M. J. , Kozubal , M. A. , Richardson , T. H. , Macur , R. E. , Hamamura N, Jennings RdM, Fouke BW, Reysenbach A-L, Roberto F, Young M, Schwartz A, Boyd ES, Badger JH, Mathur EJ, Ortmann AC, Bateson M, Geesey G, Frazier M (2010) Metagenomes from high-temperature chemotrophic systems reveal geochemical controls on microbial community structure and function. *PLoS ONE*, **5**, e9773, 1-13.

Jannasch HW, Wirsen CO, Nelson DC, Robertson LA (1985) Thiomicrospira crunogena sp. nov., a colorless, sulfur-oxidizing bacterium from a deep-sea hydrothermal vent. *International Journal of Systematic Bacteriology* **35**, 422–424.

Kato S, Nakawake M, Ohkuma M, Yamagishi A (2012) Distribution and phylogenetic diversity of cbbM genes encoding RubisCO form II in a deep-sea hydrothermal field revealed by newly designed PCR primers. *Extremophiles* **16**, 277–283.

Kormas KA, Tivey MK, Von Damm K, Teske A (2006) Bacterial and archaeal phylotypes associated with distinct mineralogical layers of a white smoker spire from a deep-sea hydrothermal vent site (9°N, East Pacific Rise). *Environmental Microbiology* **8**, 909–920.

Luton PE, Wayne JM, Sharp RJ, Riley PW (2002) The mcrA gene as an alternative to 16S rRNA in the phylogenetic analysis of methanogen populations in landfill. *Microbiology* **184**, 3521–3530.

Mandernack KW, Tebo BM (1999) In situ sulfide removal and CO2 fixation rates at deep-sea hydrothermal vents and the oxicranoxic interface in Framvaren Fjord, Norway. *Marine Chemistry* **66**, 201–213.

McCollom TM, Shock EL (1997) Geochemical constraints on chemolithoautotrophic metabolism by microorganisms in seafloor hydrothermal systems. *Geochimica Et Cosmochimica Acta* **61**, 4375–4391.

Minic Z, Thongbam PD (2011) The biological deep sea hydrothermal vent as a model to study carbon dioxide capturing enzymes. *Marine Drugs* **9**, 719–738.

Nakagawa S, Takai K (2008) Deep-sea vent chemoautotrophs: diversity, biochemistry and ecological significance. *FEMS Microbiology Ecology* **65**, 1–14.

Nakagawa S, Inagaki F, Suzuki Y, Steinsbu BO, Lever MA, Takai K, Engelen B, Sako Y, Wheat CG, Horikoshi K, Expedition IODP, 301 Scientists, (2006) Microbial community in black rust exposed to hot ridge flank crustal fluids. *Applied And Environmental Microbiology* **72**, 6789–6799.

Nedwell D (1999) Effect of low temperature on microbial growth: lowered affinity for substrates limits growth at low temperature. *FEMS Microbiology Ecology* **30**, 101–111.

Nelson DC, Wirsen CO, Jannasch HW (1989) Characterization of large, autotrophic *Beggiatoa* spp. abundant at hydrothermal vents of the guaymas basin. *Applied And Environmental Microbiology* **55**, 2909–2917.

Opatkiewicz AD, Butterfield DA, Baross JA (2009) Individual hydrothermal vents at Axial Seamount harbor distinct subseafloor microbial communities. *FEMS Microbiology Ecology* **70**, 413–424.

Orcutt B, Bach W, Becker K, Fisher A, Hentscher M, Toner B, Wheat C, Edwards KJ (2011) Colonization of subsurface microbial observatories deployed in young ocean crust. *ISME Journal* **5**, 629–703.

Pagé A, Tivey MK, Stakes DS, Reysenbach A-L (2008) Temporal and spatial archaeal colonization of hydrothermal vent deposits. *Environmental Microbiology* **10**, 874–884.

Pearson A. (2010) Pathways of carbon assimilation and their impact on organic matter values d13C. In *Handbook of Hydrocarbon and Lipid Microbiology*. (ed. Timmis K. N.). Springer, Berlin Heidelberg, pp. 143–156.

Perner M, Seifert R, Weber S, Koschinsky A, Schmidt K, Strauss H, Peters M, Haase K, Imhoff JF (2007) Microbial CO_2 fixation and sulfur cycling associated with low-temperature emissions at the Lilliput hydrothermal field, southern Mid-Atlantic Ridge (9°S). *Environmental Microbiology* **9**, 1186–1201.

Perner M, Gonnella G, Hourdez S, Böhnke S, Kurtz S, Girguis P (2012) *In situ* chemistry and microbial community compositions in five deep-sea hydrothermal fluid samples from Irina II in the Logatchev field. *Environmental Microbiology*, early online view, 1–10. doi: 10.1111/1462-2920.12038.

Polz M, Robinson J, Cavanaugh C, van Dover C (1998) Trophic ecology of massive shrimp aggregations at a Mid-Atlantic Ridge hydrothermal vent site. *Limnology and Oceanography* **43**, 1631–1638.

Proskurowski G, Lilley MD, Brown TA (2004) Isotopic evidence of magmatism and seawater bicarbonate removal at the endeavour hydrothermal system. *Earth and Planetary Science Letters* **225**, 53–61.

Reysenbach A-L (2002) Merging genomes with geochemistry in hydrothermal ecosystems. *Science* **296**, 1077–1082.

Reysenbach A-L, Longnecker K, Kirshtein J (2000) Novel bacterial and archaeal lineages from an in situ growth chamber deployed at a Mid-Atlantic Ridge hydrothermal vent. *Applied and Environmental Microbiology* **66**, 3798–3806.

Reysenbach A-L, Liu Y, Banta AB, Beveridge TJ, Kirshtein JD, Schouten S, Tivey MK, Von Damm KL, Voytek MA (2006) A ubiquitous thermoacidophilic archaeon from deep-sea hydrothermal vents. *Nature* **442**, 444–447.

Santelli CM, Orcutt BN, Banning E, Bach W, Moyer CL, Sogin ML, Staudigel H, Edwards KJ (2008) Abundance and diversity of microbial life in ocean crust. *Nature* **453**, 653–656.

Sarrazin J, Jumiper S (1999) Biological characteristics of a hydrothermal edifice mosaic community. *Marine Ecology Progress Series* **185**, 1–19.

Schloss PD, Westcott SL, Ryabin T, Hall JR, Hartmann M, Hollister EB, Lesniewski RA, Oakley BB, Parks DH, Robinson CJ, Sahl JW, Stres B, Thallinger GG, Van Horn DJ, Weber CF (2009) Introducing mothur: open-source, platform-independent, community-supported software for describing and comparing microbial communities. *Applied And Environmental Microbiology* **75**, 7537–7541.

Schrenk M, Kelley D, Delaney J, Baross J (2003) Incidence and diversity of microorganisms within the walls of an active deep-sea sulfide chimney. *Applied And Environmental Microbiology* **69**, 3580.

Scott KM, Cavanaugh CM (2007) CO_2 uptake and fixation by endosymbiotic chemoautotrophs from the Bivalve Solemya velum. *Applied and Environmental Microbiology* **73**, 1174–1179.

Scott KM, Fisher CR, Vodenichar JS, Nix ER, Minnich E (1994) Inorganic carbon and temperature requirements for autotrophic carbon fixation by the chemoautotrophic symbionts of the giant hydrothermal vent tube worm, *Riftia pachyptila*. *Physiological Zoology* **67**, 617–638.

Sievert S, Vetriani C (2012) Chemoautotrophy at deep-sea vents: past, Present, and Future. *Oceanography* **25**, 218–233.

Sievert SM, Hügler M, Taylor CD, Wirsen CO (2008) Sulfur oxidation at deep-sea hydrothermal vents. In *Microbial Sulfur Metabolism* (eds Dahl C., Friedrich C.). Springer, Berlin, Heidelberg, pp. 238–258.

Sogin ML, Morrison HG, Huber JA, Welch DM, Huse SM, Neal PR, Arrieta JM, Herndl GJ (2006) Microbial diversity in the deep sea and the underexplored "rare biosphere". *Proceedings of the National Academy of Sciences, USA* **103**, 12115–12120.

Sorokin D (1994) Dark oxidation of reduced sulfur-compounds in Kraternaya Bay. *Microbiology* **63**, 207–209.
Stein JS, Fisher AT (2001) Multiple scales of hydrothermal circulation in Middle Valle, norther Juan de Fuca Ridge: physical constraints and geologic models. *Journal of Geophysical Research* **106**, 8563–8580.
Suzuki Y, Inagaki F, Takai K, Nealson KH, Horikoshi K (2004) Microbial Diversity in Inactive Chimney Structures from Deep-Sea Hydrothermal Systems. *Microbial Ecology* **47**, 186–196.
Takai K, Komatsu T, Inagaki F, Horikoshi K (2001) Distribution of archaea in a black smoker chimney structure. *Applied And Environmental Microbiology* **67**, 3618–3629.
Takai K, Inagaki F, Nakagawa S, Hirayama H, Nunoura T, Sako Y, Nealson KH, Horikoshi K (2003) Isolation and phylogenetic diversity of members of previously uncultivated epsilon-Proteobacteria in deep-sea hydrothermal fields. *Fems Microbiology Letters* **218**, 167–174.
Takai K, Gamo T, Tsunogai U, Nakayama N, Hirayama H, Nealson K, Horikoshi K (2004) Geochemical and microbiological evidence for a hydrogen-based, hyperthermophilic subsurface lithoautotrophic microbial ecosystem (HyperSLiME) beneath an active deep-sea hydrothermal field. *Extremophiles* **8**, 269–282.
Takai K, Suzuki M, Nakagawa S, Miyazaki M, Suziki Y, Inagaki F, Horikoshi K (2006) Sulfurimonas paralvinellae sp. nov., a novel mesophilic, hydrogen- and sulfur-oxidizing chemolithoautotroph within the Epsilonproteobacteria isolated from a deep-sea hydrothermal vent polychaete nest, reclassification of Thiomicrospira denitrificans as Sulfurimonas denitrificans comb. nov. and emended description of the genus Sulfurimonas. *International Journal of Systematic and Evolutionary Microbiology* **56**, 1725–1733.
Takai K, Miyazaki M, Hirayama H, Nakagawa S, Querellou J, Godfroy A (2009) Isolation and physiological characterization of two novel, piezophilic, thermophilic chemolithoautotrophs from a deep-sea hydrothermal vent chimney. *Environmental Microbiology* **11**, 1983–1997.
Teske A, Sørensen KB (2008) Uncultured archaea in deep marine subsurface sediments: have we caught them all? *The ISME Journal* **2**, 3–18.
Tivey M (1995) The influence of hydrothermal fluid composition and advection rates on black smoker chimney mineralogy: Insights from modeling transport and reaction. *Geochimica et Cosmochim Acta* **59**, 1933–1949.
Tivey MK (2007) Generation of seafloor hydrothermal vent fluids and associated mineral deposits. *Oceanography* **20**, 50–65.
Toner BM, Lesniewski RA, Marlow JJ, Briscoe LJ, Santelli CM, Bach W, Orcutt BN, Edwards KJ (2012) Mineralogy drives bacterial biogeography of hydrothermally inactive seafloor sulfide deposits. *Geomicrobiology Journal* **30**, 313–326.
Tuttle JH (1985) The role of sulfur-oxidizing bacteria at deep-sea hydrothermal vents. *Bulletin of the Biological Society of Washington* **6**, 335–343.
Tuttle J, Wirsen C, Jannasch H (1983) Microbial activities in the emitted hydrothermal waters of the Galapagos Rift vents. *Marine Biology* **73**, 293–299.
Ver Eecke HC, Butterfield DA, Huber JA, Lilley MD, Olson EJ, Roe KK, Evans LJ, Merkel AY, Cantin HV, Holden JF (2012) Hydrogen-limited growth of hyperthermophilic methanogens at deep-sea hydrothermal vents. *Proceedings of the National Academy of Sciences, USA* **109**, 13674–13679.
Walker BD, McCarthy MD, Fisher AT, Guilderson TP (2008) Dissolved inorganic carbon isotopic composition of low-temperature axial and ridge-flank hydrothermal fluids of the Juan de Fuca Ridge. *Marine Chemistry* **108**, 123–136.
Wang F, Zhou H, Meng J, Peng X, Jiang L, Sun P, Zhang C, JdV Nostrand, He Z, Wu L, Zhou J, Xiao X (2009) GeoChip-based analysis of metabolic diversity of microbial communities at the Juan de Fuca Ridge hydrothermal vent. *Proceedings of the National Academy of Sciences, USA* **106**, 4840–4845.
Wankel SD, Joye SB, Samarkin VA, Shah SR, Friederich G, Melas-Kyriazi J, Girguis PR (2010) New constraints on methane fluxes and rates of anaerobic methane oxidation in a Gulf of Mexico brine pool via in situ mass spectrometry. *Deep Sea Research Part II: Topical Studies in Oceanography* **57**, 2022–2029.
Wankel SD, Germanovich LN, Lilley MD, Genc G, DiPerna CJ, Bradley AS, Olson EJ, Girguis PR (2011) Influence of subsurface biosphere on geochemical fluxes from diffuse hydrothermal fluids. *Nature Geoscience* **4**, 1–8.
Wirsen C, Tuttle J, Jannasch H (1986) Activities of sulfur-oxidizing bacteria at the 21-degrees-N East Pacific rise vent site. *Marine Biology* **92**, 449–456.
Wirsen C, Jannasch H, Molyneaux S (1993) Chemosynthetic microbial activity at Mid-Atlantic ridge hydrothermal vent sites. *Journal of Geophysical Research* **98**, 9693–9703.
Wirsen CO, Brinkhoff T, Kuever J, Muyzer G, Molyneaux S, Jannasch H (1998) Comparison of a new thiomicrospira strain from the Mid-Atlantic ridge with known hydrothermal vent isolates. *Applied and Environmental Microbiology* **64**, 4057–4059.
Wirsen CO, Sievert SM, Cavanaugh CM, Molyneaux SJ, Ahmad A, Taylor LT, DeLong EF, Taylor CD (2002) Characterization of an autotrophic sulfide-oxidizing marine Arcobacter sp. that produces filamentous sulfur. *Applied and Environmental Microbiology* **68**, 316–325.
Zhou H, Li J, Peng X, Meng J, Wang F, Ai Y (2009) Microbial diversity of a sulfide black smoker in main endeavour hydrothermal vent field, Juan de Fuca Ridge. *The Journal of Microbiology* **47**, 235–247.

SUPPORTING INFORMATION

Additional Supporting Information may be found in the online version of this article:

Plate S1. Chowder Hill

Plate S2. Needles (note red dots are laser sights representing 10 cm distance)

Plate S3. Dead Dog

Table S1. Published rates of carbon fixation from hydrothermal vent chimneys

Table S2. Primers and Conditions for qPCR Functional Gene Analysis.

Table S3. Diversity Metrics describing the communities in the three structures

Table S4. Percentage sequence abundance of 454 libraries by taxa corresponding to Fig. 4

Table S5. pH adjusted estimates of vent fluid CO_2

Chapter 3

Co-registered geochemistry and metatranscriptomics reveal an unexpected distribution of microbial activity within a hydrothermal vent field

(formatted for submission to the Environmental Microbiology journal)

ABSTRACT

Microbial activity at and surrounding diffuse flow hydrothermal vents is not well-understood. Co-registered metatranscriptomic and geochemical data are presented here from a range of fluids throughout ASHES vent field on the Juan de Fuca Ridge. We discuss the implications of *in* situ RNA preservations via the Deep Environmental Sample Processor compared to traditional Niskin sampling. We show that most of the fluids investigated (both diffuse flow and intra-field fluids) were characterized by the activity of seawater-derived Gammaproteobacteria sulfur oxidizers, and that only the most hydrothermally influenced diffuse flow investigated was dominated by the activity of vent-associated Epsilonproteobacteria. We also demonstrate that the intra-field habitat within a vent field between obvious diffuse flows is a high-productivity, and previously overlooked, habitat.

INTRODUCTION

Free-living microorganisms at hydrothermal vents play a fundamental role in supporting highly productive vent ecosystems, and influence local, if not global, geochemistry (Resing *et al.*, 2015). Since the discovery of hydrothermal vents in 1977 (Corliss *et al.*, 1979), scientists have sought to better understand the ecology and physiology of hydrothermal vent microbes, in particular their phylogenetic and functional diversity, their rates of primary production, and their role in supporting associated animal communities, either as free-living microbes upon which animals graze or as symbionts. To date, many of the studies on free-living microbes focused on those associated with the prominent high temperature chimneys, which can be tens of meters in height and their fluid plumes, which can reach hundreds of meters into the water column and spread over

thousands of kilometers (e.g., Klinkhammer and Hudson, 1986; Cowen *et al.*, 1990; Kadko *et al.*, 1995).

However, the less conspicuous lower temperature diffuse vents account for at least half of the total thermal and chemical flux into the overlying ocean from hydrothermal activity (Rona and Trivett, 1992a; Baker *et al.*, 1993; Bemis *et al.*, 1993; Elderfield and Schultz, 1996; Wankel *et al.*, 2011). The extent of diffuse venting underscores their relevance to, and likely influence on, global geochemical cycling. Diffuse flows seem to foster the growth of microbial communities derived from both the overlying seawater (Anderson *et al.*, 2013; Dick *et al.*, 2013) and the subsurface (e.g., Akerman *et al*, 2013; Fortunato and Huber, 2016). The lower temperatures and mix of oxygen-rich seawater with chemically reduced hydrothermal fluid is likely conducive to higher rates of primary productivity than high temperature venting (Olins *et al.*, 2013).

Despite a wealth of research on diffuse vents (Bemis *et al.*, 2012; Campbell *et al.*, 2013; Akerman *et al.*, 2013), several key questions remain. Specifically, little is known about the fate of the fluids that emanate from diffuse vents, and accordingly the phylogenetic and functional changes in the associated microbial communities as they disperse into the overlying water column. It has been suggested that diffuse plumes stay lower in the water column, pushed laterally along the vent field by bottom currents (Rona and Trivett, 1992a; Pruis *et al.*, 2004), but to our knowledge no studies have endeavored to establish this supposition through field-wide geochemical measurements while simultaneously characterizing the associated changes in microbial activity.

The goal of this work was to better understand the distribution of microbial activity and geochemistry throughout a vent field characterized by diffuse flows, and to determine

the relative contributions of vent-derived and seawater-derived microbial communities to diffuse flow microbial activity. To do this we collected samples for geochemical analyses and metatranscriptomic library construction from an extensive survey of fluids within and around diffuse hydrothermal flows at the ASHES vent field in the Axial volcano.

Previous studies of the microbial communities associated with warm diffuse flows at the Axial Volcano vent fields have demonstrated that these habitats are occupied by abundant, active populations of Epsilonproteobacteria and Gammaproteobacteria, all of which may be engaged in chemoautotrophy (Huber *et al.*, 2002; 2003; 2006), (Ver Eecke *et al.*, 2012; Anderson *et al.*, 2013; Meyer *et al.*, 2013; Akerman *et al*, 2013; Fortunato and Huber, 2016). The environmental factors that govern the abundance and activity of these and other microbial taxa, however, remain to be determined. As such, we deployed the Deep Environmental Sample Processor, or D-ESP, which is a state-of-the-art in situ microbial laboratory (Ussler *et al.*, 2013), to collect, filter, and preserve *in situ* fluids from one diffuse flow and one intra-field site. We then used Niskin sampling to collect fluids from five sites spanning three habitat types; diffuse flows (referred to as diffuse throughout), intra-field fluid between vents within the vent field (referred to as intra-field throughout), and non-vent background seawater sampled outside of Axial Caldera (referred to as background seawater throughout). We collected co-registered geochemical analyses with both sampling methods via *in situ* mass spectrometry and shipboard analyses to provide environmental context.

We looked at the resulting metatranscriptomic data through three lenses: 1) A dataset- wide investigation of the most abundant transcripts that enables a broad view of the active community and physiological poise of fluids from different habitat types; 2) a

more targeted analyses of metabolic genes relevant to chemosynthesis and elemental cycling; and 3) differential expression analysis of a subset of D-ESP samples to assess the changes in microbial activity that occur as higher temperature flows cool and mix with seawater. In brief, the data presented here indicate that low temperature diffuse flow vents in a single vent field can have dramatically different profiles of microbial activity dominated by vent-associated Epsilonproteobacteria in addition to the previously described activity profile dominated by Gammaproteobacterial Sulfur Oxidizers (GSOs). Also, these data reveal that the intra-field habitat represents a locally, and likely regionally, important zone of microbial activity that is typically not detected via common geochemical tracers, distinct from that of either seawater or hydrothermal flows, and similar to plumes from high temperature chimneys.

MATERIALS AND METHODS

Study Site

Axial Seamount Hydrothermal Emissions Study (ASHES) vent field (45° 56' N, 130° 31' W; Figure 3.1) contains a diversity of hydrothermal fluid flow types including an abundance of diffuse venting (Butterfield *et al.*, 2004). An area roughly 200 m by 1200 m, ASHES is located adjacent to the western wall of the Axial Volcano caldera along the Juan de Fuca Ridge. Patchy, diffuse venting is common throughout ASHES along the cracks in the seafloor, and discrete venting occurs at isolated sulfide chimneys as well as anhydrite mounds (Rona and Trivett, 1992a).

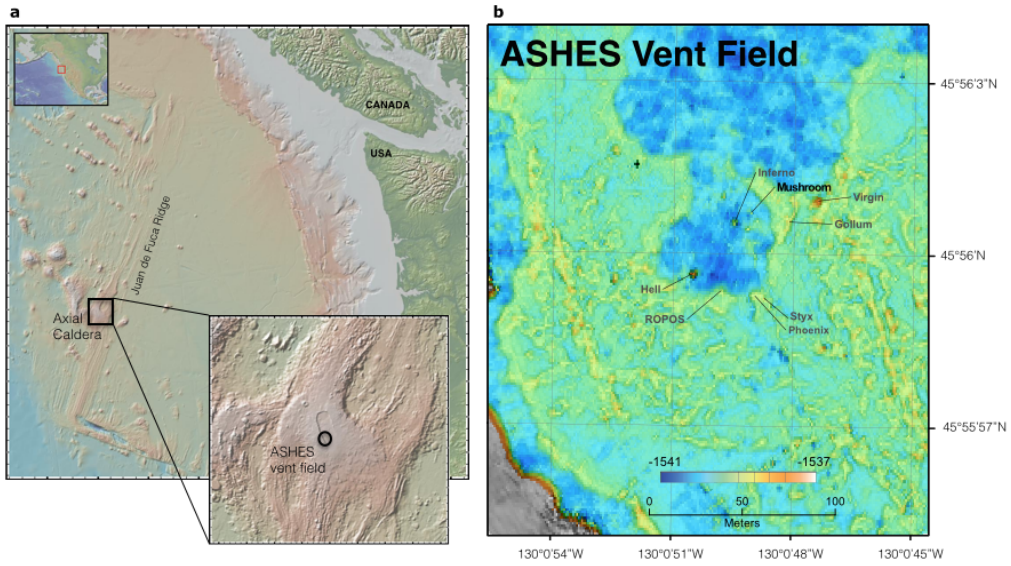

Figure 3.1 Maps of the Juan de Fuca Ridge (a) showing location of Axial Caldera and ASHES vent field, and (b) ASHES vent field showing the location of Mushroom chimney, identifying our study sites.

Sample Collection

Sampling occurred from July 14-21, 2011, aboard the *R/V Western Flyer* using the *ROV Doc Ricketts* (Monterey Bay Aquarium Research Institute). Samples were collected using the Deep Environmental Sample Processor (D-ESP; Ussler *et al.*, 2013) as well as with ROV-mounted Niskin bottles. The D-ESP is a self-contained robotic laboratory that collects and recovers particles from fluid samples *in situ* for molecular microbiological analyses (Ottesen *et al.*, 2011; Pargett *et al.*, 2013). The D-ESP was deployed near a diffuse flow vent at the base of Mushroom chimney, (~45° 56.0011' N, 130° 0.8218' W; Figure 3.1), and was programmed to collect replicate samples repeatedly over a 4 day deployment (see Supplemental Material Table 3.1 for sampling schedule). Samples were collected as in Ussler *et al.* (2013) with the addition of an extendable sampling wand that enabled sampling directly from a diffuse vent. A second sample inlet was located 1 m off the bottom

and approximately 3 m away from the diffuse vent, and was used to sample the intra-field (within vent field between diffuse flows) water (Figure 3.2b; Pargett *et al.*, 2013). The D-ESP pumped 5 L of water from one inlet at a time into a decompression module. 1 L of sample was filtered through stacked 5 and 0.2 μm Durapore filters, and immediately preserved in RNALater (Ambion Inc.). Preserved samples were stored within the D-ESP at ~8° C for 5-14 days before recovery and then stored at -80°C until processing. Additional details about D-ESP operations can be found in Supplemental Materials Methods.

Figure 3.2 (a) Schematic of samples collected for this work at 5 sites (0-4) representing 3 habitat types (seawater, intra-field, and diffuse flow) using 2 sampling methods (Niskin & Deep Environmental Sample Processorl ESP). (b) ESP deployed at sites 1 & 4 showing position of samples collected at Site 1 with Niskin and ESP. (c) ESP sampling wand deployed at Site 4 showing positions of samples collected with Niskin and ESP. (d) Site 2 Niskin samples being collected showing position of intra-field and diffuse samples collected at Site 2.

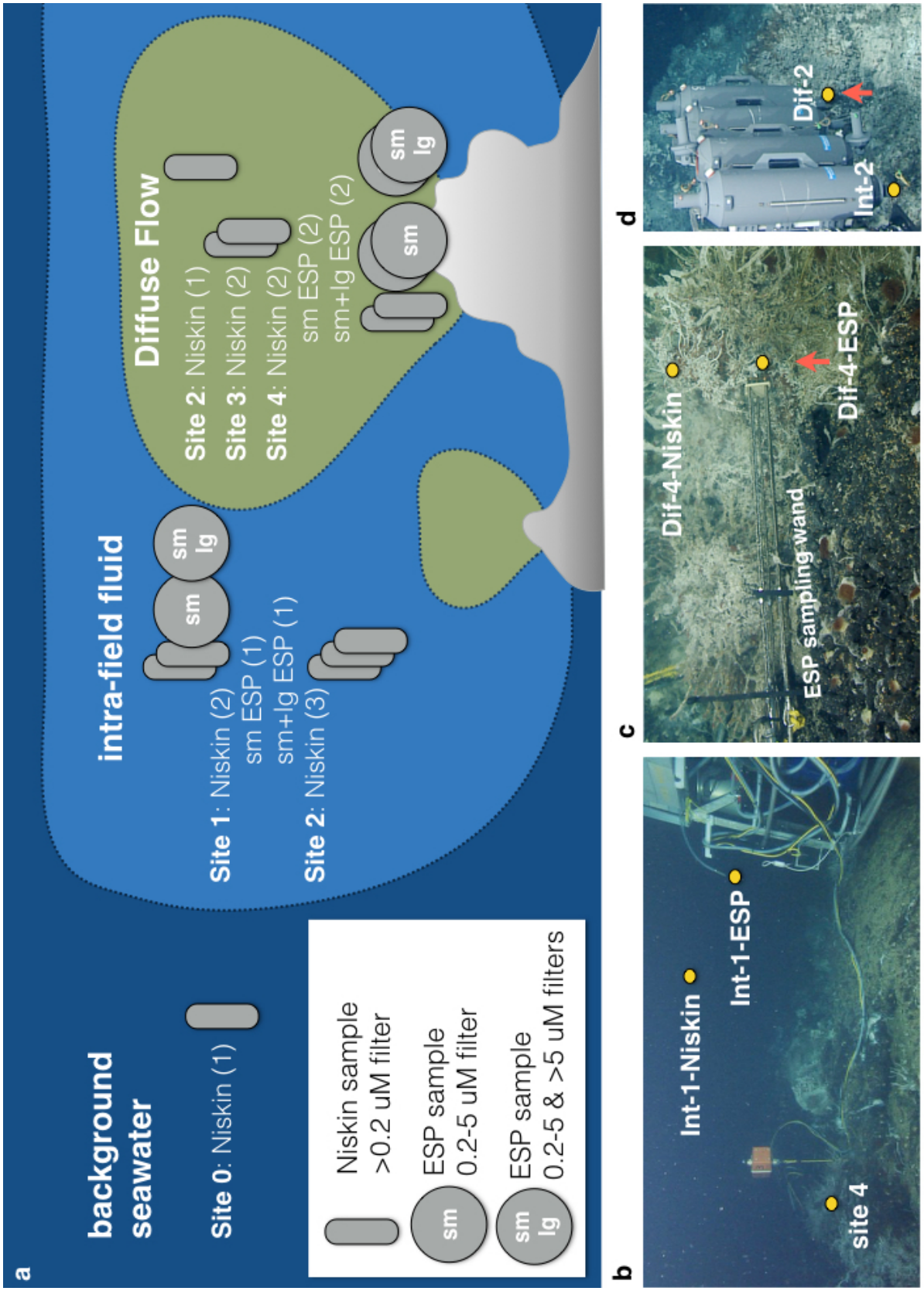

Figure 3.2 continued

Fluids were also collected using 5 L Niskin bottles affixed to a swing-arm on the ROV (Figure 3.2d). The Niskin bottles were positioned over the diffuse flows and samples collected only when shimmering water was clearly seen exiting the top of the bottle. Niskin bottles were also used to collect fluids from near both D-ESP inlets, which enabled direct comparison of D-ESP and Niskin-collected samples. Upon retrieval, water from Niskins was filtered onto 0.2 μm Durapore filters (1 L per filter), rapidly preserved in RNALater™, and stored at −80°C until processed. Time elapsed between Niskin sample collection and ROV retrieval on ship was between 3 and 9 hours. Time to process discrete samples collected by Niskin bottles was 1-2 hours.

In this work "Site X" refers to one of the 5 sampling locales (Sites 0-4) where 1 or multiple samples were collected. A sample refers to a discrete water sample that was collected and filtered either onto a single 0.2 μM filter in the case of Niskin samples or inline 0.2 and 5 μM filters in the case of the D-ESP. Individual metatranscriptomes described herein come from a single filter and therefore represent either a complete sample (for Niskin samples) or a partial sample (for D-ESP samples).

Eleven Niskin and 9 D-ESP filters were analyzed for this study. Because the D-ESP samples were run through two inline filters, six of the D-ESP filters were paired 0.2 and 5 μM filters (representing 3 discrete samples), while the additional 3 D-ESP filters were 0.2-5 μm size fractions (the corresponding 5 μM filter fraction was not sequenced). The Niskin filters, in contrast, represent an entire sample filtered >0.2 μM. See Table 3.1 for more detail. In total, paired microbiological and chemical analyses were completed at five sites (Sites 0-4; see Table 3.1). Site 0 represents background seawater, collected from 3 km outside the Axial volcano caldera approximately 2 m above the seafloor. Sites 1-4 were

within ASHES vent field and represented either diffuse flows (Sites 3 and 4), intra-field waters (Site 1), or a location where both environments were sampled (Site 2). Sites 1 and 4 were located near the base of Mushroom chimney (Figure 3.1) and Sites 2 and 3 were each located approximately 10 m away from Sites 1 and 4.

Table 3.1 Description of samples and filters sequenced

Sample ID	Sampling Method	Site #	Environment Classification	Number of filters sequenced
SW-Niskin	Niskin	0	non vent field background (seawater)	1
Int-1-Niskin	Niskin	1	vent field background (intra-field)	2
Int-1-lg-ESP & Int-1-sm-ESP	D-ESP	1	vent field background (intra-field)	1 >5um (lg) 2 0.2-5um (sm)
Int-2-Niskin	Niskin	2	vent field background (intra-field)	3
Dif-2-Niskin	Niskin	2	diffuse flow	1
Dif-3-Niskin	Niskin	3	diffuse flow	2
Dif-4-Niskin	Niskin	4	diffuse flow	2
Int-4-lg-ESP & Int-4-sm-ESP	D-ESP	4	diffuse flow	2 >5um (lg) 4 0.2-5um (sm)

Geochemical Analyses

A Seabird conductivity, temperature, depth (CTD) sensor in line with the D-ESP measured oxygen, salinity, and temperature throughout the entire deployment. Methane

concentration was quantified in 250 mL subsamples from Niskin bottles immediately upon their retrieval through headspace gas equilibration followed by shipboard gas chromatographic analysis (as in Ussler *et al.*, 2013). 10 mL subsamples from the Niskins were also filtered (through 0.2 μm Durapore filters) for major and minor element analysis acidified in hydrochloric acid, and frozen to -80°C at sea. Total concentration of major and minor elements (including Mg, Mn, Fe, and Si) were quantified using Inductively Coupled Plasma-Atomic Emission Spectrometer (ICP-AES; as in Wheat *et al.*, 2010). 10 mL Niskin subsamples were also preserved for H_2S analyses in 1M $Zn(C_2H_3O_2)_2$, stored at 4°C, and quantified via a colorimetric assay on a Spectramax Plus 384 absorbance microplate reader (Molecular Devices, LLC; Cline, 1969).

Nucleic Acid Extraction

For RNA extraction from both D-ESP and Niskin samples, filters were rinsed with TE buffer to remove RNALater™ (Ambion Inc.), the cells were lysed by incubating filters with Trizol™ (Life Technologies Inc.) for 20 minutes at 25°C then 10 minutes at 85°C. Nucleic acids were separated using 24:1 chloroform:isoamyl alcohol. RNA was precipitated in isopropanol with 100 mg of Glycoblue™ (Ambion Inc.) to improve recovery. RNA was resuspended in RNA Storage buffer (Ambion Inc.). Residual DNA was removed with TurboDNase (Ambion Inc.) per manufacturer's instructions. RNA was quantified with a Qubit 2.0 fluorometer (Life Technologies Inc.) and the RNA high specificity assay (Life Technologies, Inc.).

Metatranscriptomic Sequencing

RNA sample quality control, Illumina TruSeq Stranded mRNA sample preparation (without rRNA removal), and Illumina HiSeq2000 101 cycle paired end sequencing were carried out by the University of Utah Microarray Core Facility (Salt Lake City, UT; see Supplemental Materials methods for details). To constrain the extent of bias between the two lanes used for sequencing, a subset of samples from the first sequencing run were re-run on the second lane. Statistical analyses of taxonomic and functional groups did not show any significant differences between sequencing runs (data not shown).

Global Metatranscriptomic Analyses

Sequence data from all 20 metatranscriptomic libraries were analyzed in MG-RAST (http://metagenomics.anl.gov/) using default quality control parameters at submission with the exception of running Duplicate Read Inferred Sequencing Error Estimation (DRISEE), which is designed to remove artificial duplicate read sequences, but can inadvertently eliminate biologically relevant sequences from illumina data (Eren *et al.*, 2014). For analysis or identified reads, the following parameters were selected: maximum e- value cutoff of 10, minimum percent identity of 80%, and minimum alignment length cutoff of 25. The Non-redundant multisource ribosomal RNA annotation (M5RNA) database was used for taxonomic classifications, and SEED and Subsystem classification were used for functional gene identification. Read abundances for genes of interest were manually curated by searching for variations of gene names and then compiled. Reads were normalized to total identified functional reads for functional analyses and to total predicted rRNA reads (see Supplemental Materials Table 3.2 for values) that were classified at the domain level for taxonomic analyses.

Targeted *de novo* transcriptomic assembly and differential expression analyses

A subset of 6 filters were selected for targeted differential expression analyses between one diffuse and one intra-field site. The selected filters consisted of all D-ESP samples where both the 0.2 and 5 μM filters were extracted and sequenced (1 intra-field Site 1 sample and 2 diffuse Site 4 samples). These samples were selected to minimize variables introduced by different sampling methods and to target the ends of the geochemical spectrum of sites sampled. In total, six metatranscriptomic libraries representing three fluid samples, one from Site 1 (intra-field) and two from Site 4 (diffuse flow) were used in this analysis.

Metatranscriptomic reads were trimmed and adapters were removed using Trimmomatic (Bolger *et al.*, 2014) with the following parameters: -LEADING:3, -TRAILING:3, -SLIDINGWINDOW:4:15, -MINLEN:50. RiboPickr (Schmieder and Edwards, 2011) was used to remove ribosomal rRNA reads prior to assembly of functional transcripts (80% alignment coverage threshold, 90% alignment identity threshold, using the non-redundant ribosomal rRNA database; 4/15/2015 update version).

Metatranscriptomic functional paired reads from all six libraries were assembled *de novo* using Trinity (Grabherr *et al.*, 2011); minimum contig length of 50). Differential expression between Site 1 and Site 4 was calculated using DESeq2 (Love *et al.*, 2014) in R using the trans.counts.matrix file generated in Trinity. Results were filtered by adjusted p-value (>0.05), and for contigs that had 100 or more reads from the Site 1 sample (consisting of the 2 paired filters) or 200 or more reads from the 2 Site 4 samples (from 4 paired filters). The remaining differentially expressed contigs were identified using blastx

(Altschul *et al.*, 1990) on NCBI's nr database (Pruitt, 2005); version updated April 15, 2015) using default parameters.

Transcripts from the resulting list were manually pooled according to replicate functions (i.e., all ribosomal proteins). Log odds ratios were calculated to compare relative over and under expression of this curated transcript list between the two sites.

Statistical analyses

To statistically examine the patterns in microbial gene expression, we posed 5 testable scenarios that could explain patterns in gene expression. Differences could be not significant (null hypothesis) or they could be significant as a function of (1) Site, (2) environment, (3) an outlier single Site (one that is distinct from all the others), (4) sampling method. To test which of these scenarios best explained the variation in our data, we grouped samples accordingly (i.e., by Site – 1-4, by environment – diffuse flow or intra-field seawater, by separating out the most hydrothermally influenced Site – Sites 1-3 vs. Site 4, or by method – Niskin vs. ESP) and performed statistical tests in R (Mann Whitney U or Kruskal-Wallis for 4 or 2 groups respectively). We used p-value = 0.05 for a significance cut-off after correcting for multiple comparisons. Gene categories that were significant after correction with the conservative Bonferroni correction were considered highly significant, while those significant after the less conservative Benjamini-Hochberg test were considered significant. Site 0 (seawater) was not used in statistical analyses because it was represented by a single sample (see Table 3.1 for number of samples in each grouping). These statistical tests were performed on the selected genes of interest as well

as the SEED subsystem categories. See Supplemental Material Table 3.3 (Appendix B) for P-Values.

Cluster analysis (Figure 3.4) was carried out in R on taxomonic IDs with singleton and doubletons removed. The vegdist function in the vegan package was used to calculate Bray-Curtis dissimilarity matrix, and clustering was carried out using the hclust function and the complete linkage method.

RESULTS

Fluid geochemistry

The geochemical samples, including additional samples not used for metatranscriptome sequencing, show a wide range of chemistry among diffuse flows, and only subtle chemical differences between seawater and intra-field fluids (Table 3.2; Supplemental Figure 3.1). Methane concentrations, however, distinguish the seawater from intra-field samples, demonstrating hydrothermal influence throughout the intra-field samples (average of 21.8 nmol/L as opposed to 0.55 nmol/L in seawater, and 668.8 nmol/L in the diffuse flows; Table 3.2). Sulfide (another proxy for hydrothermal influence) was not detected in either seawater or intra-field fluids, and varied from non-detectable to 90.6 µMol in the diffuse flow fluids. The only fluids measured with pH below 7 came from diffuse flows. Similarly, other chemical markers of hydrothermal fluid (increased silica and manganese and decreased magnesium relative to seawater) show clear hydrothermal influence in only some of the diffuse flows analyzed. For all geochemical measurements, diffuse flow samples showed the highest variation. The diffuse flows sampled at Sites 2, 3, and 4 spanned a range of temperatures and higher concentrations of vent-derived reduced

compounds such as methane and sulfide. The seawater (Site 0) and intra-field samples (Sites 1 and 2) differed in their methane and magnesium concentrations, but not in silica, sulfide, manganese concentrations, or pH (Figure 3.3, Table 3.2).

Table 3.2 Geocemical data including samples not sequenced for this work. Mg, Mn, and Si represent total elemental concentration.

Sample Type	Dive	Niskin	Mg mmol/kg	Mn umol/kg	Si umol/kg	pH	H_2S µmol/kg	CH4 nmol/kg
seawater	ESP upcast	ESP upcast	50.6	1.0	120.7	7.2	0	nm
	ESP upcast	ESP upcast	50.9	0.9	119.6	nm	0	nm
	DR-261	Niskin 7	51.4	0.0	97.6	7.5	0	0.5
	DR-261	Niskin 5	51.6	0.0	67.9	nm	0	0.6
	DR-261	Niskin 6	51.5	0.0	86.6	nm	0	0.6
	DR-261	Niskin 8	nm	nm	nm	nm	nm	0.5
		Average	51.2	0.4	98.5	7.4	0	0.5
		St. Err.	0.2	0.2	10.0	0.2	0	0.0
		n	5	5	5	2	5	4
intra-field	DR-258	Niskin 5	50.7	0.2	97.6	7.6	0	29.1
	DR-259	Niskin 5	nm	nm	nm	nm	nm	4.7
	DR-259	Niskin 6	nm	nm	nm	nm	nm	7.3
	DR-259	Niskin 7	nm	nm	nm	7.6	0	26.2
	DR-259	Niskin 8	nm	nm	nm	7.5	0	24.5
	DR-254	Niskin 8	nm	nm	nm	nm	nm	13.0
	DR-252	Niskin 5	nm	nm	nm	nm	nm	9.9
	DR-254	Niskin 5	nm	nm	nm	nm	nm	45.1
	DR-257	Niskin 5	51.2	0.1	92.1	7.6	0	31.7
		Average	50.9	0.1	94.9	7.6	0	21.3
		St. Err.	0.2	0.1	2.8	0.0	0	4.8
		n	2	2	2	4	3	8
diffuse	DR-257	Niskin 7	51.3	0.2	85.5	7.5	0	18.8
	DR-258	Niskin 6	50.1	4.7	252.7	6.6	35.9	1365.5
	DR-258	Niskin 7	50.7	8.7	367.1	6.3	88.5	2499.0
	DR-258	Niskin 8	50.3	2.7	169.1	7.3	10.6	175.3
	DR-254	Niskin 7	nm	nm	nm	nm	nm	118.1
	DR-252	Niskin 6	nm	nm	nm	nm	nm	624.0

Table 3.2 continued

	DR-252	Niskin 7	nm	nm	nm	nm	nm	641.8
diffuse	DR-252	Niskin 8	nm	nm	nm	nm	nm	374.8
	DR-257	Niskin 8	nm	nm	nm	nm	nm	61.1
		Average	50.6	4.1	218.6	6.9	45.0	653.2
		St. Err.	0.3	1.8	60.1	0.3	19.9	270.3
		n	4	4	4	4	4	9
chimney	DR-254	Niskin 6	nm	nm	nm	nm	nm	120.5

Measurements that correspond to the samples that were sequenced (Figure 3.3) show that Site 2 intra-field (Int-2) and diffuse (Dif-2) samples shared similar chemistry and that diffuse samples from Sites 3 and 4 had increasing hydrothermal influence. Among the diffuse flow samples, methane, sulfide, silica, and manganese increase from Site 2 to Site 3 to Site 4, indicating increasing hydrothermal influence in these samples. pH correspondingly decreased among these samples.

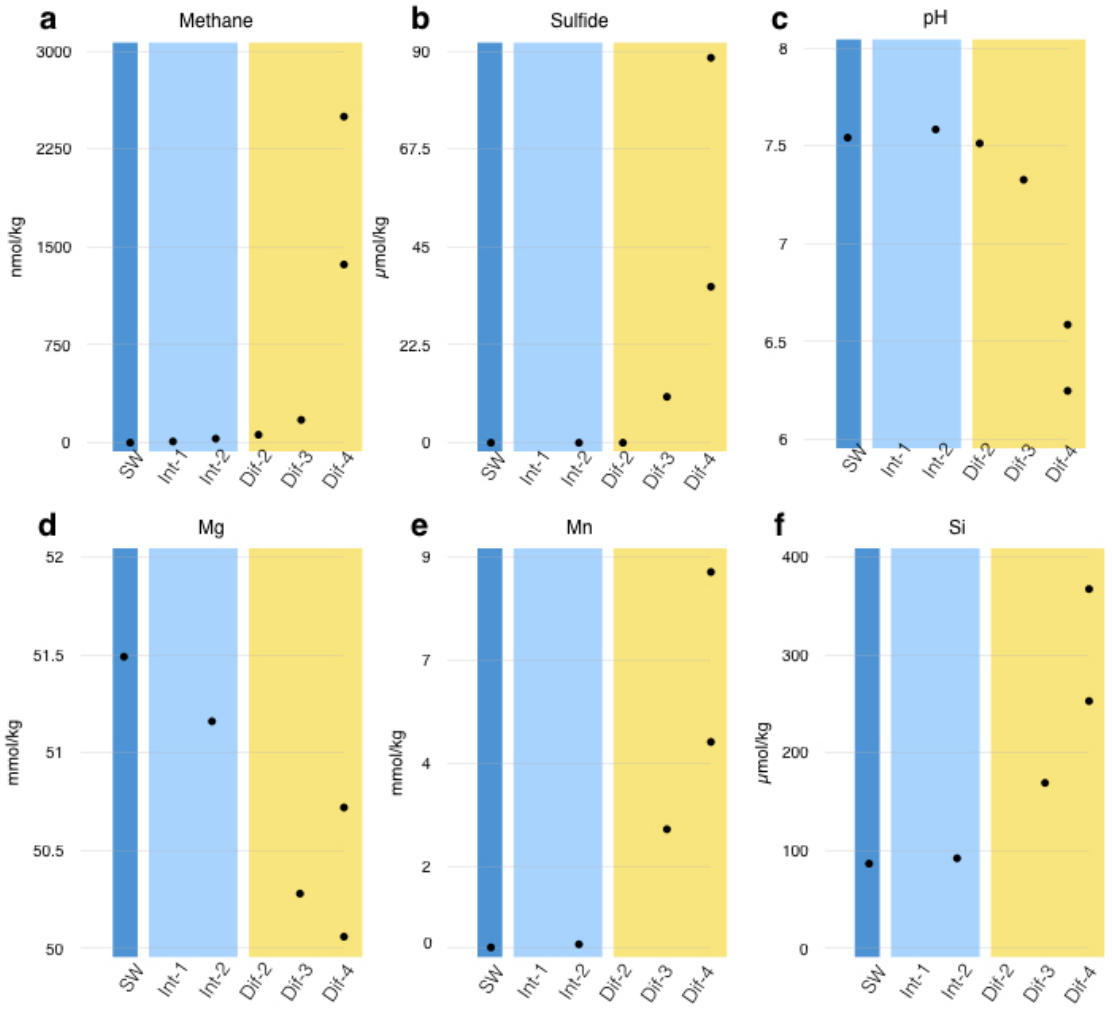

Figure 3.3 Chemical measurements corresponding to sequenced filters (site numbers noted in X-axis). (a) methane, (b) sulfide, (c) pH, (d) magnesium, (e) manganese, and (f) silica measurements are arranged by habitat type; dark blue – seawater (SW), light blue – intra-field (Int), and yellow – diffuse flow (Dif). Note than Mn and Si were not measured at Site 2.

Oxygen and temperature measurements were only available for the ESP samples, and therefore are limited to Site 1, representing the intra-field fluids, and Site 4, the most hydrothermally influenced diffuse flow. However, based on the patterns of the chemical markers measured in both types of samples, and by assuming linear mixing between seawater and vent fluid (as in Baker *et al.*, 1993), we assume that temperature and oxygen concentration of the samples represented solely by Niskin samples (i.e. at Sites 2 and 3)

would fall between those measured at Sites 1 and 4. Oxygen was substantially lower in the Site 4 diffuse flow (0.03 ml L^{-1}) than in the intra-field water at Site 1 (0.96 ml L^{-1}). The temperature was substantially higher at the Site 4 diffuse flow (34.2°C) than the intra-field water at Site 1 (2.5°C).

Composition of the Active Microbial Community

Diversity analyses

Community composition, based on taxonomic assignments of metatranscriptomic data, was similar among replicate samples (Supplemental Figure 3.2). Cluster analysis showed that the samples grouped into 3 main groups based on similarity; the seawater sample, all samples from Site 4, and the remaining samples from Sites 1-3 (Figure 3.4).

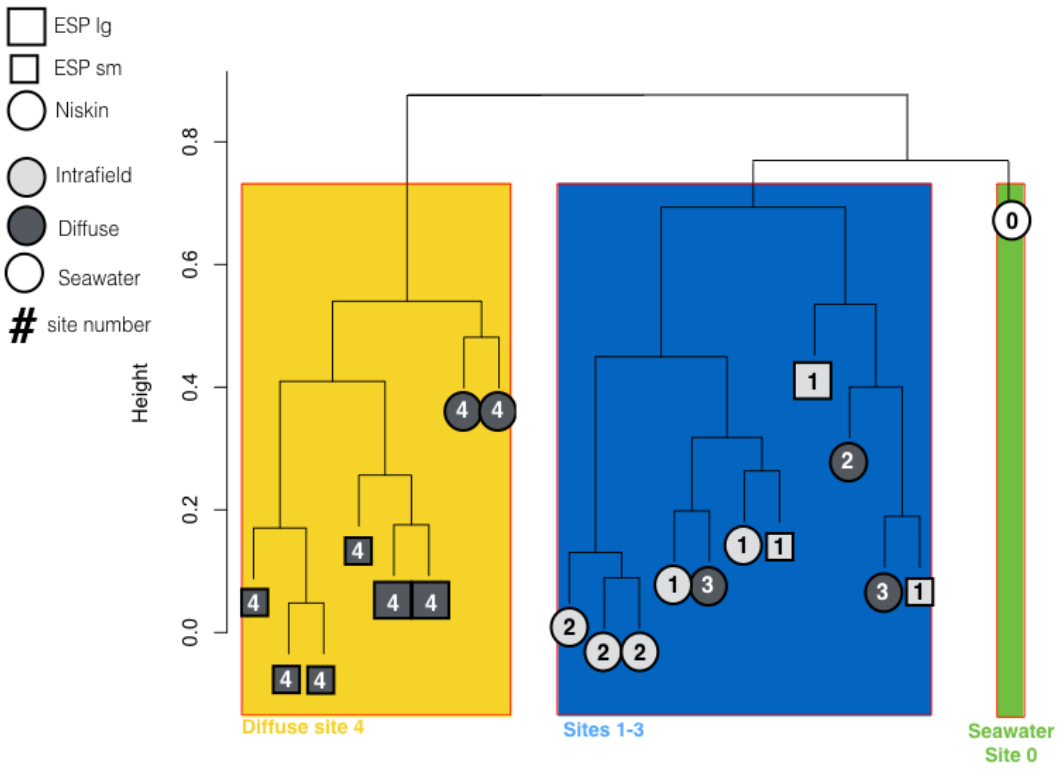

Figure 3.4 Cluster diagram generated with Complete Linkage method showing similarity of metatranscriptomes based on identified rRNA reads not including singleton or doubleton reads. Major groupings show seawater, Site 4 diffuse flows, and Sites 1-3 samples as distinct.

Simpson's diversity was not significantly different between seawater and Sites 1-3, but diversity was substantially lower in Site 4 (Figure 3.5a). Niskin samples had, on average, higher diversity than ESP samples, but this difference was not statistically significant (Figure 3.5b). When samples were compared by environment type (i.e., diffuse vs. intra-field), they did not show nearly as obvious differences in diversity as alternately grouping Sites 1-3 for comparison with Site 4 (Figure 3.5c&d), even though Sites 1-3 contained samples from both intra-field and diffuse vent locations.

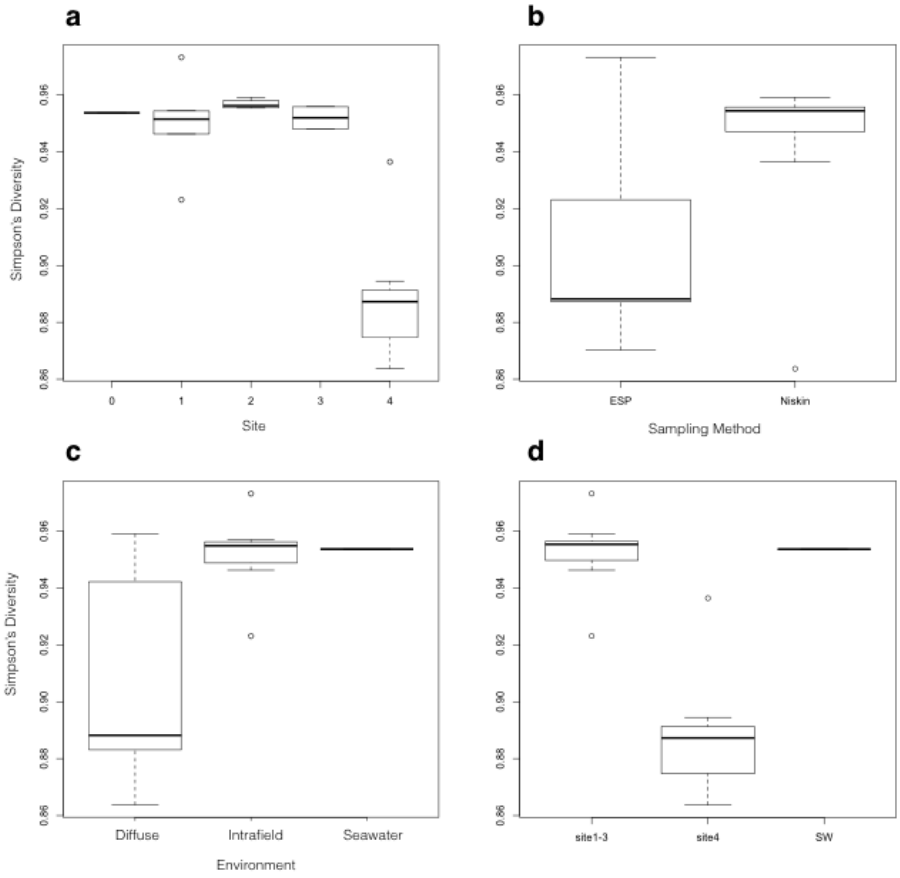

Figure 3.5 Box and whisker plots showing Simpson's Diversity of the 20 metatranscriptomes grouped by (a) site, (b) sampling method, (c) environment or habitat type, and (d) cluster analysis grouping (distinct groups shown in Figure 3.4).

Broad Taxonomic Description

The identified rRNA from all samples was dominated by bacterial sequences (Figure 3.6a), which represented 56-96% of a given sample's identified rRNA reads. Individual replicate filters were similar, and so we present the averages of all replicates of the same filter type (e.g., all 0.2-5 μm ESP filters from Site 4) in these figures. Archaea represented 0.007-0.6% of rRNA reads in all vent field samples, and were least abundant at Site 4 (with the exception of a single filter). Archaea were most abundant in the seawater sample (1.7% of rRNA reads; Figure 3.6a). Eukaryotic transcripts represented 1-7% of transcripts in all

samples with one exception (the >5 μm ESP Site 1 intra-field sample contained 40% Eukaryote rRNA where the most abundant Eukaryote sequences came from Fungi).

Bacterial communities were dominated by Proteobacteria, which represented 76-86% of all bacterial rRNA sequences (Figure 3.6b). Reads assigned to Bacteroidetes, Firmicutes, and Actinobacteria were the next most abundant bacterial phyla (Figure 3.6b). Bacteroidetes affiliated reads represented 2-4% of rRNA reads in most samples, with ESP samples from Site 4 containing 0.3-0.5%. Reads assigned to Firmicutes and Actinobacteria both were most abundant in the seawater sample (1 and 1.5% respectively), and less abundant in all vent field samples (less than 1%). Additionally, ESP Site 4 samples contained the lowest relative abundances of Actinobacteria and Firmicutes rRNA reads. Unclassified bacterial rRNA reads were least abundant in the seawater sample (9.5%), most abundant in Site 4 (17-22%). Sites 1-3 contained 11-18% unclassified bacterial rRNA sequences (Figure 3.6b).

Gammaproteobacteria

Gammaproteobacteria dominated the rRNA transcripts from all samples except those collected from Site 4 (Figure 3.6c). They represented 88% of proteobacterial rRNA reads from seawater, 48-89% from Sites 1-3, and 2-35% from Site 4 with all ESP Site 4 samples having 5% or less (Figure 3.6c). The most abundant Gammaproteobacteria rRNA reads in the seawater sample were from the genera *Idomarina*, *Alteromonadales*, *Marinobacter*, and *Pseudoalteromonas* (Figure 3.6d). In contrast, the most highly represented Gammaproteobacteria in the rRNA reads from Sites 1-3 were closely aligned to the symbionts of vent animals or to SUP05 chemoautotrophs (Figure 3.6e).

Epsilonproteobacteria

The transcriptomic libraries from the most hydrothermally influenced diffuse flow revealed an active, autotrophic community dominated by vent-associated Epsilonproteobacteria such as *Sulfurovum* and *Sulfurimonas*. Epsilonproteobacteria dominated all Site 4 samples (58-95% of proteobacteria; Figure 3.6c). The seawater sample had the lowest representation at 1% Epsilonproteobacterial rRNA, while Site 4 ESP samples were all above 90%. Proteobacterial rRNA from Sites 1-3 were 5-22% Epsilonproteobacteria. The most highly represented taxa within this class were from the genera *Arcobacter*, *Nitratiruptor*, *Sulfurimonas*, *Sulfurovum*, and *Campylobacteriales* (Figure 3.6f). These are all taxa known to be vent associated and typically found in warmer, less oxic vent environments (Huber *et al.*, 2010; Yamamoto and Takai, 2011; Wright *et al.*, 2012; Meyer *et al.*, 2013; Anderson *et al.*, 2013; Akerman *et al*, 2013).

Other Proteobacteria

Representation of Betaproteobacteria in rRNA reads varied among samples (Figure 3.6c). Proteobacteria communities from seawater and Site 4 were less than 2% Betaproteobacteria, while those from Sites 1-3 were 2-15% with one striking exception of Dif-2-Niskin at 34%. Alphaproteobacteria expression was less variable with Sites (Figure 3.6c). In samples from Sites 0-3, the proteobacteria rRNA reads were 1-12% Alphaproteobacteria, with all but one ESP sample above 3%. At Site 4, Alphaproteobacteria values ranged from 0.3-2%. Deltaproteobacteria expression was still more consistant, with no sample having greater than 2% of proteobacteria rRNA reads represented by

Deltaproteobacteria and all ESP Site 4 samples having 0.2-0.6% (Figure 3.6c). Similarly, Zetaproteobacteria expression was consistant with only a single sample containing more than 1% of proteobacterial rRNA reads (at ESP Site 1, 1.3%; Figure 3.6c). Unclassified proteobacteria represented 0.2-0.6% of proteobacterial rRNA reads at Sites 0-3, and 1-9% at Site 4 (Figure 3.6c).

Figure 3.6 Taxonomic identification of rRNA reads, averaged by sample type. (a) Domain-level distribution of all rRNA identifications, (b) phylum-level distribution of bacterial reads, and (c) class-level identification of proteobacterial reads. 10 most abundant genus-level identifications from (d) seawater, (e) Sites 1-3, and (f) Site 4.

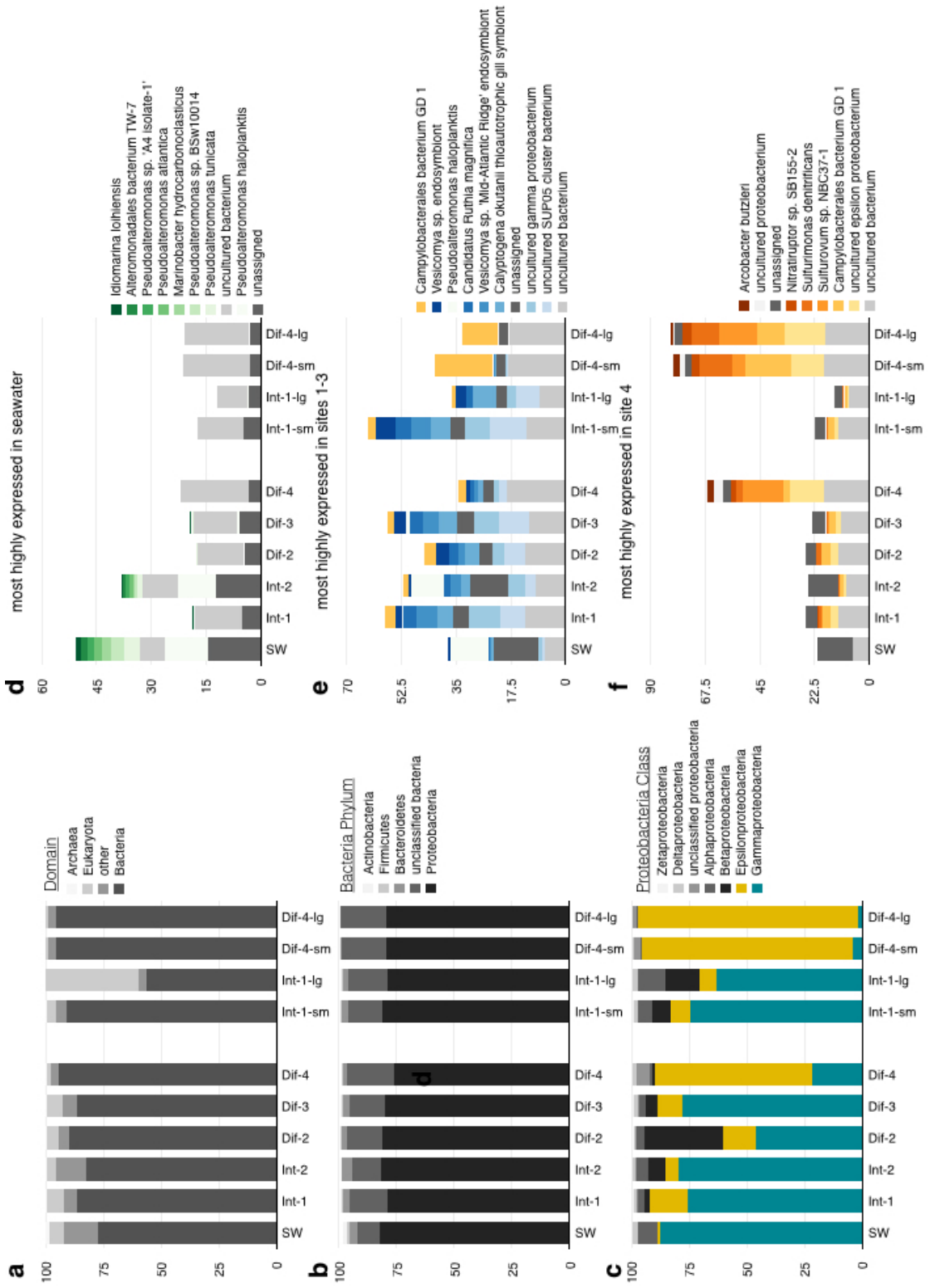

Figure 3.6 continued

Dataset-wide Microbial Activity

Subsystem Overview

Hierarchical SEED Subsystem functional gene classification showed that all samples had a fairly similar broadly categorized (Subsystem Level 1) profile of transcriptional activity. Most highly expressed categories are shows in Figure 3.7a. There were notable differences, however, in categories of elemental metabolism (Figure 3.7b). Some L1 subsystem categories did show statistically significant differences in expression between Sites 1-3 and Site 4 (Figure 3.7c). The following L1 subsystems were more highly expressed in Sites 1-3 than Site 4; metabolism of aromatic compounds; P metabolism; membrane transport; stress response; and carbohydrates. In contrast, the following L1 subsystems were more highly expressed in Site 4: secondary metabolism; nucleosides and nucleotides; N Metabolism; and cofactors, vitamins, prosthetic groups & pigments.

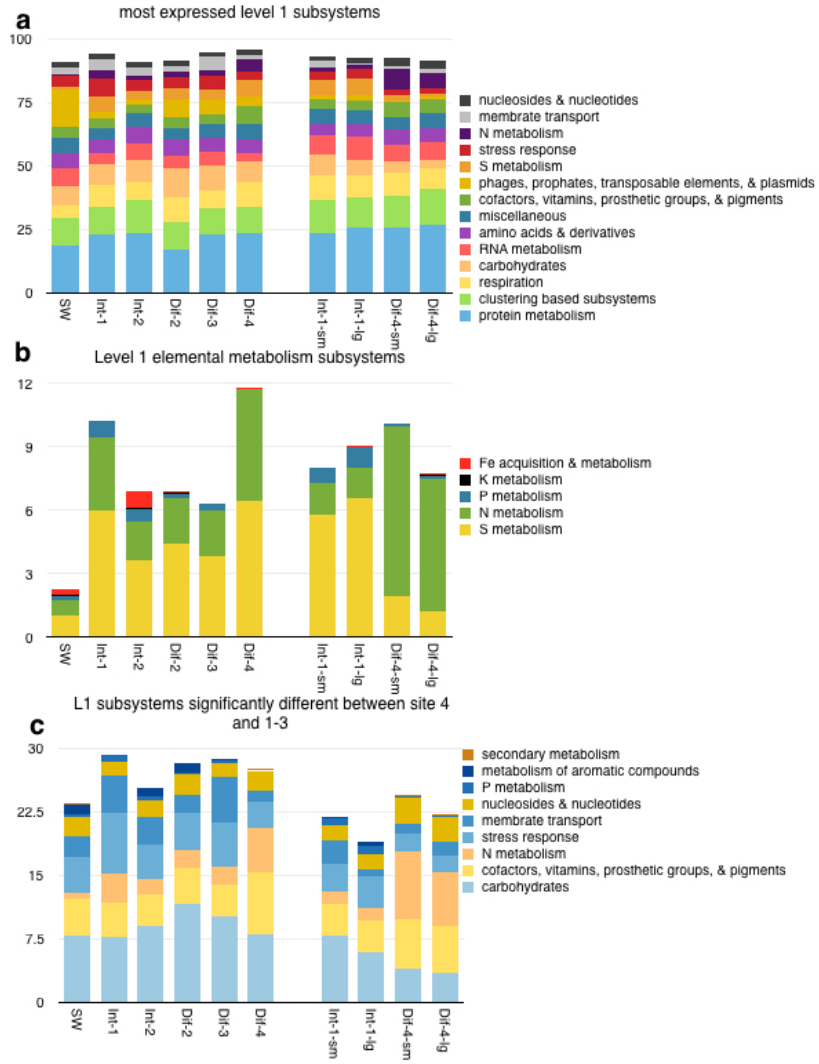

Figure 3.7 (a) Distribution of functional reads assigned to the most highly expressed Level 1 SEED subsystems. (b) Distribution of functional reads assigned to Level 1 subsystems specific to elemental metabolism. (c) Distribution of functional reads of Level 1 subsystems that showed significantly different expression between Sites 1-3 and Site 4. See Supplemental Table 3.3 for P-Values.

Expression of Selected Functional Genes

In addition to the most highly expressed transcripts, we were interested in the expression certain genes related to chemosynthetic metabolisms and related to elemental cycling of carbon, nitrogen, sulfur, and iron, and hydrogen. These genes did not necessarily

show up in the dataset-wide analyses of most highly expressed genes due to lower levels of transcription.

First and foremost we were interested in genes associated with carbon cycling (Figure 3.8a), which were expressed in all samples. The relative expression of genes allied to different carbon fixation pathways varied among the samples. Total RuBisCO expression, indicative of the Calvin Benson Bassham (CBB) cycle, was highest at Site 2 and lowest at Site 4. ATP citrate lyase, indicative of the reductive Tricarboxylic Acid (rTCA) Cycle, was most highly expressed at Site 4. Cumulatively, these carbon fixation genes were least highly expressed in the seawater sample. Both of these genes showed statistically significant differences in expression between Site 4 and Sites 1-3 (see Supplemental Materials Table 3.3 for P-Values).

Methanogenesis is another metabolic process at vents that is related to carbon cycling. Relative expression of methyl-coenzyme M reducatase (mcr; a diagnostic gene for the process of methanogenesis), was highest in Site 1 Niskin samples and Site 4 ESP samples (Figure 3.8a). However, the differences in mcr expression by sample type were not statistically significant.

Sulfur metabolism genes were also expressed in all samples, but were least expressed in the seawater sample and Site 4 ESP samples (Figure 3.8b). Sulfur oxidation (all identified sox genes, including soxABCXYZ), dissimilatory sulfite reductase (all dsr genes including dsrMKOP; transcripts identified as assimilatory sulfite reductase are not included in Figure 3.8), and adenylylsulfate reductase (including aprAB) all showed significantly higher expression in Sites 1-3 than Site 4. Sulfide-quinone reductase (*sqr*) was most highly expressed in Site 4 Niskin samples, but these differences were not statistically

significant. Ferric iron transporters showed significantly more expression in Sites 1-3 than Site 4 (Figure 3.8e). Genes related to ferrous iron, on the other hand, showed higher expression in Site 4, but the difference was not statistically significant. The relative expression of genes used to oxidize hydrogen (i.e., hydrogenases) was also significantly higher in Sites 1-3 than Site 4 (Figure 3.8g).

The expression of genes involved in denitrification was highest in the Site 4 samples (Figure 3.8b). Nitrate and nitrite reductases were expressed in all samples, were predominantly dissimilatory (Supplemental Figures 3.3 & 3.4), and had statistically significant differences in expression between Sites 1-3 and Site 4. Nitrate reductases were more highly expressed in Site 4, while nitrite reductases were more highly expressed in Sites 1-3. However, overall nitrate reductases were expressed far more highly than nitrite reductases. Nitric oxide reductases followed a similar pattern as nitrate reductases, but nitrous oxide reductases showed very little expression overall (data not shown). Ammonia monooxygenases showed a pattern opposite that of nitrate reductases, being both highly expressed and significantly more expressed in Sites 1-3 than Site 4.

Figure 3.8 Expression of selected functional genes across the whole dataset related to (a) carbon fixation, (b) nitrogen metabolisms, (c) methanogenesis, (d) sulfur oxidation, (e) other sulfur metabolisms, (f) iron, and (g) hydrogen. Of these genes, only ammonia monooxygenase showed statistically significant difference in expression between sampling methods (higher expression in Niskin samples). Genes shown in blue showed statistically significantly more expression in Sites 1-4, while those in yellow were statistically significantly more expressed in Site 4 samples.

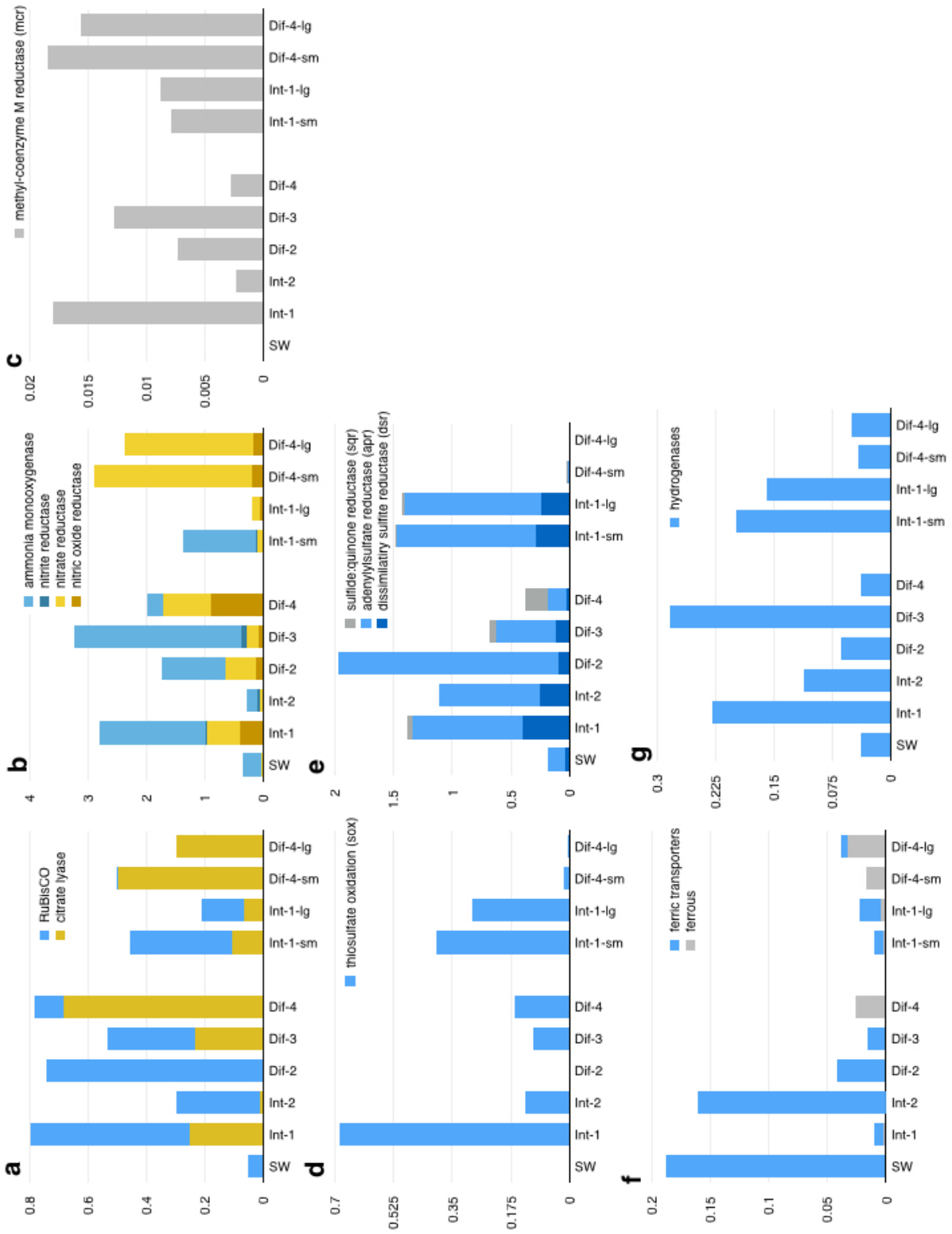

Figure 3.8 continued

Sampling Method Comparison

While the two methods used in this work did not collect truly comparable samples at Site 4 (the ESP sampled from within a tubeworm clump while Niskin bottles sampled just above), we were interested in how community composition and expression activity varied between them. Certain level 1 subsystems showed statistically significant differences in expression between the two sampling methods (Figure 3.9). Two categories (Carbohydrates and Stress Response) were more highly expressed in Niskin samples than D-ESP samples. The Carbohydrates category was dominated by expression of genes related to the Glyoxylate bypass, the TCA Cycle, the Calvin-Benson Cycle, and the Pentose Phosphate Pathway among others. The Stress Response category was dominated by expression of genes related to heat shock, cold shock, oxidative stress, and redox-dependent regulation of nucleus processes. RNA metabolism (a category that was dominated by expression of DNA-directed RNA polymerase) was expressed more highly in D-ESP samples. The final L1 subsystem that was showed significant difference of expression between sampling methods was Fatty Acids, Lipids, and Isoprenoids (Figure 3.9d).

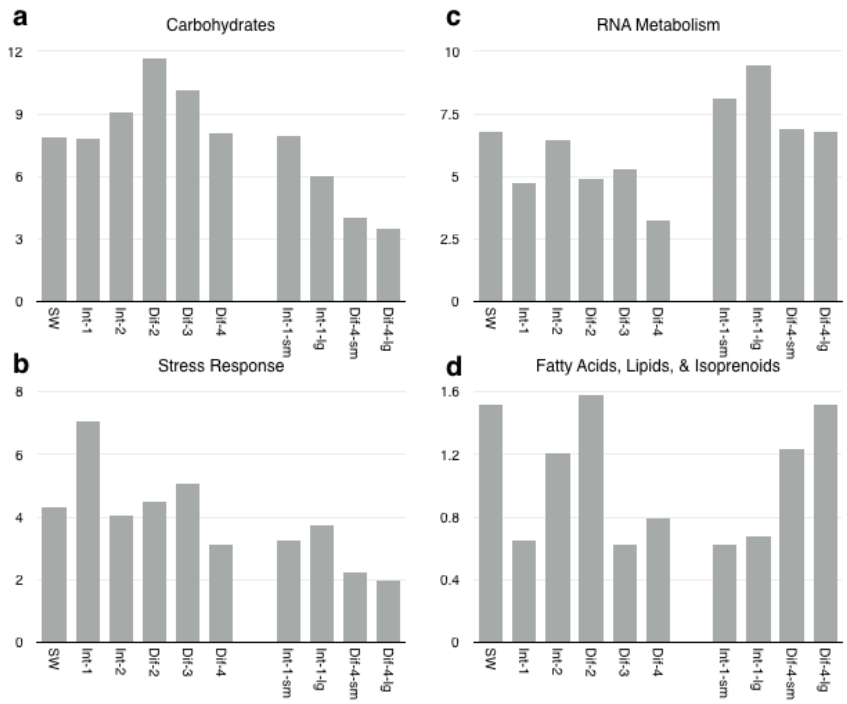

Figure 3.9 Level 1 SEED subsystems with expression that showed statistically significant difference in expression between sampling methods (Niskin vs. D-ESP) were (a) Carbohydrates, (b) Stress Response, (c) RNA Metabolism, and (d) Fatty Acids, Lipids, and Isoprenoids.

Despite significant differences between the sampling methods overall, both methods showed the same pattern of expression differences between Sites 1-3 and Site 4 in the RNA Metabolism and Stress Response categories. In both of these cases Site 4 showed lower expression than Sites 1-3. In contrast, the carbohydrates and fatty acids, lipids, and isoprenoids did not show a consistent pattern between Sites 1-3 and Site 4.

Of the selected functional genes described in the previous section, the only one to have statistically significant difference in expression between the sampling methods was ammonia monooxygenase (Figure 3.8b). Ammonia monooxygenases were more highly expressed in Niskin samples than D-ESP samples, but both sampling methods showed higher expression in Sites 1-3 than Site 4. Of the taxonomic groupings, the only taxa to have

statistically significant differences in representation between sampling methods was Gammaproteobacteria (Figure 3.6c). Like ammonia monooxygenase, Gammaproteobacteria reads were more abundant in the Niskin samples, but both sampling methods showed higher abundance in Sites 1-3 than Site 4.

Differential Expression Analysis of ESP Samples

Differential expression analysis on selected samples (the 3 ESP samples with Paired 0.2-5 and >5 μM size fragments, one from Site 1 and two from Site 4) highlighted transcripts that were differentially expressed between samples collected *in situ* by the ESP at Site 1 (intra-field) and Site 4 (the most hydrothermally influenced diffuse flow). FigFF shows the most abundant differentially expressed transcripts, plotting relative abundance and log odds ratio of those where average Site 1 and Site 4 relative abundance sum to greater than 0.5%. A putative senescence associated protein, adenylylsulfate reductase (aprA), and particulate methane monooxygenase are among those transcripts most over-expressed in ESP Site 1 samples, whereas thiosulfate reductase, flagellin and flagellar proteins, nitrate and nitrite reductases, and hydrolase are among the most over-expressed in ESP Site 4 samples.

Figure 3.10 Differential expression analysis of D-ESP samples with sequenced filters of both 0.2-5 μM and >5 μM. Shown here are functional assignments with the hightest log odds ratio or without log odds ratio due to expression in only the D-ESP wand (Site 4) or elevator (Site 1) samples. Log odds ratio between the two sites is shown in grey. Yellow and Blue bars represent Site 4 (wand) and Site 1 (elevator) expression, respectively.

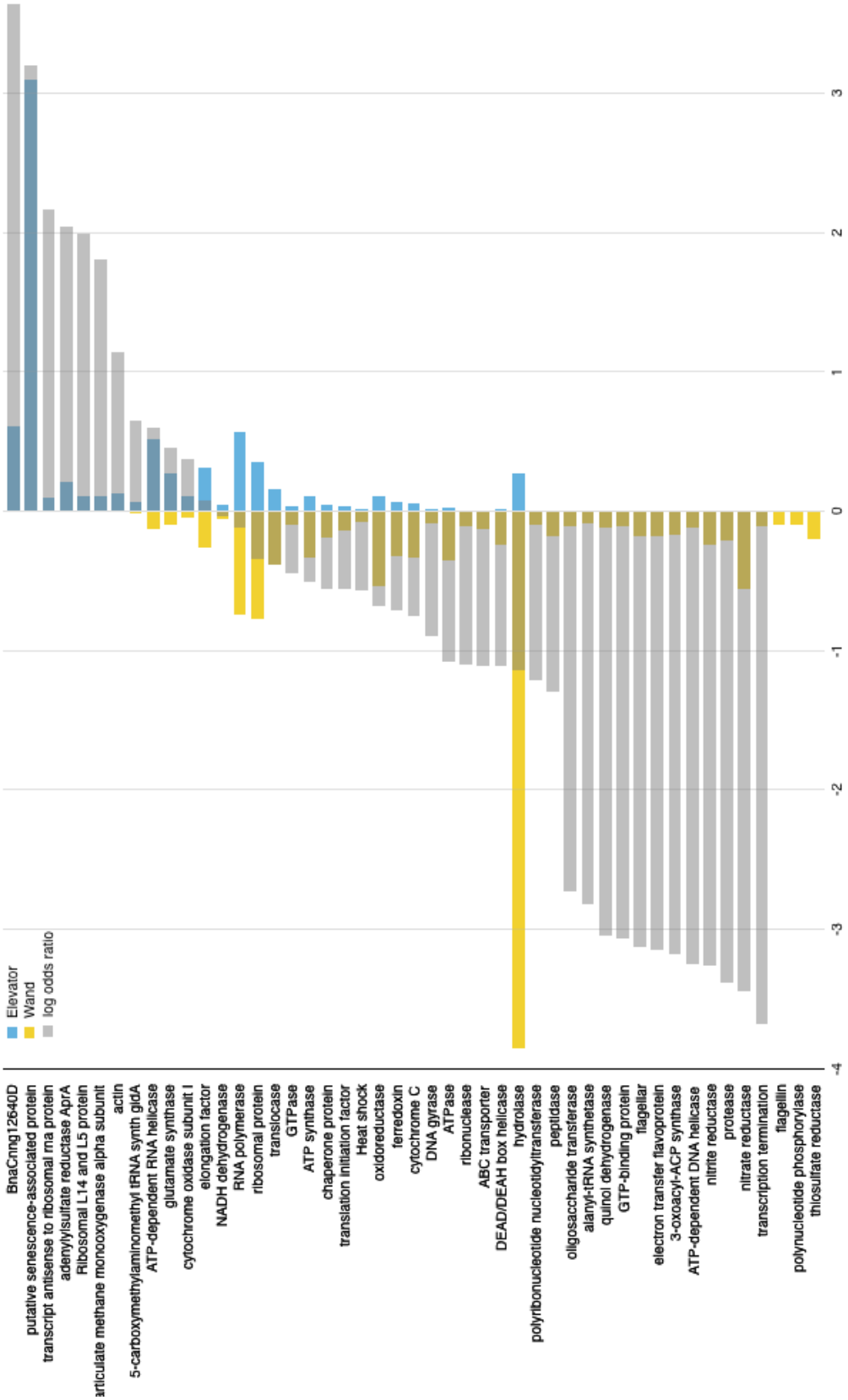

Figure 3.10 continued

DISCUSSION

Our data reveal that hydrothermal influence on microbial processes may be more widespread than currently assumed. This influence extends outside of the high temperature fluids and plumes, and likely beyond diffuse flows, into and throughout the intra-field habitat, potentially encompassing entire vent fields. Specifically, via our analyses we found two distinct profiles of microbial activity within the vent field, both likely relying on the oxidation of sulfur compounds for energy. In one, the more active members of the community appear to be derived from the bottom seawater, and another the most active members of the community appear to be vent-derived. Further, we found that most, but not all, of the microbial activity in the samples collected throughout ASHES vent field were dominated by microbes most closely related to known seawater-derived Gammaproteobacterial sulfur oxidizers (GSOs). Only the most hydrothermally influenced diffuse vent we sampled was instead dominated by vent-derived Epsilonproteobacteria. Additionally we found that the seawater among these diffuse vents, the intra-field waters, was nearly indistinguishable from most diffuse flows.

To date, the work that has been done in low temperature, hydrothermally-influenced environments has focused largely on understanding the diversity and distribution of microbial taxa (Huber *et al.*, 2002; Opatkiewicz *et al.*, 2009; Meyer *et al.*, 2013; Anderson *et al.*, 2013; Perner *et al.*, 2013b; Campbell *et al.*, 2013). Other studies have focused on physiological capacities of target genotypes (e.g., the Epsilonproteobacteria in (Akerman *et al.*, 2013), H_2 oxidizers in (Perner *et al.*, 2010), or denitrifying bacteria in (Bourbonnais *et al.*, 2012). However, the extent to which both seawater and vent-derived microbes are active in these regions, as well as the extent to which geochemistry directly

influences or determines microbial processes, remain poorly constrained. It has also been shown that community composition (as determined by metagenomics or 16S rDNA sequencing) is not an especially robust indicator of activity. Specifically, striking differences were found in the relative representation of Gamma- and Epsilonproteobacteria sequences recovered in DNA and RNA libraries constructed from ASHES diffuse flow fluids (Akerman *et al*., 2013). Our finding that the intra-field seawater among these diffuse vents was nearly indistinguishable, in terms of microbial activity, from most diffuse flows is of fundamental importance for any modeling efforts (discussed in Huber and Holden, 2008) or for predicting global influence of hydrothermal vent microbial metabolism on geochemistry.

Influence of geochemistry on the active microbial communities

In order to compare patterns of geochemistry and gene expression, we sampled three geochemically distinct habitats; non-vent seawater; intra-field fluid; and diffuse flow. All of the vent field microbial communities sampled here, both from diffuse flows or in intra-field fluid, were functionally distinct from our background seawater sample (Figure 3.8), indicating that the influence of diffuse hydrothermal venting extends beyond the obvious flows and potentially across the whole vent field. This is, however, despite the fact that most geochemical parameters measured (sulfide, pH, total Mn, & total Si concentrations) did not vary between intra-field and diffuse fluid sample types, instead intra-field and seawater appeared more geochemically similar. While methane concentrations were higher in the intra-field than is typically found in background seawater (commonly single digit nM), and may explain some of the differences observed in

gene expression, it seems quite unlikely that methane availability alone is the primary factor driving the drastic differences observed in the community composition and activity. Collectively these data reveal that the intra-field fluid habitat is more similar to the non-buoyant plumes typically associated with focused, higher temperature chimneys than it is to the surrounding seawater.

It is often assumed that microbial activity is controlled by local geochemistry, and there are well-documented correlations between chemistry and community composition (e.g., Nakagawa *et al.*, 2005; Huber *et al.*, 2006; Flores *et al.*, 2011; Anderson *et al.*, 2013; Akerman *et al.*, 2013; Anantharaman *et al.*, 2015). Our data, however, paint a picture that is more complicated than a direct relationship between chemistry and microbial activity, indicating that much of vent microbial activity is not solely determined by the geochemical parameters measured here. The active communities from diffuse flow Site 4 were distinct from those of diffuse flows at Sites 1-3 (Figure 3.4). This is despite the fact that Site 2 and 3 were also diffuse flows, and that Site 3 had detectable sulfide and elevated methane concentrations.

Two distinct active vent field communities imply ecological niches that cross-cut canonical habitat boundaries

The active community at Site 4 was dominated by Epsilonproteobacteria, which are associated with hydrothermal vent diffuse flows (Nakagawa *et al.*, 2005; Huber *et al.*, 2007; Meyer *et al.*, 2013; Anderson *et al.*, 2013; Akerman *et al.*, 2013). At the cooler diffuse Sites 2 and 3, where we might have predicted a proportional contribution of transcripts from canoncially vent-associated microbes, fluids were dominated by marine

Gammaproteobacterial sulfur oxidizers (SUP05) commonly associated with hydrothermal buoyant plumes (Mattes *et al.*, 2013) and anoxic waters (Wright *et al.*, 2012). These organisms are typically found in low abundances in deep seawater, but are thought to become active in hydrothermal plumes (Sunamura *et al.*, 2004; Dick and Tebo, 2010; Lesniewski *et al.*, 2012; Anderson *et al.*, 2013; Sheik *et al.*, 2015; Anantharaman *et al.*, 2015). Moreover, these diffuse flow communities were significantly more similar to those found at intra-field Sites 1 and 2, despite the differences in geochemistry (for P-Values see Supplemental Material Table 3.3). The active microbial communities at Sites 1-3 (both diffuse and intra-field samples) were, therefore, dominated by SUP05-like Gammaproteobacteria described above. This is similar to the community identified in a post-eruption "Snowblower" vent sampled shortly after our samples were collected (Meyer *et al.*, 2013).

Rather than the canonical view of different environments (e.g., chimney, diffuse flow, plume, background seawater) being dominated by distinct microbial communities, we posit that microbial ecological niches (defined here as regions that host microbial communities of similar activity) cross the apparent "geochemical boundaries" associated with these different environments. These realized niches are represented as markedly different communities engaged in distinct metabolisms (see activity section below). The activity profile seen at Sites 1-3 spanned both diffuse flows and intra-field water, while that of Site 4 was limited to the most hydrothermally influenced diffuse flow.

However, our Site 4 Epsilonproteobacteria-dominated diffuse flow appears to have less hydrothermal influence than other ASHES diffuse flows that have been shown to host more canonically vent-like activity profiles. One such vent had a Gammaproteobacteria-

dominated activity profiles (Akerman *et al.*, 2013), and a recently published metatranscriptome of a diffuse flow at Marker 113 within the Axial caldera outside the ASHES vent field had a diverse expression profile characterized by substantial expression of Alphaproteobacteria, and *Methanococcus*, in addition to Epsilonproteobacteria (Fortunato and Huber, 2016). This implies that factors other than geochemistry (such as fluid dynamics or biological interactions) may explain why Site 4 was dominated by vent Epsilonproteobacteria. In essence, these distributions imply that the active microbial community does not, as one might predict from thermodynamic models, directly mirror geochemistry. It has previously been demonstrated that vents in close proximity can host significantly different communities despite geochemical similarities (e.g., Opatkiewicz *et al.*, 2009; Perner *et al.*, 2013a; Perner *et al.*, 2013b; Sheik *et al.*, 2015). It is important to note, however that we cannot rule out all geochemical factors as determinants of community activity, as microbial energy metabolism in plumes may be determined in part by plume chemistry, such as sulfur availability (Anantharaman *et al.*, 2015).

One possible explanation is that oxygen concentration is responsible for this difference in overall activity. Fortunato and Huber (2016) characterized an *in situ* preserved active community from a diffuse flow vent at a different vent (Marker 113) within Axial caldera, and interestingly showed a strikingly different active community far less dominated by either Gamma- or Epsilonproteobacteria than our diffuse flow metatranscriptomes. While oxygen was not quantified in their work, oxygen concentration could explain this difference if we assume temperature is a proxy for oxygen concentration, because our Site 4 was 34.2°C whereas the Marker 113 metatranscriptome was 24.1°C. However, it is impossible to rule out the effect of temperature itself some other aspect of

geochemistry (despite lower temperature, Marker 113 had concentrations of methane, hydrogen sulfide, magnesium, and silica that indicate it had a greater hydrothermal influence than our Site 4 flow). Additionally, non-geochemical factors such as spatial variation between vent fields (Butterfield and Merle, 2007), or simply the substantial heterogeneity inherent in microbial activity are also likely to influence community activity. Further research is needed to determine the relative influence of these factors.

Functional gene expression patterns at Sites 1-3: a ubiquitous seawater-derived Gammaproteobacterial community

Supplemental Figure 3.5b shows the 10 genes that are most highly expressed only in Sites 1-3. Included are two versions of soluble methane monooxygenase (EC 1.14.13.25), which are the 8th and 9th most highly expressed identified gene in Sites 1-3, but are not detected at all in the seawater sample, and rank 87th and 89th in Site 4 diffuse samples. This implies the community representing Sites 1-3 is involved in oxidizing methane for energy generation.

Sulfite reductase Alpha subunit (EC 1.8.1.2, formerly 1.8.99.1), and adenylyl-sulfate reductase (aka APS reductase – aprA & aprB, EC 1.8.99.2) are also highly expressed in Sites 1-3 (ranking 13th and 14th most highly expressed, respectively), not expressed in the seawater sample, and far less highly expressed in Site 4 (ranking 284th and 166th, respectively). Both of these genes catalyze reversible reactions that can be part of either sulfate reduction or sulfide oxidation. Sulfite reductase works between sulfate to sulfide, and APS reductase between sulfite and adenylyl sulfate. From its expression alone one cannot determine definitively whether it is playing a role in sulfate reduction and sulfide

oxidation. However, given Sites 1-3 are oxic and therefore not likely conducive to sulfate reduction, it seems likely they are indicative of sulfur oxidation. Additionally, the vast majority of sequences identified as APS reductase and sulfite reductase were most similar to sequences from Gammaproteobacterial symbionts, *Thiobacillus denitrificans*, and *Thioalkalivibrio* sp., most of which are known to carry out sulfur oxidation. While sulfide was not detected at Sites 1 and 2 and was relatively low at Site 3 (detection limit: ~1 uM), we suggest this habitat may be conducive to oxidation of partially reduced sulfur species such as thiosulfate, or elemental sulfur.

Expression of selected genes of interest further indicates that sulfur species oxidation appears to be an important aspect of metabolism throughout the vent field. Dissimilatory sulfate reductase (*dsr*) genes are used both by anaerobic sulfate reducers and microaerophilic or aerobic sulfur oxidizers for sulfate reduction and sulfur oxidation, respectively. Because *dsr* genes were more highly expressed in the more oxic Sites (1-3), we infer they indicate oxidation of reduced sulfur compounds. Other sulfur oxidation genes (*sox* and *apr*) showed similar expression patterns, further indicating that this process may be more pronounced in Sites 1-3 (Figure 3.8d & 3.8e). This activity profile is similar to those observed in a proteomic-based study of ASHES hydrothermal plumes sampled roughly 2 months after our samples were collected (Mattes *et al.*, 2013).

Patterns of gene expression associated with carbon fixation indicate that primary productivity in Sites 1-3 is occurring primarily through the Calvin Benson Bassham (CBB) cycle (Figure 3.8a). The CBB cycle tends to be favorable wherever oxygen is abundant, and as such it is not surprising that CBB genes (represented by total RuBisCO gene expression) dominated at the more oxic Sites 1-3. Different carbon fixation pathways are predicted to

dominate in different environments primarily because of the oxygen tolerance of key enzymes (Hügler and Sievert, 2011), the data are consistent with a transition from oxygen-tolerant to oxygen-sensitive pathways at Sites 3 and 4 respectively. Because oxygen concentration was lower in Site 4 than Site 1, it is plausible that oxygen was the primary driver for the observed patterns, as it has been implicated in defining ecological niches for other marine microbes such as marine ammonia-oxidizing archaea (e.g., Erguder *et al.*, 2009), anaerobic and microaerophilic sulfate reducing bacteria (reviewed in Baumgartner *et al.*, 2006), and even soil microbial communities (e.g., Pett-Ridge and Firestone, 2005). It is likely that the ubiquity of CBB genes relates to the relatively higher oxygen concentrations in the field. It appears that, like the buoyant plumes from high temperature chimneys, intra-field environments may be areas of increased primary productivity and therefore an ecologically important deep sea environment. However, it should also be noted that other factors co-vary with oxygen, including sulfide, temperature, and pH. Further work is needed to determine the extent of intra-field habitats on local and global scales.

Activity Profile at Site 4: A vent derived Epsilonproteobacteria-dominated community

Sulfur oxidation also appeared to be important at Site 4, though mediated by different biochemical pathways. Relative to Sites 1-3, sulfide:quinone reductase (*sqr*) was more highly expressed (though the differences were not statistically significant), and *dsr* genes were less highly expressed. This is consistent with sulfide oxidation to elemental sulfur at Site 4, and similar to patterns of gene expression found in other low temperature

vent environments where transcription from Gammaproteobacterial and Epsilonproteobacteria symbionts were shown to express different profiles of genes for sulfur metabolism (Yamamoto and Takai, 2011; Sanders *et al.*, 2013).

We also found elevated expression of genes associated with denitrification at Site 4 (Figure 3.8b). Since denitrification is favored in lower oxygen regimes, these data are consistent with the lower oxygen concentrations accompanying the elevated hydrothermal contribution to chemistry at this Site in conjunction with nitrate from seawater. Organisms similar to *Sulfurimonas denitrificans* and *Sulfurovum* sp. NBC37-1 (the most abundant species-level identifications at Site 4) dominated the overall active community at Site 4. *Sulfurimonas denitrificans* has genes for sulfide oxidation, hydrogen oxidation, and denitrification (Sievert *et al.*, 2008) and has been long known to oxidize thiosulfate and reduce nitrate (Hoor 1975), and *Sulfurovum* sp. NBC37-1 has been shown to utilize nitrate as a terminal electron acceptor (Nakagawa *et al.*, 2007). We posit that denitrification is linked to sulfide oxidation –and ultimately carbon fixation– at Site 4. Denitrification could, theoretically, also be linked with hydrogen oxidation, although we are not aware of microbes that have been shown to actively couple these two processes.

Based on ATP citrate lyase expression, carbon fixation at Site 4 may be dominated by the rTCA cycle. RuBisCO expression was also detected, though ~7 and 100- fold lower in abundance in Nisken and D-ESP samples, respectively (Figure 3.8a). The rTCA cycle is carried out by enzymes with higher oxygen sensitivity, and is thought to dominate chemically reduced hydrothermal vent environments (e.g., Campbell and Cary, 2004, and reviewed in Hügler et al., 2011).

Implications of different sampling methods

There is great interest in quantifying or describing the differences in microbial community gene expression with and without *in situ* sample preservation. We might expect that *in situ* preservation would provide a more accurate representation of gene expression because microbes sampled via traditional methods are subject to various "bottle effects" (changes in temperature and pressure, biological interactions, etc.) during collection and sample retrieval. In this study, we employed two different sampling methods: *in situ* pumping and preservation via the D-ESP as well as ROV-based fluid sampling via 5L Niskin bottles and *ex situ* preservation. The D-ESP sampling wand allows greater precision of sampling than the Niskin bottles, which collects a parcel of water from a larger area. Additionally, the sampling wand from the D-ESP can be positioned within a tubeworm clump at a diffuse vent orifice, while the Niskin bottles from the same Site have to be positioned above the tubeworms to enable the bottles to close and seal properly. At Site 4, therefore, the two sampling methods were sampling a similar, but not identical, environment. At Site 1, in contrast, the two methods sampled the same environment.

While considering the differences in sampling method, there were a few differences between our two sampling methods that could reflect the sampling method (described in results). Surprisingly however, the majority of functional and taxonomic genes and gene categories investigated in this work did not show statistically significant differences in expression between Niskin bottles and ESP samples. This indicates that Niskin sampling provides a fairly accurate picture of microbial gene expression in these samples. More research is needed to determine under what conditions and for what types of samples, Niskin sampling accurately represents *in situ* activity.

Differential expression analysis of paired ESP samples

To minimize variables and perform an in-depth analysis on a subset of the data representing the ends of our geochemical spectrum, we analyzed a subset of the ESP samples to quantitatively examine differences in gene expression between intra-field and diffuse flow fluids. Paired 0.2-5.0 and >5.0 μm ESP samples from the ESP elevator (Site 1) and ESP wand (Site 4) were used for this analysis (see methods for details). Figure 3.10 shows the most the most highly expressed transcripts showing statistically significant differential expression between these two environments. Those more highly expressed at the ESP elevator (intra-field Site 1) include aprA (one of the targeted genes showing a similar profile across the whole dataset, Figure 3.8), and a particulate methane monooxygenase (one of the most highly expressed genes in Sites 1-3, Supplemental Figure 3.5 in Appendix B).

Genes more highly expressed at the ESP wand (Diffuse Site 4) span a wide functional range. Increased thiosulfate reductase expression potentially indicates thiosulfate oxidation, likely coupled to nitrate reduction. Increased expression of nitrate and nitrite reductases (Figure 3.10, similar to the pattern of expression across the whole dataset – Figure 3.8) is consistent with a lower oxygen environment. Increased expression of flagellin and other flagellar genes potentially indicate increased motility in diffuse flows relative to intra-field fluids, and may be related to environment, but may also be associated with organisms that are dominant in these warmer waters, and not directly tied to environmental factors. ABC transporters and ferredoxin potentially indicate increased of uptake of metabolic substrates from the environment for biological redox reactions.

Whole vent fields as non-buoyant plumes

We posit that intra-field water is a diffuse flow-derived non-buoyant plume, the physical extent of which remains unknown. Geochemical and gene expression data presented here are consistent with what has been observed in studies of buoyant plumes emitted from high temperature hydrothermal flows (Dick and Tebo, 2010; Lesniewski *et al.*, 2012; Anantharaman *et al.*, 2015). However, the data presented here are from cooler diffuse flows. Our data would be consistent with this non-buoyant plume being large enough to span multiple diffuse flow vents. Given that the volume of fluids emitted by diffuse flow vents is comparable to or greater than that coming out of high temperature vents (Rona and Trivett, 1992b; Baker *et al.*, 1993; Bemis *et al.*, 1993; Elderfield and Schultz, 1996; Wankel *et al.*, 2011), the questions arise: how widespread are non-buoyant vent-field scale plumes, and how much of the Axial caldera is enveloped by such a plume? Future work in vent fields characterized by diffuse venting should aim to further characterize the microbial communities in the intra-field fluids.

Conclusions

Deep sea hydrothermal vents and their plumes are known to have a substantial impact on global ocean chemistry (e.g., Resing *et al.*, 2015). As the global mid-ocean ridge system cycles the entire ocean volume-equivalent every 70,000-200,000 years (Johnson and Pruis, 2003; Wheat *et al.*, 2003). This cycling is an important contribution to deep ocean iron and copper concentrations (Sander and Koschinsky, 2011), has influenced the global sulfur cycle over geologic time (reviewed in Bottrell and Newton, 2006), and likely

plays an indirect, but important, role in governing total carbon export in certain locations of the ocean (Tagliabue *et al.*, 2010). It is likely that microbes play key roles in these elemental cycles, but the details of how their activities both influence and are influenced by the surrounding geochemistry remains an open area of investigation (discussed in Anantharaman *et al.*, 2015).

At the outset of this work, we asked whether microbial activity varies systematically among geochemically distinct environments. Surprisingly, activity in intra-field waters was very similar to activity within certain diffuse flows. We found the majority of activity in these environments likely came from seawater-derived microbes, but certain diffuse flows, such as Site 4, appear to be dominated by mesophilic and thermophilic microbes derived to warmer vents or the subsurface. We found evidence for one profile of gammaproteobacteria-dominated activity throughout most of the vent field, and a distinct activity profile dominated by epsilonproteobacteria at only the most hydrothermally influenced site. The stark contrast in microbial gene expression among our diffuse flow sites highlights that realized niches crosscut our traditional definitions of a vent habitat, and intra-field samples emphasize the extent to which microbes associated with hydrothermal systems –from warm diffuse flows to highly oxic intra-field fluids– are active beyond the confines of the easily distinguishable vent features.

Conflict of Interest Statement

The authors declare no conflict of interest

Acknowledgements

This study is based upon work supported by grants from the National Science Foundation (Graduate Research Fellowship under Grant No. DGE-1144152 to H. Olins, NSF IOS- 1257755 and OCE-1344241 to P. R. Girguis, NSF OCE-0314222 and EF-0424599 to C. Scholin), the National Aeronautic and Space Administration (NASA-ASTEP NN X09AB78G and NN G06GB34G to C. Scholin and P. R. Girguis), and the David and Lucille Packard Foundation (to C. Scholin) through funds allocated by the Monterey Bay Aquarium Research Institute (MBARI), as well as the Gordon and Betty Moore Foundation (ERG731 to C. Scholin).

We thank Andrew Richardson, Jon Sanders, Talia Moore, Wai-ki Yip, and Matt Hayek for providing feedback on early versions of this manuscript, and Roxanne Beinart, Colleen Cavanaugh, and Andrew Knoll for feedback on a later version. We also thank Julie Huber for assistance with chimney identification. We thank the engineering technicians and machinists at MBARI for their invaluable help and dedication toward instrument development, Geoff Wheat for assistance with chemical analyses, Dave Clague and Jenny Paduan for assistance with bathymetric map of ASHES vent field, and the crews of the *R/V Western Flyer* and *ROV Doc Rickets* for facilitating and enabling these sample collections.

References

Akerman, N.H., Butterfield, D.A., and Huber, J.A. (2013) Phylogenetic diversity and functional gene patterns of sulfur-oxidizing subseafloor Epsilonproteobacteria in diffuse hydrothermal vent fluids. *Front. Microbio.* **4**: 185.

Altschul, S.F., Gish, W., Miller, W., Myers, E.W., and Lipman, D.J. (1990) Basic local alignment search tool. *J. Mol. Biol.* **215**: 403–410.

Anantharaman, K., Breier, J.A., and Dick, G.J. (2015) Metagenomic resolution of microbial functions in deep-sea hydrothermal plumes across the Eastern Lau Spreading Center. *ISME J* **10**: 225–239.

Anderson, R.E., Beltrán, M.T., Hallam, S.J., and Baross, J.A. (2013) Microbial community

structure across fluid gradients in the Juan de Fuca Ridge hydrothermal system. *FEMS Microbiology Ecology* **83**: 324–339.
Baker, E.T., Massoth, G.J., and Walker, S.L. (1993) A method for quantitatively estimating diffuse and discrete hydrothermal discharge. *Earth and planetary science letters* **118**: 235–249.
Baumgartner, L.K., Reid, R.P., Dupraz, C., Decho, A.W., Buckley, D.H., Spear, J.R., et al. (2006) Sulfate reducing bacteria in microbial mats: Changing paradigms, new discoveries. **185**: 131–145.
Bemis, K., Lowell, R., and Farough, A. (2012) Diffuse Flow On and Around Hydrothermal Vents at Mid-Ocean Ridges. *oceanog* **25**: 182–191.
Bemis, K.G., Herzen, von, R.P., and Mottl, M.J. (1993) Geothermal heat flux from hydrothermal plumes on the Juan de Fuca Ridge. *J. Geophys. Res.* **98**: 6351–6365.
Bolger, A.M., Lohse, M., and Usadel, B. (2014) Trimmomatic: a flexible trimmer for Illumina sequence data. *Bioinformatics* **30**: 2114–2120.
Bottrell, S.H. and Newton, R.J. (2006) Reconstruction of changes in global sulfur cycling from marine sulfate isotopes. *Earth-Science Reviews* **75**: 59–83.
Bourbonnais, A., Juniper, S.K., Butterfield, D.A., Devol, A.H., Kuypers, M.M.M., Lavik, G., et al. (2012) Activity and abundance of denitrifying bacteria in the subsurface biosphere of diffuse hydrothermal vents of the Juan de Fuca Ridge. *Biogeosciences* **9**: 4661–4678.
Butterfield, D.A. and Merle, S. (2007) NeMO 2006 Cruise Report.
Butterfield, D.A., Roe, K.K., Lilley, M.D., Huber, J.A., Baross, J.A., Embley, R.W., and Massoth, G.J. (2004) Mixing, Reaction and Microbial Activity in the Sub-Seafloor Revealed by Temporal and Spatial Variation in Diffuse Flow Vents at Axial Volcano. *The Subseafloor Biosphere at Mid-Ocean Ridges* 269–289.
Campbell, B.J. and Cary, S.C. (2004) Abundance of Reverse Tricarboxylic Acid Cycle Genes in Free-Living Microorganisms at Deep-Sea Hydrothermal Vents. *Applied and Environmental Microbiology* **70**: 6282–6289.
Campbell, B.J., Polson, S.W., Allen, L.Z., Williamson, S.J., Lee, C.K., Wommack, K.E., and Cary, S.C. (2013) Diffuse flow environments within basalt- and sediment-based hydrothermal vent ecosystems harbor specialized microbial communities. *Front. Microbio.* **4**:.
Corliss, J.B., Dymond, J., Gordon, L.I., Edmond, J.M., Herzen, von, R.P., Ballard, R.D., et al. (1979) Submarine Thermal Sprirngs on the Galapagos Rift. *Science* **203**: 1073–1083.
Cowen, J.P., Massoth, G.J., and Feely, R.A. (1990) Scavenging rates of dissolved manganese in a hydrothermal vent plume. *Deep Sea Research Part A. Oceanographic Research Papers* **37**: 1619–1637.
Dick, G.J. and Tebo, B.M. (2010) Microbial diversity and biogeochemistry of the Guaymas Basin deep-sea hydrothermal plume. *Environmental Microbiology* **12**: 1334–1347.
Dick, G.J., Anantharaman, K., Baker, B.J., Li, M., Reed, D.C., and Sheik, C.S. (2013) The microbiology of deep-sea hydrothermal vent plumes: ecological and biogeographic linkages to seafloor and water column habitats. *Front. Microbio.* **4**:.
Elderfield, H. and Schultz, A. (1996) Mid-ocean ridge hydrothermal fluxes and the chemical composition of the ocean. *Annual Review of Earth and Planetary Sciences* **24**: 191–224.
Eren, A.M., Morrison, H.G., Huse, S.M., and Sogin, M.L. (2014) DRISEE overestimates errors in metagenomic sequencing data. *Briefings in Bioinformatics* **15**: 783–787.
Erguder, T.H., Boon, N., Wittebolle, L., Marzorati, M., and Verstraete, W. (2009) Environmental factors shaping the ecological niches of ammonia-oxidizing archaea. **33**:

855–869.
Flores, G.E., Campbell, J.H., Kirshtein, J.D., Meneghin, J., Podar, M., Steinberg, J.I., et al. (2011) Microbial community structure of hydrothermal deposits from geochemically different vent fields along the Mid-Atlantic Ridge. *Environmental Microbiology* **13**: 2158–2171.
Fortunato, C.S. and Huber, J.A. (2016) Coupled RNA-SIP and metatranscriptomics of active chemolithoautotrophic communities at a deep-sea hydrothermal vent. *ISME J* 1–14.
Grabherr, M.G., Haas, B.J., Yassour, M., Levin, J.Z., Thompson, D.A., Amit, I., et al. (2011) Full-length transcriptome assembly from RNA-Seq data without a reference genome. *Nat Biotechnol* **29**: 644–652.
Hoor, A. T.-T. (1975). A new type of thiosulphate oxidizing, nitrate reducing microorganism: Thiomicrospira denitrificans sp. nov. *Netherlands Journal of Sea Research*, **9**(3-4), 344–350.
Huber, J.A. and Holden, J.F. (2008) Modeling the impact of diffuse vent microorganisms along mid-ocean ridges and flanks. In, *Magma to Microbe: Modeling Hydrothermal Processes at Ocean Spreading Centers*, Geophysical Monograph Series. American Geophysical Union, Washington, D. C., pp. 215–231.
Huber, J.A., Butterfield, D.A., and Baross, J.A. (2003) Bacterial diversity in a subseafloor habitat following a deep-sea volcanic eruption. *FEMS Microbiology Ecology* **43**: 393–409.
Huber, J.A., Butterfield, D.A., and Baross, J.A. (2006) Diversity and distribution of subseafloor Thermococcales populations in diffuse hydrothermal vents at an active deep-sea volcano in the northeast Pacific Ocean. *J. Geophys. Res.* **111**: 1–13.
Huber, J.A., Butterfield, D.A., and Baross, J.A. (2002) Temporal Changes in Archaeal Diversity and Chemistry in a Mid-Ocean Ridge Subseafloor Habitat. *Applied and Environmental Microbiology* **68**: 1585–1594.
Huber, J.A., Cantin, H.V., Huse, S.M., Mark Welch, D.B., Sogin, M.L., and Butterfield, D.A. (2010) Isolated communities of Epsilonproteobacteria in hydrothermal vent fluids of the Mariana Arc seamounts. *FEMS Microbiology Ecology* no–no.
Huber, J.A., Mark Welch, D.B., Morrison, H.G., Huse, S.M., Neal, P.R., Butterfield, D.A., and Sogin, M.L. (2007) Microbial Population Structures in the Deep Marine Biosphere. *Science* **318**: 97–100.
Hügler, M. and Sievert, S.M. (2011) Beyond the Calvin Cycle: Autotrophic Carbon Fixation in the Ocean. *Annu. Rev. Marine. Sci.* **3**: 261–289.
Johnson, H.P. and Pruis, M.J. (2003) Fluxes of fluid and heat from the oceanic crustal reservoir. *Earth and planetary science letters* **216**: 565–574.
Kadko, D., Baross, J., and Alt, J. (1995) The Magnitude and Global Implications of Hydrothermal Flux American Geophysical Union, Washington, D. C.
Klinkhammer, G. and Hudson, A. (1986) Dispersal patterns for hydrothermal plumes in the South Pacific using manganese as a tracer. *Earth and planetary science letters* **79**: 241–249.
Lesniewski, R.A., Jain, S., Anantharaman, K., Schloss, P.D., and Dick, G.J. (2012) The metatranscriptome of a deep-sea hydrothermal plume is dominated by water column methanotrophs and lithotrophs. *ISME J* **6**: 2257–2268.
Love, M.I., Huber, W., and Anders, S. (2014) Moderated estimation of fold change and dispersion for RNA-seq data with DESeq2. *Genome Biol* **15**: 31–21.
Mattes, T.E., Nunn, B.L., Marshall, K.T., Proskurowski, G., Kelley, D.S., Kawka, O.E., et al.

(2013) Sulfur oxidizers dominate carbon fixation at a biogeochemical hot spot in the dark ocean. *ISME J* **7**: 2349–2360.
Meyer, J.L., Akerman, N.H., Proskurowski, G., and Huber, J.A. (2013) Microbiological characterization of post-eruption "snowblower" vents at Axial Seamount, Juan de Fuca Ridge. *Front. Microbio.* **4**:.
Nakagawa, S., Takai, K., Inagaki, F., Hirayama, H., Nunoura, T., Horikoshi, K., and Sako, Y. (2005) Distribution, phylogenetic diversity and physiological characteristics of epsilon-Proteobacteria in a deep-sea hydrothermal field. *Environmental Microbiology* **7**: 1619–1632.
Nakagawa, S., Takaki, Y., Shimamura, S., Reysenbach, A.-L., Takai, K., and Horikoshi, K. (2007) Deep-sea vent epsilon-proteobacterial genomes provide insights into emergence of pathogens. *Proc. Natl. Acad. Sci. U.S.A.* **104**: 12146–12150.
Olins, H.C., Rogers, D.R., Frank, K.L., Vidoudez, C., and Girguis, P.R. (2013) Assessing the influence of physical, geochemical and biological factors on anaerobic microbial primary productivity within hydrothermal vent chimneys. *Geobiology* 279–293.
Opatkiewicz, A.D., Butterfield, D.A., and Baross, J.A. (2009) Individual hydrothermal vents at Axial Seamount harbor distinct subseafloor microbial communities. *FEMS Microbiology Ecology* **70**: 413–424.
Ottesen, E.A., Marin, R., Preston, C.M., Young, C.R., Ryan, J.P., Scholin, C.A., and DeLong, E.F. (2011) Metatranscriptomic analysis of autonomously collected and preserved marine bacterioplankton. *ISME J* **5**: 1881–1895.
Pargett, D.M., Jensen, S.D., Roman, B.A., Preston, C.M., III, W.U., Girguis, P.R., et al. (2013) Deep Water Instrument for Microbial Identification, Quantification, and Archiving. *Oceans San Diego, IEEE Conference Publication* 1–6.
Perner, M., Gonnella, G., Hourdez, S., Böhnke, S., Kurtz, S., and Girguis, P. (2013a) In situ chemistry and microbial community compositions in five deep-sea hydrothermal fluid samples from Irina II in the Logatchev field. *Environmental Microbiology* **15**: 1551–1560.
Perner, M., Hansen, M., Seifert, R., Strauss, H., Koschinsky, A., and Petersen, S. (2013b) Linking geology, fluid chemistry, and microbial activity of basalt- and ultramafic-hosted deep-sea hydrothermal vent environments. *Geobiology* **11**: 340–355.
Perner, M., Petersen, J.M., Zielinski, F., Gennerich, H.-H., and Seifert, R. (2010) Geochemical constraints on the diversity and activity of H2-oxidizing microorganisms in diffuse hydrothermal fluids from a basalt- and an ultramafic-hosted vent. *FEMS Microbiology Ecology* **74**: 55–71.
Pett-Ridge, J. and Firestone, M.K. (2005) Redox Fluctuation Structures Microbial Communities in a Wet Tropical Soil. **71**: 6998–7007.
Pruis, M.J., Hautala, S.L., Johnson, H.P., and Berdeal, I.G. (2004) Turbulent heat flux in the deep ocean above diffuse hydrothermal vents. *… in preparation for Deep- ….*
Pruitt, K.D. (2005) NCBI Reference Sequence (RefSeq): a curated non-redundant sequence database of genomes, transcripts and proteins. *Nucleic Acids Research* **33**: D501–D504.
Resing, J.A., Sedwick, P.N., German, C.R., Jenkins, W.J., Moffett, J.W., Sohst, B.M., and Tagliabue, A. (2015) Basin-scale transport of hydrothermal dissolved metals across the South Pacific Ocean. *Nature* **523**: 200–203.
Rona, P.A. and Trivett, D.A. (1992a) Discrete and diffuse heat transfer atashes vent field, Axial Volcano, Juan de Fuca Ridge. *Earth and planetary science letters* **109**: 57–71.

Rona, P.A. and Trivett, D.A. (1992b) Discrete and diffuse heat transfer atashes vent field, Axial Volcano, Juan de Fuca Ridge. *Earth and planetary science letters* **109**: 57–71.
Sander, S.G. and Koschinsky, A. (2011) Metal flux from hydrothermal vents increased by organic complexation. *Nature Geosci* **4**: 145–150.
Sanders, J.G., Beinart, R.A., Stewart, F.J., Delong, E.F., and Girguis, P.R. (2013) Metatranscriptomics reveal differences in in situ energy and nitrogen metabolism among hydrothermal vent snail symbionts. *ISME J* **7**: 1556–1567.
Schmieder, R. and Edwards, R. (2011) Quality control and preprocessing of metagenomic datasets. *Bioinformatics* **27**: 863–864.
Sheik, C.S., Anantharaman, K., Breier, J.A., Sylvan, J.B., Edwards, K.J., and Dick, G.J. (2015) Spatially resolved sampling reveals dynamic microbial communities in rising hydrothermal plumes across a back-arc basin. *ISME J* **9**: 1434–1445.
Sievert, S.M., Scott, K.M., Klotz, M.G., Chain, P.S.G., Hauser, L.J., Hemp, J., et al. (2008) Genome of the Epsilonproteobacterial Chemolithoautotroph Sulfurimonas denitrificans. *Applied and Environmental Microbiology* **74**: 1145–1156.
Sunamura, M., Higashi, Y., Miyako, C., Ishibashi, J.I., and Maruyama, A. (2004) Two Bacteria Phylotypes Are Predominant in the Suiyo Seamount Hydrothermal Plume. *Applied and Environmental Microbiology* **70**: 1190–1198.
Tagliabue, A., Bopp, L., Dutay, J.-C., Bowie, A.R., Chever, F., Jean-Baptiste, P., et al. (2010) Hydrothermal contribution to the oceanic dissolved iron inventory. *Nature Geosci* **3**: 252–256.
Ussler, W., III, Preston, C., Tavormina, P., Pargett, D., Jensen, S., Roman, B., et al. (2013) Autonomous Application of Quantitative PCR in the Deep Sea: In Situ Surveys of Aerobic Methanotrophs Using the Deep-Sea Environmental Sample Processor. *Environ. Sci. Technol.* **47**: 9339–9346.
Ver Eecke, H.C., Butterfield, D.A., Huber, J.A., Lilley, M.D., Olson, E.J., Roe, K.K., et al. (2012) Hydrogen-limited growth of hyperthermophilic methanogens at deep-sea hydrothermal vents. *Proceedings of the National Academy of Sciences* **109**: 13674–13679.
Wankel, S.D., Germanovich, L.N., Lilley, M.D., Genc, G., DiPerna, C.J., Bradley, A.S., et al. (2011) Influence of subsurface biosphere on geochemical fluxes from diffuse hydrothermal fluids. *Nature Geosci* **4**: 1–8.
Wheat, C.G., Jannasch, H.W., Fisher, A.T., Becker, K., Sharkey, J., and Hulme, S. (2010) Subseafloor seawater-basalt-microbe reactions: Continuous sampling of borehole fluids in a ridge flank environment. *Geochem. Geophys. Geosyst.* **11**: n/a–n/a.
Wheat, C.G., McManus, J., Mottl, M.J., and Giambalvo, E. (2003) Oceanic phosphorus imbalance: Magnitude of the mid-ocean ridge flank hydrothermal sink. *Geophys. Res. Lett.* **30**: 1–4.
Wright, J.J., Konwar, K.M., and Hallam, S.J. (2012) Microbial ecology of expanding oxygen minimum zones. *Nat Rev Micro* **10**: 381–394.
Yamamoto, M. and Takai, K. (2011) Sulfur Metabolisms in Epsilon- and Gamma-Proteobacteria in Deep-Sea Hydrothermal Fields. *Front. Microbio.* **2**:.

Chapter 4

In situ mineral colonization samplers reveal patterns in microbial community composition, structure, and succession

ABSTRACT

Microbes can use solid phase minerals as both electron donors and acceptors, and thus minerals may exert a selective pressure on microbes colonizing their surfaces. Little is known about the extent of this selection. Hydrothermal vent chimneys are ideal to investigate these microbe-mineral interactions. In order to examine the extent to which solid-state minerals influence community structure in hydrothermal vent chimneys, we designed and deployed novel sampling devices called ISMACS (*in situ* mineral associated colonization samplers), with which we incubated a variety of minerals in vent fluid. Gross community composition did not vary significantly with mineralogy. Certain taxa did appear to be significantly more abundant on specific minerals. We found evidence that communities exposed to a mix of mineral substrates were more diverse than single-mineral communities, and that hematite-hosted communities were less diverse than other minerals. We also identified taxa that may represent early and late colonizers in this ecosystem. These data indicate that mineral substrate is not the primary driver of community structure in hydrothermal vent chimneys, but that it plays an important role in the diversity, succession, and metabolism of these microbial communities – especially in rare taxa.

INTRODUCTION

Iron and sulfur are two of the key elements involved in microbial mineral oxidation and reduction. Microbes can use solid phase minerals as electron donors, for example Fe(II) sulfides such as pyrite (Nordstrom and Southam, 1997; Edwards *et al.*, 1998; Weber *et al.*, 2006; Juncher Jørgensen *et al.*, 2009). They can also use minerals as electron

acceptors, for example Iron(III) oxides such as magnetite (Kostka and Nealson, 1995; Weber *et al.*, 2006) and hematite (Lovley, 1991). Hydrothermal vents are an ideal location to investigate these processes because reduced and oxidized iron and sulfur are both available in the form of iron oxide and iron sulfide minerals.

Some microbes are known to preferentially colonize certain minerals. For example, *Thiobacillus ferrooxidans'* selective colonization of pyrite over other minerals (described in (Hutchens, 2009), or an uncultured group of microbes related to *Magnetobacterium bavaricum* found only in regions of extinct vent chimneys containing metal sulfides (Suzuki *et al.*, 2004). More broadly, epi- and endolithic microbial community structure has been shown to be substantially influenced by rock type in low temperature deep sea environments such as hydrothermally inactive sulfide chimneys (Toner *et al.*, 2013; Sylvan *et al.*, 2013), sea floor basalts (Toner *et al.*, 2013), seafloor basaltic andesite (Sylvan *et al.*, 2013), and methane seep carbonates (Case *et al.*, 2015). Microbial communities have also been shown to vary across different mineral layers that make up active hydrothermal vent chimney structures (Schrenk *et al.*, 2003; Suzuki *et al.*, 2004; Kormas *et al.*, 2006; Harrison and Orphan, 2012). These studies have identified patterns at the scale of bulk mineralogical composition, but have not demonstrated a functional link between individual taxa and particular minerals. Colonization studies are necessary to demonstrate such linkages.

Colonization studies in boreholes in the subsurface crustal aquifer of the Juan de Fuca Ridge have shown that distinct communities colonize rock chip, mineral, and basalt glass substrates, that surface attached communities are distinct from planktonic communities, and that there are mineral-specific differences in community structure (Orcutt *et al.*, 2010; 2011; Smith *et al.*, 2011; 2016). Additionally, iron-rich and iron-poor

minerals were recently shown to be colonized by distinct communities of bacteria in the subsurface (Smith *et al.*, 2016). *In situ* colonization studies of basalts and minerals have also been carried out in a number of hydrothermal environments including sediments (Callac *et al.*, 2013) and diffuse flows (Edwards *et al.*, 2003; Toner *et al.*, 2009; Gulmann *et al.*, 2015).

Together, these experimental and observational studies clearly demonstrate that mineral substrate influences microbial community structure in a variety of deep sea habitats. However, the coupling of particular minerals and specific taxa has not been clearly demonstrated in actively venting hydrothermal structures. We hypothesize that minerals in active hydrothermal flows are exerting a selective pressure on the microbial communities that colonize their surfaces. Hydrothermal vent chimneys are a habitat characterized by steep gradients in chemistry and temperature, and predictable layering of minerals. Because minerals precipitate at specific thermal and chemical conditions, mineralogy tends to be a record vent fluid chemistry and temperature at the time of mineral precipitation. As such, the mineralogy of a chimney is a record of past chemistry and temperature, and it is difficult to connect differences in microbial community to specific mineral substrates formed *in situ*. This is challenging because minerals in vents form at specific thermal and chemical conditions, and thermal gradients tend to co-occur with mineral layers in vent chimney walls. Because of this co-occurrence and the dynamic nature of the vent habitat, microbial community composition and structure could also be driven by fluid chemistry, temperature, succession patterns, or other ecological factors.

The goal of the work presented here is to examine the extent to which substrate mineralogy influences microbial community structure in hydrothermal vent chimneys. We

designed and deployed novel sampling devices called ISMACS (*in situ* mineral associated colonization samplers) to incubate a variety of hydrothermal vent-relevant minerals in diffuse vent fluids while recording temperature throughout the incubation in order to infer changes in fluid chemistry. ISMACS were deployed in triplicate for 2, 3, 4-5, 40, and 685 day periods. Community composition of 107 mineral samples was assessed *via* 16S Illumina MiSeq™ sequencing. Phylogenetic analyses revealed that gross community composition (principle component analysis of weighted UniFrac distance) did not vary significantly with mineralogy, but that hematite-hosted communities were the least diverse after 2 years. Suprisingly, we found evidence that communities that colonized a mixture of mineral substrates (as opposed to only one mineral) were more diverse than single-mineral communities, with significantly increased diversity among the Deltaproteobacteria. From time series analyses, we identified certain taxa that may represent early and late colonizers in this ecosystem. These data indicate that mineral substrates may play an important role in the diversity, succession, and metabolism of epi- and endolithic communities in low and high temperature hydrothermal vent structures– especially in rare taxa.

MATERIALS & METHODS

ISMACS design

ISMACS samplers were fabricated from high-density polyethylene plastic funnels, PVC pipe and couplings, 5 ml cryovials, and 2 x 2.5mm screen mesh. Mineral substrates are held within each ISMACS unit in individual mineral tubes (Figure 4.1). Mineral tubes were created by cutting off the rounded tube bottom and affixing screen mesh with epoxy and zip ties. This became the top of the mineral tube. Holes were drilled in the cryo vial caps,

which were then used to hold screen mesh on the bottom of the mineral tubes. The 6 mineral tubes in each unit were held in place by custom-fabricated Delrin plastic discs that also blocked fluid from flowing around, rather than through, the mineral tubes. 6 mineral tubes were each filled with a different mineral or substrate and were installed in the holding disk forming the sampling module.

Figure 4.1 a) Schematic of ISMACS units showing mixing module that contains the iButton temperature logger, and sampling module that contains mineral/substrate tubes. (b) Photo of ISMACS pre-deployment. (c) Photo of ISMACS #3 during deployment with white flocculant matter as evidence of colonization. (d) Photo of ISMACS #10 after deployment during sampling with mineral tubes exposed.

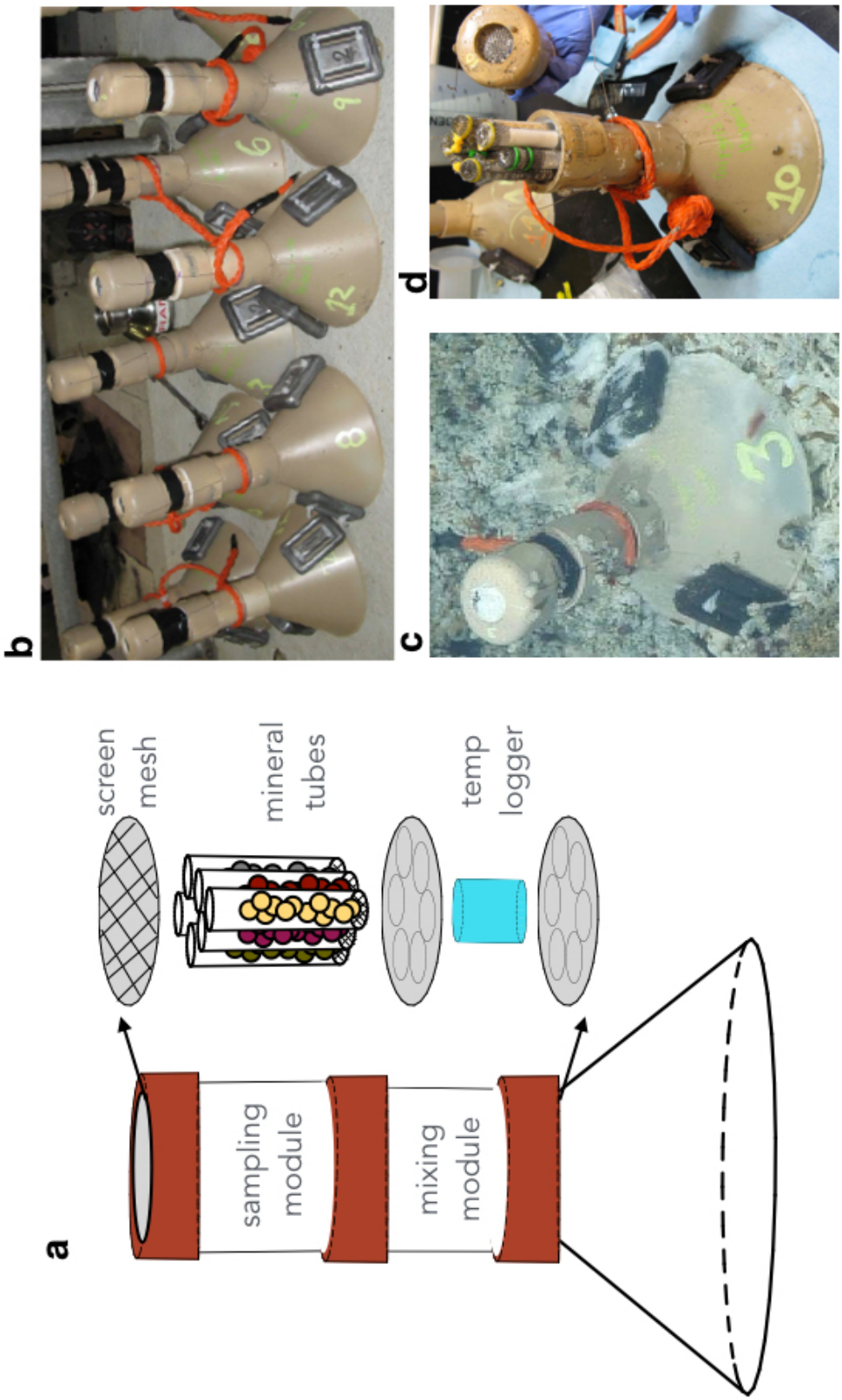

Figure 4.1 continued

Below the sampling module, a section of PVC pipe formed the mixing module. An iButton™ temperature logger (Maxim Inc.) was installed in the mixing module in a small 1 atm housing made of either stainless steel with a Delrin™ plastic top (for shorter incubations) or grade 1 titanium (for the longer incubations). In all cases the tops were fastened to the body with 22 gauge titanium wire, which was also used to hang the pressure vessel inside the mixing module.

The top of the unit consisted of a 1.5 inch PVC pipe coupling with screen mesh to prevent animals from entering the unit and disrupting fluid flow. The base of each unit consisted of an inverted plastic funnel (20cm diameter) modified by removing the narrow end until the funnel adequately fit the mixing and sampling modules. This funnel was then connected with epoxy and titanium wire. For the 2-year incubation, units were reinforced with a custom titanium bracket connecting the funnel to the mixing module. Titanium wire was used to seal the unit for deployment. Units were ~33 cm tall.

Study Site and ISMACS collection and deployment

ISMACS were prepared for the initial deployment as follows. Mineral tubes (except anhydrite) were sterilized in a 70% EtOH. To avoid dissolution, anhydrite was sterilized in weigh boats in the UV Stratolinker before being put into tubes soaked in EtOH. Mineral tubes were shipped in a glass jar, wet with EtOH, and were wet upon arrival. This extended soak may have been problematic for the adhesive, as some of the tube tops were no longer fixed to the tubes when the jar was opened. One tube of beads spilled and beads were replaced with gloved hands. On board, mineral tubes were soaked in 10% HCl for ~12

hours to remove any oxide rind. Tubes were then taken out of the HCl and stored in anoxic (bubbled with He gas) DI water until they were placed into the ISMACS units the evening before deployment. Mineral tubes were therefore exposed to O_2 overnight before deployment, which was necessary so that the pilots could load the submersible the night before.

ISMACS units were deployed at two sites in Ashes vent field within Axial Caldera on the Juan de Fuca Ridge. Ashes is characterized by widespread diffuse venting, making it ideal for ISMACS deployment. Initial deployments took place during the Monterey Bay Aquarium Research Institute's 2011 Pacific Northwest Expedition aboard the *R/V Western Flyer* using the *ROV Doc Ricketts*. The 12 ISMACS units (number 1-12) were placed in the vent field using the ROV on the same dive, and positioned in diffuse flows on the following dive. 3 units (#7, 2, and 8) were placed on a diffuse flow near Phoenix Chimney and the location of the ESP deployment (described in Chapter 3), and 9 were placed at the base of the southern side of Mushroom chimney. All units were placed over active diffuse flow, and it was confirmed visually that warm water was flowing through each unit. Unit 3 had substantially more obvious flow running through it than the other units.

ISMACS collection was carried out using the submersible manipulator arms. Units were placed together into a sealed biobox. Upon retrieval, units were opened, mineral grains were sampled from the top of each mineral tube for microscopy, and the remainder of the grains in their tube were placed in whirlpaks and frozen at -80°C for later analyses. Units 3, 7, and 12 were collected after 2 days. Units 2, 6, and 10 were collected after 3 days. Units 5, 8, and 9 were collected after 4-5 days. Units 1, 4, and 11 were left in place and were collected after 40 days by University of Washington colleagues during the Visions 2011

cruise. At the same time units 6, 9, and 12 were re-deployed (and are referred to as 6b, 9b, and 12b) for a roughly two-year deployment (685 days), after which they were collected during the Visions 2013 cruise.

DNA Extraction and Sequencing

DNA was extracted from mineral samples using the MoBio™ Power Soil kit (MoBio Inc.) according to manufacturers instructions with the following modifications: A) Instead of a specific mass of soil, mineral grains were added to the PowerBead™ tubes, filling them up to the top of the textured portion of the tube; B) After adding solution C1, tubes were incubated at 70°C for 12 minutes; then C) after this incubation 200 ug of polyadenylic acid (PolyA) was added to each tube. Tubes were vortexed at maximum speed for 15 minutes. DNA was stored frozen at -80°C.

A total of 107 ISMACS samples were concurrently prepared for iTag sequencing via Illumina MiSeq™ at the Argonne National Laboratory using Earth Microbiome recently updated bacterial/archaeal forward barcoded 515f/806r primers (Caporaso *et al.*, 2012; and modification described in Apprill *et al.*, 2015). 71 samples were extracted from the bottom third of the mineral tubes recovered from the 15 ISMACS deployments. 33 samples were extracted from the top third of the same mineral tubes extracted above. 3 samples were extracted from microbial mats scraped from minerals or sampling devices.

Bioinformatics

Bioinformatic analyses were carried out primarily using QIIME1.9.1 with default protocols (as in Caporaso *et al.*, 2010). Variations from the default settings are described

below. Paired end reads were joined (join_paired_ends.py), and FASTQC was used to assess overall quality of joined reads. Fastq sequences were demultiplexed (split_libraries_fastq.py) and filtered using a Phred quality score of 19. OTUs were generated using open reference OTU picking (pick_open_reference_otus.py) against a 99% identity representative set from the Silva database (Silva_119_rep_set99_aligned.fna). Statistical significance of differences between extraction, incubation length, mineral, and deployment site were analyzed (compare_categories.py) using the adonis method and default parameters (999 permutations). Initial diversity analyses (core_diversity_analyses.py) were run on individual samples rarefied to the number of sequences in the smallest sample (14,287 sequences). This analysis included comparing samples based on the following categories: ISMACS unit, mineral, extraction number, site, and incubation length.

The following alpha diversity metrics were calculated (alpha_diversity.py) for each sample: dominance, equitability, fisher_alpha, osd, shannon, simpson, simpson_e, chao1, PD_whole_tree, observed_otus. To assess the impact of rare taxa on diversity, OTUs were filtered (filter_otus_from_otu_table.py) to remove those with fewer than 2 sequences or that were not observed in at least 10 samples. OTU frequencies across categories were compared (group_significance.py) to identify specific OTUs that were differentially expressed by incubation length, mineral, site, or unit (whether or not statistically significant differences between OTU abundance in different sample groups). Significances were calculated with and without rare taxa (see OTU filtering above) to see if rare taxa (potentially artificial) were influencing results using multiple tests (ANOVA, Gtest, mann-whitney, and non-parametric T test). OTUs were summarized and plotted via

summarize_taxa_through_plots.py. otu_category_significance.py to identify whether OTUs were significantly associated with a category.

Succession analysis

To examine broad patterns of succession, diversity metrics were averaged across each ISMACS units (Supplemental Table 1). Because only marcasite, hematite, pyrite and zirconia bead communities were available for all units (except unit 7 which was not used in this analysis). These unit-wide averages were based only on these 4 minerals. Sphalerite and mineral mix communities were not included because they were not available for each unit.

Calculation of standard redox potentials

The values of the standard reduction potentials (E^0; Supplemental Figure 1) under standard conditions for the half-cell reactions were obtained from the HSC Chemistry Database (Roine, 2002). The standard conditions refer to 25°C temperature, 1 atm pressure, and concentrations of 1M for all ions involved in the respective reactions.

RESULTS

Temperature records

Temperature records show that most of the ISMACS units were below 20°C for their deployments (Figure 4.2). Units 3 and 4, in contrast, had average temperatures above 80°C during their deployments. The short (2-5 day) incubations were relatively stable in temperature over the course of their deployments (with the exception of Units 3 and 9;

Supplemental Figure 3). The 40-day incubations (Units 1, 4, and 11; Supplemental Figure 4.4) all showed daily variation likely due in part to tidal influences. Unit 11 fluctuated regularly between 5 and 15°C through the incubation. Unit 1 started out warm, spending most of the first 7 days above 40°C, but by day 16 was similar in temperature to Unit 11. Unit 4, in contrast was above 60°C for nearly the entire deployment, and above 80°C for more than half of it.

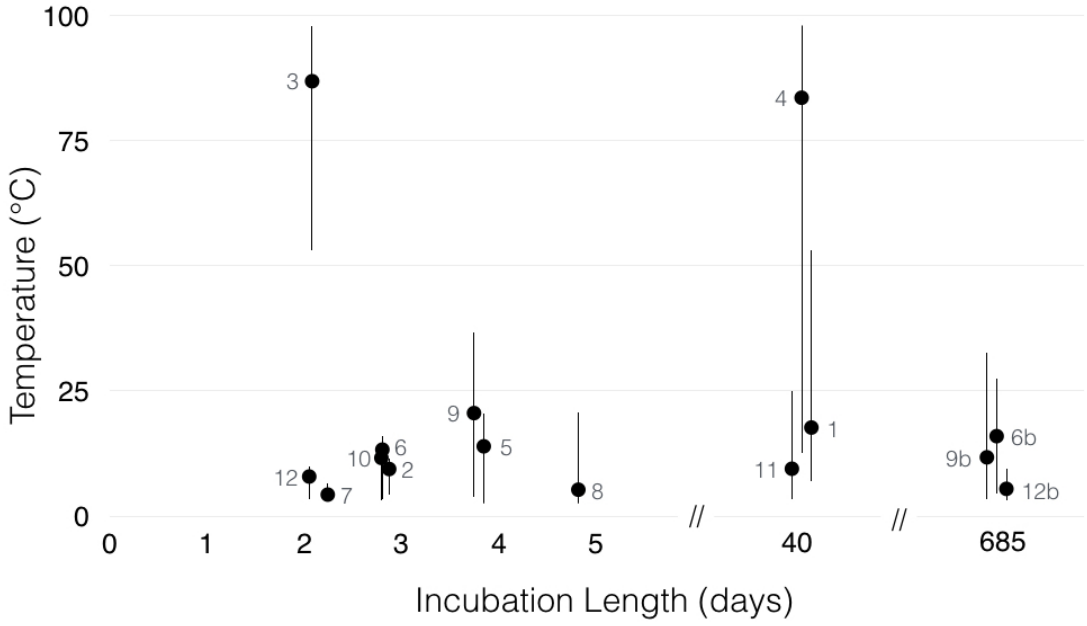

Figure 4.2 Summary of temperature records for all ISMACS. Dots represent average temperature over incubation. Bars represent the temperature range (highest and lowest temperature recorded during incubation). Dot label represent the ISMACS number. Note broken x-axis scale.

The two-year incubations, which are the main focus of this work, varied substantially on both short and long term time scales (Figure 4.3). Unit 12b was below 5°C for the first ~200 days, and then remained between 5 and 10°C (with a few excursions below 5°C) for the remainder of the incubation period. Unit 6b was initially the warmest showed frequent 5-10°C shifts in temperature for the first ~300 days. For the last third of

the incubation, unit 6b held relatively stable temperature around 15-17°C. Around day 375 Unit 9b became the warmest and started registering regular shifts in temperature similar to those of unit 6b in the beginning of the deployment. Around day 530 temperatures dropped in unit 9b to below 10°C and then rose again above 20°C around day 660.

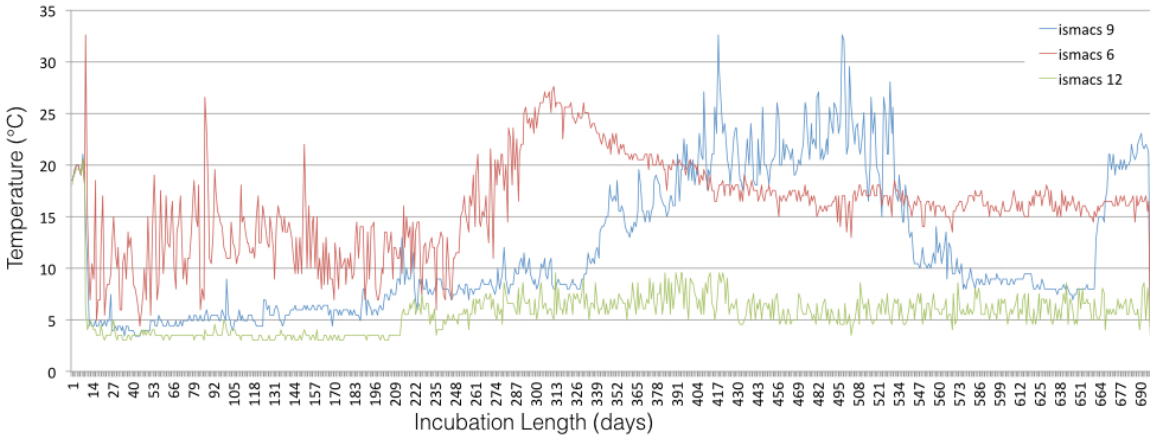

Figure 4.3 Temperature records from the 2-year incubations show substantial variation on short (day) and long (month) time scales. Unit 9b is shown in blue, Unit 6b in red, and Unit 12b in green.

Sequencing

A total of 11,609,745 sequences were generated. The median sequence length from the Illumina run was 253 bp. Joined reads had sequence lengths of 151-296 base pairs. Overall GC content was 51%. After quality filtering (described in bioinformatics section) 5 of the samples sequenced returned fewer than 250 sequences and were removed from all downstream analyses. Of the remaining samples, the smallest number of sequences was 14,631. All samples were rarefied to this number of sequences for comparative analyses. The average number of sequences from ISMACS mineral extraction samples was 72,322, and the largest number of sequences from any of these samples was 121,860.

Overall (whole data set) diversity

Beta diversity (both weighted and unweighted UniFrac principle coordinates) did not show clear grouping by site, mineral, incubation length, or extraction (Figure 4.4). Comparisons based on the weighted UniFrac distance matrix of all ISMACS mineral samples showed that categorization of samples by extraction number, incubation length, mineral substrate, or site, were not statistically significant (data not shown).

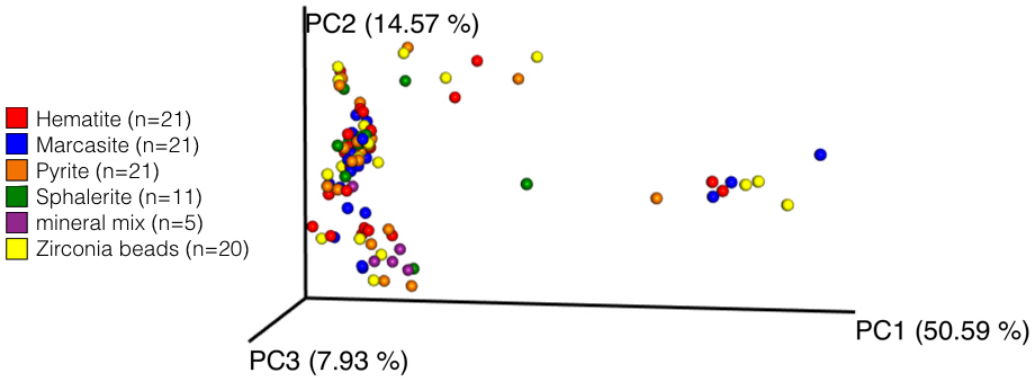

Figure 4.4 Weighted UniFrac distance of all ISMACS samples showing no clear grouping by mineral. Unweighted UniFrac distances (not shown) were similar.

Alpha diversity metrics (CHAO1, PD Whole Tree, and Observed OTUs) did not show statistically significant differences in diversity among mineral substrate at the level of the whole ISMACS dataset (Figure 4.5a, Supplemental Figure 4.5). However, other diversity metrics (Shannon Diversity, Equitability, Simpson's Evenness) seemed to indicate that the mineral mix was more diverse than the single mineral substrates (Figure 4.5b, Supplemental Figure 4.5). Because the mineral mix was only used in the 2-year incubations, it was unclear if this apparent difference in diversity was an artifact of comparisons to samples without that substrate. Therefore, we focused subsequent alpha diversity analysis on only the two-year incubations (see two-year incubations section for description).

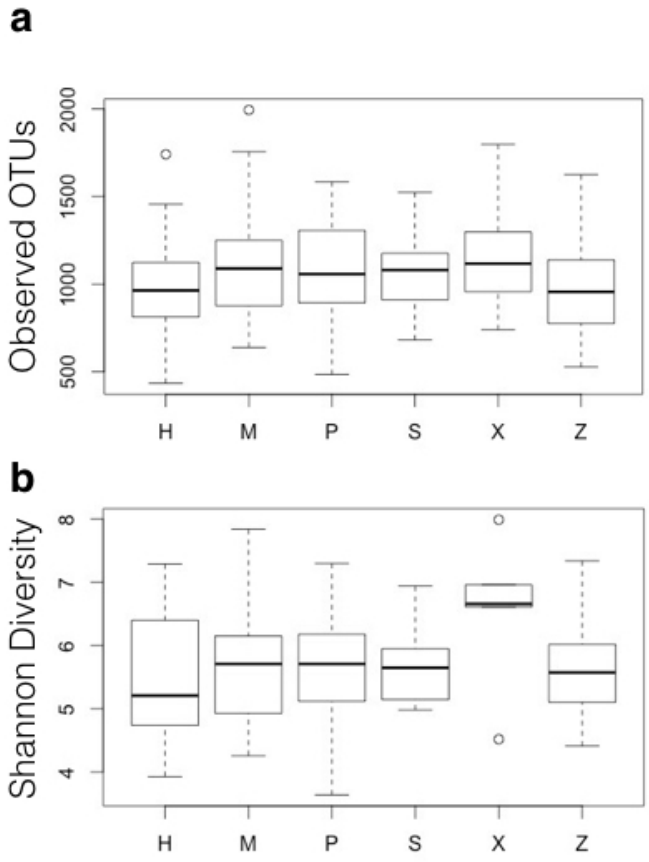

Figure 4.5 Box and whisker plot of alpha diversity of all ISMACS communities by mineral/substrate: H – hematite, M – marcasite, P – pyrite, S – sphalerite, x – mineral mix, and Z – zirconia beads. Boxplots were made in R with default settings (ends of whiskers represent the limits of the nominal range of data inferred from upper and lower quartiles, box defines lower and upper quartiles, heavy line represents median, circles values outside the nominal range of the data). Plots show (a) total observed OTUs, and (b) Simpson's Diversity metric.

Analysis of dominance

The number of dominant taxa (those taxa that represented a dataset-wide average of greater than 10% of all sequences) did not vary significantly among minerals (data not shown). There were 22 taxa (based on genus-level identification) that were dominant (>10% of sequences) in this dataset (Table 4.1). 19 of these were dominant in 10 or fewer samples. The remaining three taxa, all Epsilonproteobacteria, were unidentified

Epsilonproteobacteria, unidentified Helicobacteraceae, and *Sulfurimonas* (a genus within Helicobacteraceae). These were dominant in 36, 69, and 73 samples respectively. Where we have grouped these three taxa, we refer to them jointly as dominant Epsilonproteobacteria. Dominant Epsilonproteobacteria represented an average of 57% of each sample in this dataset (Figure 4.6).

Table 4.1 Dominant taxa (>10% of identified sequences; Epsilonproteobacteria are highlighted in orange and Deltaproteobacteria are highlighted in green)

OTU ID	average relative abundance	# samples taxa is dominant
k__Bacteria;p__Proteobacteria;c__Epsilonproteobacteria;o__Campylobacterales;f__Helicobacteraceae;g__Sulfurimonas	0.243	73
k__Bacteria;p__Proteobacteria;c__Epsilonproteobacteria;o__Campylobacterales;f__Helicobacteraceae;g__	0.207	69
k__Bacteria;p__Proteobacteria;c__Epsilonproteobacteria;o__;f__;g__	0.123	36
k__Bacteria;p__Bacteroidetes;c__Bacteroidia;o__Bacteroidales;f__VC21_Bac22;g__	0.040	10
k__Archaea;p__Euryarchaeota;c__Thermoplasmata;o__Thermoplasmatales;f__[Aciduliprofundaceae];g__	0.024	8
k__Bacteria;p__Proteobacteria;c__Deltaproteobacteria;o__;f__;g__	0.024	8
k__Bacteria;p__Proteobacteria;c__Epsilonproteobacteria;o__Campylobacterales;f__Campylobacteraceae;g__Arcobacter	0.021	6
k__Bacteria;p__Bacteroidetes;c__Bacteroidia;o__Bacteroidales;f__;g__	0.018	3
k__Bacteria;p__Proteobacteria;c__Epsilonproteobacteria;o__Campylobacterales;f__Campylobacteraceae;g__	0.018	2
k__Bacteria;p__Proteobacteria;c__Epsilonproteobacteria;o__Nautiliales;f__Nautiliaceae;g__	0.017	6
Unassigned;Other;Other;Other;Other;Other	0.015	0
k__Bacteria;p__Aquificae;c__Aquificae;o__Aquificales;f__Desulfurobacteriaceae;Other	0.013	6
k__Archaea;p__Crenarchaeota;c__Thermoprotei;o__;f__;g__	0.012	2
k__Bacteria;p__Proteobacteria;c__Deltaproteobacteria;o__Desulfurellales;f__Desulfurellaceae;g__	0.011	6
k__Bacteria;p__Proteobacteria;c__Deltaproteobacteria;o__Desulfobacterales;f__Desulfobulbaceae;g__Desulfocapsa	0.010	2
k__Bacteria;p__Proteobacteria;c__Deltaproteobacteria;o__Desulfobacterales;f__Desulfobulbaceae;g__	0.009	1
k__Bacteria;p__Proteobacteria;c__Gammaproteobacteria;o__;f__;g__	0.009	1
k__Bacteria;p__Proteobacteria;c__Deltaproteobacteria;o__AF420338;f__;g__	0.009	3
k__Bacteria;p__Proteobacteria;c__Alphaproteobacteria;o__Rhizobiales;f__;g__	0.009	4
k__Bacteria;p__Proteobacteria;c__Epsilonproteobacteria;o__Nautiliales;f__Nautiliaceae;g__Caminibacter	0.008	1
k__Bacteria;p__Proteobacteria;c__Deltaproteobacteria;o__Desulfobacterales;f__Desulfobacteraceae;g__	0.008	1

Table 4.1 continued

k__Bacteria;p__Bacteroidetes;c__Flavobacteriia;o__Flavobacteriales;f__Flavobacteriaceae;g__	0.007	1
k__Bacteria;p__Thermotogae;c__MS9;o__;f__;g__	0.005	2

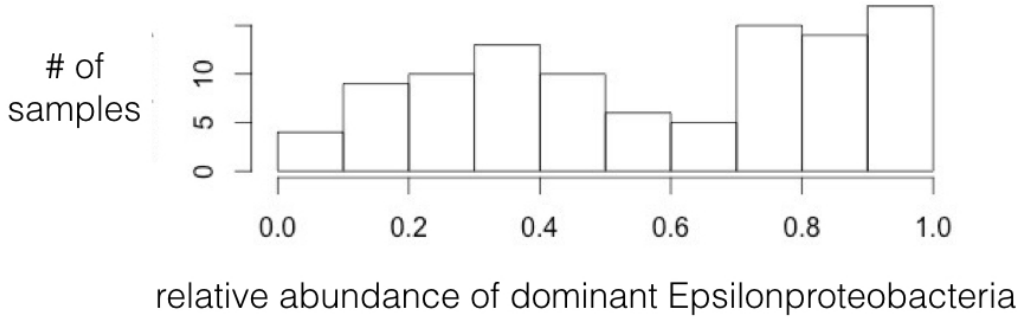

Figure 4.6 Histogram of the relative abundance of dominant Epsilonproteobacteria (combination of unidentified Epsilonproteobacteria, unidentified Helicobacteraceae and *Sulfurimonas*). These taxa jointly represent a dataset-wide averate of 57% of identified sequences.

Taxa that differed by mineral

ANOVA identified 38 OTUs with significant difference (p-value < 0.05 after correcting for multiple comparisons) in representation among the minerals and 17 in the 2-year incubations (Table 4.2), and most of these were more abundant in the mineral mix. 8 of the 17 were Deltaproteobacteria, mostly from the Desulfobacteriales, which represented about half of all Deltaproteoabcteria (Figure 4.11).

Table 4.2 Taxa demonstrating statistically significant difference in relative abundance among mineral/substrates.

Sig dif by mineral (ANOVA, P-value <0.05 after BonFerroni correction) whole data set	# of OTUs
k__Archaea; p__[Parvarchaeota]; c__[Parvarchaea]; o__WCHD3-30; f__; g__; s__	1
k__Bacteria; p__Planctomycetes; c__Planctomycetia; o__Planctomycetales; f__Planctomycetaceae; g__Planctomyces; s__	1
k__Bacteria; p__Proteobacteria; c__Alphaproteobacteria; o__Rhodobacterales; f__Rhodobacteraceae; g__; s__	1
k__Bacteria; p__Proteobacteria; c__Deltaproteobacteria; o__Desulfobacterales; f__Desulfobacteraceae; g__; s__	2
k__Bacteria; p__Proteobacteria; c__Deltaproteobacteria; o__Desulfobacterales; f__Desulfobulbaceae; g__; s__	2
k__Bacteria; p__Proteobacteria; c__Deltaproteobacteria; o__Desulfobacterales; f__Desulfobulbaceae; g__Desulfocapsa; s__	21
k__Bacteria; p__Proteobacteria; c__Deltaproteobacteria; o__Myxococcales; f__OM27; g__; s__	2
k__Bacteria; p__Proteobacteria; c__Epsilonproteobacteria; o__Campylobacterales; f__Campylobacteraceae; g__; s__	1
k__Bacteria; p__Proteobacteria; c__Epsilonproteobacteria; o__Campylobacterales; f__Helicobacteraceae; g__Sulfurimonas; s__	4
k__Bacteria; p__Proteobacteria; c__Epsilonproteobacteria; o__Campylobacterales; f__Helicobacteraceae; g__Sulfurimonas; s__autotrophica	1
k__Bacteria; p__Proteobacteria; c__Gammaproteobacteria; o__Thiotrichales; f__Thiotrichaceae; g__B46; s__	1
k__Bacteria; p__Proteobacteria; c__Gammaproteobacteria; o__Thiotrichales; f__Thiotrichaceae; g__Cocleimonas; s__	1
total	38

Sig dif by mineral (ANOVA, P-value <0.05 after BonFerroni correction) 2 year data set	
k__Archaea;p__[Parvarchaeota];c__[Parvarchaea];o__WCHD3-30;f__;g__	1
k__Bacteria;p__Planctomycetes;c__Planctomycetia;o__Planctomycetales;f__Planctomycetaceae;g__Planctomyces	1
k__Bacteria;p__Proteobacteria;c__Alphaproteobacteria;o__Rhodobacterales;f__Rhodobacteraceae;g__	1
k__Bacteria;p__Proteobacteria;c__Alphaproteobacteria;o__Rhodobacterales;f__Rhodobacteraceae;Other	1
k__Bacteria;p__Proteobacteria;c__Deltaproteobacteria;o__Desulfobacterales;f__Desulfobacteraceae;g__	1
k__Bacteria;p__Proteobacteria;c__Deltaproteobacteria;o__Desulfobacterales;f__Desulfobacteraceae;Other	1
k__Bacteria;p__Proteobacteria;c__Deltaproteobacteria;o__Desulfobacterales;f__Desulfobulbaceae;g__	2
k__Bacteria;p__Proteobacteria;c__Deltaproteobacteria;o__Desulfobacterales;f__Desulfobulbaceae;g__Desulfocapsa	1
k__Bacteria;p__Proteobacteria;c__Deltaproteobacteria;o__Desulfobacterales;f__Desulfobulbaceae;Other	2
k__Bacteria;p__Proteobacteria;c__Deltaproteobacteria;o__Myxococcales;f__OM27;g__	1
k__Bacteria;p__Proteobacteria;c__Epsilonproteobacteria;o__Campylobacterales;f__Campylobacteraceae;g__	1
k__Bacteria;p__Proteobacteria;c__Epsilonproteobacteria;o__Campylobacterales;f__Campylobacteraceae;Other	1
k__Bacteria;p__Proteobacteria;c__Epsilonproteobacteria;o__Campylobacterales;f__Helicobacteraceae;g__Sulfurimonas	1
k__Bacteria;p__Proteobacteria;c__Gammaproteobacteria;o__Thiotrichales;f__Thiotrichaceae;g__B46	1
k__Bacteria;p__Proteobacteria;c__Gammaproteobacteria;o__Thiotrichales;f__Thiotrichaceae;g__Cocleimonas	1
total	17

Additionally, Deltaproteobacteria as a whole were significantly more abundant on the mineral mix than the other minerals in the 2-year incubations (Wilcoxon Rank Sum Test between, P-Value = 0.009). Showing the opposite pattern as Deltaproteobacteria, but not statistically significant, the dominant Epsilonproteobacteria were least abundant on the mineral mix (Figure 4.7).

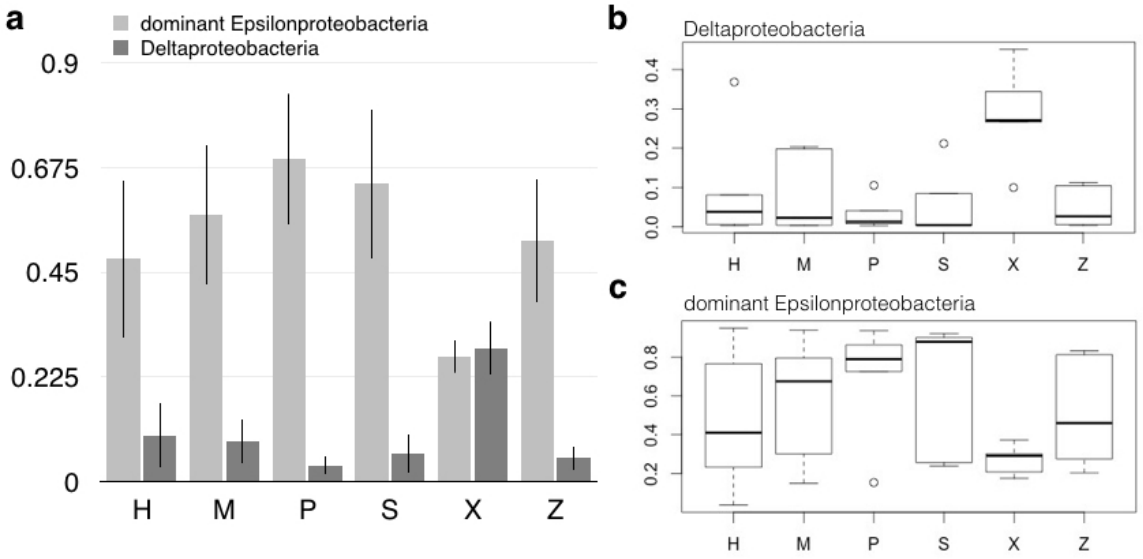

Figure 4.7 (a) Relative abundance of dominant Epsilonproteobacteria compared to total Deltaproteobacteria sequences (error bars represent standard error). Box and whisker plots of (b) Deltaproteobacteria and (c) dominant Epsilonproteobacteria relative abundance.

Succession

Initial succession analysis (described in methods) did not identify statistically significant changes in diversity over time (Supplemental Table 1). However a comparison of selected communities based on similar temperature units and only the marcasite, hematite, pyrite, and zirconia bead substrates common to all (described below), showed

that diversity (as measured by observed OTUs, CHAO1 diversity estimate, or Shannon-Wiener Diversity Index) increased with time (Table 4.3).

Table 4.3 Alpha diversity averages based on hematite, marcasite, pyrite, and zirconia bead samples

	Days Deployed	Observed OTUs	Chao1	Shannon	Simpson's evenness
low	2	1011	2481	5.40	0.015
temp.	40	1139	2823	6.14	0.019
units	685	1246	3175	6.22	0.018
high					
temp.	2	982	2379	5.45	0.014
units	40	1211	3088	5.86	0.015

To investigate patterns in succession, while minimizing heterogeneity among ISMACS incubated at different temperatures, we selected Units 12, 11, and 12b which were incubated fairly consistently around 10°C for 2, 40, and 685 days respectively. We examined the most abundant 25 taxa from these units and identified taxa that showed either increase or decrease over time (from 2 to 40 to 685 days). Taxa represent the lowest taxonomic identification (for example a class means unidentified within that class). Seven of these taxa decreased over time and 14 increased with time (Table 4.4).

Table 4.4 Low temperature time series: Units 12, 11, & 12b

	Taxa	2 day ave.	40 day ave.	685 day ave.	3-5 day standard error	40 day standard error	685 day standard error	abundance rank (1-25)
potential early colonizers	k__Bacteria;p__Proteobacteria;c__Epsilonproteobacteria;o__Campylobacterales;f__Helicobacteraceae;g__Sulfurimonas	0.4221	0.2573	0.1455	0.1070	0.0738	0.0489	1
	k__Bacteria;p__Proteobacteria;c__Epsilonproteobacteria;o__;f__;g__	0.1522	0.0478	0.0293	0.0483	0.0160	0.0164	3
	k__Bacteria;p__Proteobacteria;c__Epsilonproteobacteria;o__Campylobacterales;f__Campylobacteraceae;g__Arcobacter	0.0536	0.0403	0.0157	0.0231	0.0213	0.0084	5
	k__Archaea;p__Euryarchaeota;c__Thermoplasmata;o__Thermoplasmatales;f__[Aciduliprofundaceae];g__	0.0448	0.0002	0.0003	0.0422	0.0001	0.0001	11
	k__Bacteria;p__Proteobacteria;c__Epsilonproteobacteria;o__Nautiliales;f__Nautiliaceae;g__	0.0280	0.0020	0.0030	0.0167	0.0006	0.0022	16
	k__Bacteria;p__Proteobacteria;c__Deltaproteobacteria;o__Desulfurellales;f__Desulfurellaceae;g__	0.0185	0.0002	0.0001	0.0169	0.0001	0.0000	20
	k__Bacteria;p__Proteobacteria;c__Gammaproteobacteria;o__Oceanospirillales;f__SUP05;g__	0.0105	0.0023	0.0051	0.0040	0.0009	0.0028	23
potential late successional taxa	k__Bacteria;p__Proteobacteria;c__Epsilonproteobacteria;o__Campylobacterales;f__Helicobacteraceae;g__	0.0776	0.2541	0.2330	0.0156	0.0478	0.0498	2
	k__Bacteria;p__Bacteroidetes;c__Bacteroidia;o__Bacteroidales;f__VC21_Bac22;g__	0.0093	0.0552	0.0731	0.0075	0.0314	0.0396	4
	k__Bacteria;p__Proteobacteria;c__Epsilonproteobacteria;o__Campylobacterales;f__Campylobacteraceae;g__	0.0049	0.0307	0.0418	0.0017	0.0112	0.0137	6
	k__Bacteria;p__Proteobacteria;c__Alphaproteobacteria;o__Rhizobiales;f__;g__	0.0001	0.0196	0.0419	0.0000	0.0195	0.0146	7
	k__Bacteria;p__Bacteroidetes;c__Bacteroidia;o__Bacteroidales;f__;g__	0.0033	0.0227	0.0294	0.0023	0.0080	0.0052	8
	Unassigned;Other;Other;Other;Other;Other	0.0137	0.0138	0.0205	0.0071	0.0038	0.0058	9
	k__Bacteria;p__Proteobacteria;c__Deltaproteobacteria;o__Desulfobacterales;f__Desulfobacteraceae;g__	0.0039	0.0119	0.0285	0.0038	0.0055	0.0148	12
	k__Bacteria;p__Proteobacteria;c__Deltaproteobacteria;o__Desulfobacterales;f__Desulfobulbaceae;g__Desulfocapsa	0.0012	0.0124	0.0290	0.0009	0.0107	0.0080	13
	k__Bacteria;p__Proteobacteria;c__Deltaproteobacteria;o__Desulfobacterales;f__Desulfobulbaceae;g__	0.0016	0.0112	0.0261	0.0011	0.0059	0.0099	14
	k__Bacteria;p__Proteobacteria;c__Gammaproteobacteria;o__;f__;g__	0.0024	0.0186	0.0177	0.0008	0.0102	0.0059	15
	k__Bacteria;p__Bacteroidetes;c__Bacteroidia;o__Bacteroidales;f__SB-1;g__	0.0033	0.0081	0.0188	0.0033	0.0047	0.0061	17
	k__Bacteria;p__Bacteroidetes;c__Flavobacteriia;o__Flavobacteriales;f__Flavobacteriaceae;g__	0.0008	0.0038	0.0256	0.0002	0.0015	0.0090	18
	k__Bacteria;p__Proteobacteria;c__Deltaproteobacteria;o__Desulfuromonadales;f__Desulfuromonadaceae;g__	0.0006	0.0037	0.0140	0.0003	0.0018	0.0044	21
	k__Bacteria;p__Proteobacteria;c__Gammaproteobacteria;o__Chromatiales;f__;g__	0.0015	0.0054	0.0109	0.0004	0.0020	0.0047	24

Table 4.4 continued

	Taxa	2 day average	40 day average	685 day average	3-5 day standard error	40 day standard error	685 day standard error	abundance rank (1-25)
	k__Bacteria;p__Proteobacteria;c__Deltaproteobacteria;o__;f__;g__	0.0020	0.0371	0.0076	0.0006	0.0267	0.0025	10
no successional pattern	k__Bacteria;p__Spirochaetes;c__Spirochaetes;o__Spirochaetales;f__Spirochaetaceae;g__	0.0018	0.0131	0.0061	0.0017	0.0060	0.0032	19
	k__Bacteria;p__Proteobacteria;c__Deltaproteobacteria;o__Desulfuromonadales;f__Desulfuromonadaceae;g__Desulfuromonas	0.0066	0.0023	0.0095	0.0065	0.0016	0.0057	22
	k__Bacteria;p__WWE1;c__[Cloacamonae];o__[Cloacamonales];f__MSBL8;g__	0.0047	0.0064	0.0064	0.0046	0.0058	0.0058	25

We then examined our high temperature ISMACS (Units 3 & 4) in a similar manner to see if any of the most abundant high temperature taxa showed similar patterns to the low temperature taxa (Supplemental Table 2). The abundant epsilonproteobacteria showed opposite patterns (those from the cold units decreasing over time, and those from hot increasing). Four taxa decreased over time in both the hot and cold units: Desulfurellaceae, Arcobacter, Nautiliaceae, and Aciduliprofundaceae (Figure 4.8). Five taxa increased over time in both hot and cold units: Flavobacteraceae, Camplylobacteraceae, Bacteroidales, VC21 Bac22, and Desulfobacteraceae (Figure 4.9).

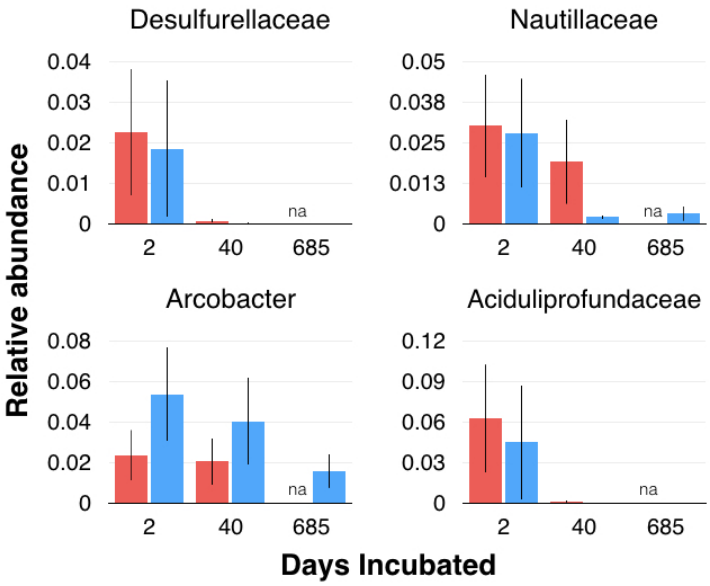

Figure 4.8 Taxa that decreased over time in both high (red bars) and cold (blue bars) time series. Note that long-term (685 day) data was not available at high temperature because none of the units incubated long-term maintained high enough temperature consistently (see Figure 4.3).

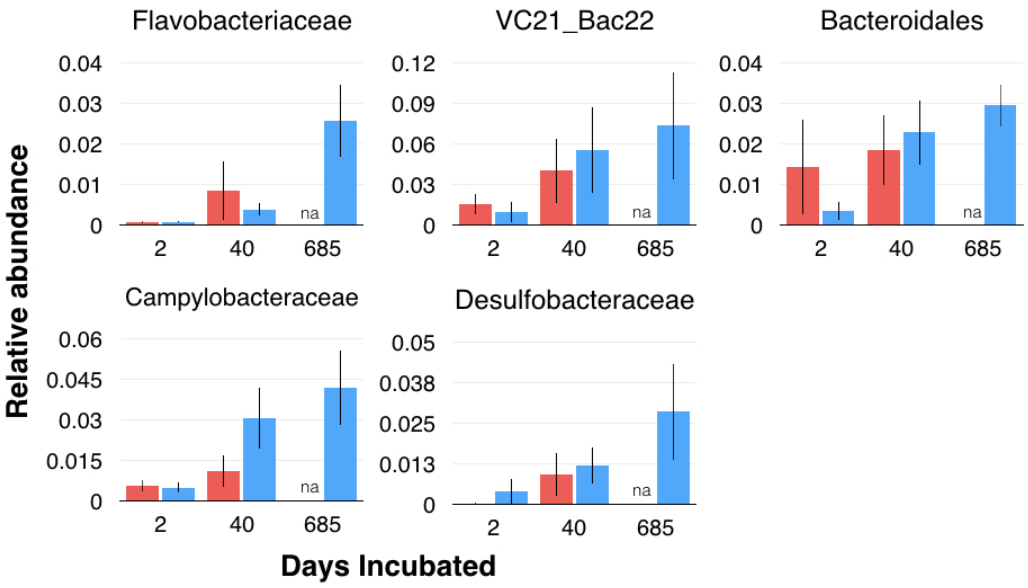

Figure 4.9 Taxa that increased over time in both high (red bars) and cold (blue bars) time series.

Two-year incubations

Among the two-year incubations, hematite communities were the least diverse and mineral mix communities the most diverse (Figure 4.10). The difference in diversity between these mineral conditions was statistically significant, (Wilcoxon Rank Sum test, P-Value =0.05). Communities from other minerals had diversities intermediate in diversity between those two. The increased diversity on the mineral mix substrate appears to be due to Deltaproteobacteria, in particular Desulfobacteriales in the families Desulfobacteraceae and Desulfobulbaceae (Figure 4.11). Additionally, the relative abundance of Epsilonproteobacteria was lower on the mineral mix than the single mineral in the two-year deployments (Figure 4.7), although this difference was not statistically significant.

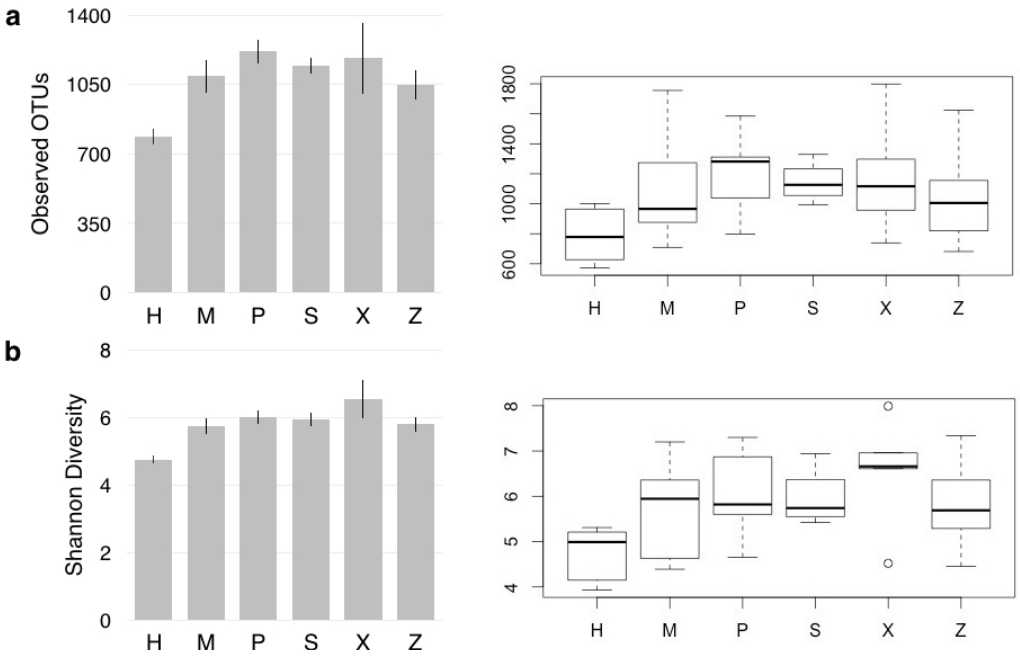

Figure 4.10 Alpha diversity of 2-year incubation communities by mineral substrate (H – hematite, M – marcasite, P – pyrite, S – sphalerite, X – mineral mix, Z – zirconia beads). Average (a) Observed OTUs and (b) Shannon diversity values depicted as bar plot with error bar representing standard error and box and whisker plot. Hematite communities are significantly less diverse than those from other mineral/substrates (Wilcoxon Rank Sum Test, p-values = 0.008 (Observed OTUs) and 0.006 (Shannon Diversity). Mineral mix communities were are the most diverse, but differences were not statistically significant.

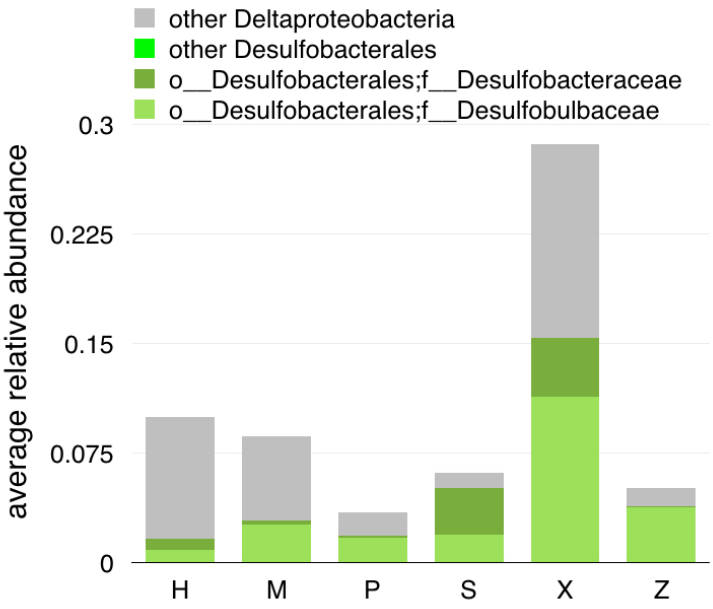

Figure 4.11 Differences in Deltaproteobacteria relative abundance in the 2-year incubations were statistically significant (Wilcoxon Rank Sum Test, P-Value = 0.009). In particular, the families Desulfobacteraceae and Desulfobulbaceae, which were the vast majority of identified Desulfobacterales, identified as individual taxa that showed significant difference in relative abundance by mineral (Table 4.2).

DISCUSSION

Patterns in microbial colonization of solid phase substrates in hydrothermal settings could be predicted simply based on mineral reactivity and thermodynamics. The data presented here, however, reveal patterns of colonization that are (not surprisingly) far more complex. These observations likely reflect the concurrent influences of fluid geochemistry, ecological interactions, and –to a lesser extent- the substrate mineralogy. We observed Epsilonproteobacteria dominating most communities regardless of mineral, temperature, or incubation length. We observed lower diversity on hematite than other single mineral treatments. We identified some potential early and late colonizer taxa (irrespective of mineralogy). Finally, we observed a surprising increase in diversity

(particularly of Deltaproteobacteria) on mixed mineral assemblages, which may point to the role of cryptic elemental cycling or electrochemical gradients in enabling certain taxa to outcompete the dominant Epsilonproteobacteria when in close proximity to a diversity of mineral substrates. The paragraphs below present these points in further detail.

Epsilonproteobacteria, rather than mineral substrate, appears to be the dominant aspect of community structure

In these experiments, mineralogy did not appear to structure microbial communities at the level of comparing whole samples (Figure 4.4). We initially set out to decouple the influence of temperature, chemistry, and mineralogy on surface-attached microbial communities in diffuse flows. It is likely that chemistry, temperature or other ecological processes such as founder effects may be exerting stronger overall influence on these communities than mineral substrate.

The vast majority of samples had communities that were dominated by Epsilonproteobacteria - specifically unidentified Epsilonprotebacteria, unidentified Helicobacteraceae, and the genus *Sulfimonas* within the family Helicobacteraceae. Only 4 ISMACS mineral communities were less than 10% sequences from these taxa, and more than half of the communities were more than 50% sequences from these taxa. It is likely that this is a reflection of the microbial community being transported in the vent fluid (described in Akerman *et al.*, 2013). It is unclear from these data whether these organisms are active members of the surface attached community, or simply so abundant because there is a constant influx of them from the subsurface. Previous work at Axial Seamount has shown 16S rRNA DNA libraries from diffuse flow fluid communities to be between 18%

and 52% Epsilonproteobacteria, with *Sulfurovum* and *Sulfurimonas* being the most abundant (Akerman *et al.*, 2013). This is broadly consistent with our data, although our communities were far more dominated by sequences identified as *Sulfurimonas*, and showed even higher relative abundance of total Epsilonproteobacteria (more than half of ISMACS mineral communities were greater than 60% Epsilonproteobacteria). This increased relative abundance of Epsonproteobacteria (particularly *Sulfurimonas*) in mineral associated communities relative to fluid communities from Akerman *et al.* (2013) suggests that these microbes are being selected for in the surface attached communities, but not due to any mineral-specific metabolic process.

Hematite hosts lower diversity communities

While community structure as a whole did not appear to be substantially influenced by minerals, there were some differences that were attributable to mineral substrate. In the two-year incubations the communities on hematite were significantly less diverse than those on the other minerals (Figure 4.10). This is likely because hematite is most stable, and therefore least available to microbes, of the mineral substrates incubated. Sulfide minerals (e.g. pyrite, marcasite, and sphalerite) are subject to physical dissolution as well as chemical oxidation of Fe(II). Iron oxides on the other hand (e.g., hematite) are only subject to dissolution under oxic and near neutral pH conditions of these incubations (described in detail in Rickard and Luther, 2007). Additionally, hematite is one of the less reactive, and slower to dissolve iron oxides (Sidhu *et al.*, 1981). In contrast to the oxides, iron sulfides dissolved and oxidized under our incubation conditions, making them much more available to microbes. When Edwards and colleagues (2003) incubated iron sulfides

and other substrates in a low temperature hydrothermal environment, they found the cell densities on these substrates generally correlated with oxidative dissolution rate (the most reactive minerals to oxidizing species were the most heavily colonized; marcasite > pyrite > sphalerite > chalcopyrite). One caveat, however, is that if stability and metabolic inaccessibility of the mineral is the reason hematite showed lower diversity, it is unclear why the zirconia bead communities would not have had similarly low diversity.

Time series produced hypotheses for future investigation

While we lacked the replication to carry out robust statistical analyses of patterns in succession, our data were sufficient to produce testable hypotheses for future analyses, and are consistent with other recent studies of succession in hydrothermal environments. Gulmann and colleagues (2015) incubated basalt panels in diffuse flows on the East Pacific Rise. Consistent with our results, they found that diversity increased over their 9 month incubation from almost entirely Epsilonproteobacteria to a much more diverse community of Epsilon-, Gamma-, Deltaproteobacteria and Bacteroidetes. We, similarly, found an increase in diversity in our temperature controlled, time-series analyses (Table 4.3). Gulmann *et al.* (2015) also found that *Sulfurovum* was dominant at early time points (we found *Sulfurovum* dominant at all time points and decreased in abundance over time at low temperature; Supplemental Figure 2). Similar to Gulmann *et al.* (2015) this work identifies *Sulfurovum* and *Arcobacter* as low temperature early colonists (in our work, *Arcobacter* seems to follow this pattern at high temperature as well).

The abundance and dominance of *Sulfurovum* and other unidentified Epsilonproteobacteria across so many of our samples (Figure 4.6) is likely due to their

abundance in the source vent fluids. Epsilonproteobacteria are well established as being abundant in diffuse flows in ASHES vent field (e.g., Huber *et al.*, 2003; Akerman *et al.*, 2013). It has been proposed that these vent-associated Epsilonproteobacteria use their EPS production and quorum sensing abilities to establish a persistent biofilm, perhaps paving the way for a more diverse community over time (Gulmann *et al.*, 2015). Their decrease in abundance over time in our cold time series samples could be explained as a product of biofilm formation facilitating the eventual establishment of metabolically mineral-associated taxa.

We propose that taxa that decrease in abundance in these selected time series units are potentially early successional organisms that have an advantage colonizing bare substrates. The taxa that decreased over time in both our low and high temperature time series are the families Aciduliprofundaceae, Nautiliaceae, and Desulfurellaceae, and the genus *Arcobacter* (Figure 4.8). Similarly we propose that taxa that increase over time in these communities are potentially late successional taxa, which have a selective advantage once an initial biofilm has formed. Taxa that increased in relative abundance over time in both the high and low temperature time series are the order Bacteroidales, families VC21 Bac22, Campylobacteraceae, Flavobacteriaceae, and Desulfobacteraceae (Figure 4.9). These incubations lack the replication at similar temperatures and time points that would be necessary to analyze the significance of these successional patterns. We therefore suggest these early and late successional taxa as hypotheses to be tested in future studies.

The mineral mix supports a diverse Deltaproteobacteria community

In addition to overall diversity, the abundance of certain taxa was correlated with mineralogy. Again in the two-year incubation, Deltaproteobacteria were significantly more abundant on the mineral mix substrate than the other minerals or zirconia beads. In particular, two families of Deltaproteobacteria (Desulfobacteraceae and Desulfobulbaceae) made up roughly half of all the Deltaproteobacteria (Figure 4.11). Desulfobacteraceae are known to be anaerobic sulfate reducers, while Desulfobulbaceae are aerobic sulfide oxidizers. Their co-occurrence highlights the heterogeneity of these communities, and can be explained by coexistence in a biofilm that may have aerobic and anaerobic portions. While the water entering the colonization units was not anaerobic, portions of mineral-attached biofilms certainly could have been. This underscores the need for chemical measurements made at microbially relevant scales.

Both of these families (as well as other Deltaproteobacteria) have been demonstrated to be capable of extracellular electron transfer (EET; Ishii *et al.*, 2013). We hypothesize that the different minerals in close contact in the mineral mix condition produce an electrochemical gradient that these EET-capable microbes are able to take metabolic advantage of, conferring them a selective advantage. The standard redox potentials of the possible redox couples in the mineral mix condition indicate that using pyrite (or marcasite) as an electron donor and hematite as an electron acceptor could establish a favorable electrochemical gradient (ΔE up to 1.705 volts; Supplemental Figure 1). While this gradient is less favorable than using oxygen or nitrate as an electron acceptor, it opens up additional electrochemical niches for microbes capable of EET that are not available in the single mineral conditions.

Conclusions

Despite Epsilonproteobacteria, (in particular the family Helicobacteraceae and genus *Sulfurimonas*) dominating most of our samples, significant mineral-specific trends were apparent in these data. In our long-term incubations, we observed lower diversity on hematite, and a higher diversity and abundance of Deltaproteobacteria on the mineral mix than on the individual mineral substrates. This indicates that while the abundance of dominant taxa in this system is likely influenced by factors other than mineralogy, mineralogy (specifically the condition of having access to multiple minerals) appears to confer selective advantage on some rarer taxa. Taxa such as the Deltaproteobacteria families Desulfobacteraceae and Desulfobulbaceae are known to be capable of extracellular electron transfer and may be specialized to take advantage of electrochemical gradients between minerals that would be common in hydrothermal vent chimney. In addition to mineral-specific trends, we identified potential early successional taxa (Desulfurellaceae, Nautiliaceae, Arcobacter, and Aciduliprofundaceae) and late successional taxa (Flavobacteriaceae, Campylobacteraceae, Bacteroidales, VC21 Bac22, and Desulfobacteraceae).

The dynamic geochemical environment of hydrothermal vents makes it inherently challenging to draw causal relationships between microbial communities and the abiotic factors that influence them. The data described herein underscore the substantial heterogeneity inherent to these microbial communities, but more importantly offer insight into their structure, succession, and primary productivity. This work extends our thinking about microbe-mineral interactions at vents to include the possibility that specific

combinations of minerals, in addition to individual mineral substrates, may influence the metabolism and structure of microbial communities.

REFERENCES

Akerman, N.H., Butterfield, D.A., and Huber, J.A. (2013) Phylogenetic diversity and functional gene patterns of sulfur-oxidizing subseafloor Epsilonproteobacteria in diffuse hydrothermal vent fluids. *Front. Microbio.* **4**: 185.

Apprill, A., McNally, S., Parson, R., Weber, L., (2015) Minor revision to V4 region SSU rRNA 806R gene primer greatly increases detection of SAR11 bacterioplankton. *Aquatic Microb. Eco.* **75** 129-137.

Callac, N., Rommevaux-Jestin, C., Rouxel, O., Lesongeur, F., Liorzou, C., Bollinger, C., et al. (2013) Microbial colonization of basaltic glasses in hydrothermal organic-rich sediments at Guaymas Basin. *Front. Microbio.* **4**: 1-20.

Caporaso, J.G., Kuczynski, J., Stombaugh, J., Bittinger, K., Bushman, F.D., Costello, E.K., et al. (2010) QIIME allows analysis of high-throughput community sequencing data. *Nat. Methods* **7**: 335–336.

Caporaso, J.G., Lauber, C.L., Walters, W.A., Berg-Lyons, D., Huntley, J., Fierer, N., et al. (2012) Ultra-high-throughput microbial community analysis on the Illumina HiSeq and MiSeq platforms. *ISME J* **6**: 1621–1624.

Case, D.H., Pasulka, A.L., Marlow, J.J., Grupe, B.M., Levin, L.A., and Orphan, V.J. (2015) Methane Seep Carbonates Host Distinct, Diverse, and Dynamic Microbial Assemblages. *MBio* **6**: e01348–15.

Edwards, K.J., McCollom, T.M., Konishi, H., and Buseck, P.R. (2003) Seafloor bioalteration of sulfide minerals: results from in situ incubation studies. *Geochimica et Cosmochimica Acta* **67**: 2843–2856.

Edwards, K.J., Schrenk, M.O., Hamers, R., and Banfield, J.F. (1998) Microbial oxidation of pyrite; experiments using microorganisms from an extreme acidic environment. *American Mineralogist* **83**: 1444–1453.

Gulmann, L.K., Beaulieu, S.E., Shank, T.M., Ding, K., Seyfried, W.E., and Sievert, S.M. (2015) Bacterial diversity and successional patterns during biofilm formation on freshly exposed basalt surfaces at diffuse-flow deep-sea vents. *Front. Microbio.* **6**: 227–16.

Harrison, B.K. and Orphan, V.J. (2012) Method for Assessing Mineral Composition-Dependent Patterns in Microbial Diversity Using Magnetic and Density Separation. *Geomicrobiology Journal* **29**: 435–449.

Huber, J.A., Butterfield, D.A., and Baross, J.A. (2003) Bacterial diversity in a subseafloor habitat following a deep-sea volcanic eruption. *FEMS Microbiology Ecology* **43**: 393–409.

Hutchens, E. (2009) Microbial selectivity on mineral surfaces: possible implications for weathering processes. *Fungal Biology Reviews* **23**: 115–121.

Ishii, S.R.I., Suzuki, S., Norden-Krichmar, T.M., Tenney, A., Chain, P.S.G., Scholz, M.B., et al. (2013) A novel metatranscriptomic approach to identify gene expression dynamics during extracellular electron transfer. *Nat Comms* **4**: 1601–10.

Juncher Jørgensen, C., Jacobsen, O.S., Elberling, B., and Aamand, J. (2009) Microbial Oxidation of Pyrite Coupled to Nitrate Reduction in Anoxic Groundwater Sediment. *Environ. Sci. Technol.* **43**: 4851–4857.

Kormas, K.A., Tivey, M.K., Damm, Von, K., and Teske, A. (2006) Bacterial and archaeal phylotypes associated with distinct mineralogical layers of a white smoker spire from a deep-sea hydrothermal vent site (9oN, East Pacific Rise). *Environmental Microbiology* **8**: 909–920.

Kostka, J.E. and Nealson, K.H. (1995) Dissolution and reduction of magnetite by bacteria. *Environ. Sci. Technol.* **29**: 2535–2540.

Lovley, D.R. (1991) Dissimilatory Fe(III) and Mn(IV) Reducion. *Microbiological Reviews* **55**: 259–287.

Nordstrom, D.K. and Southam, G. (1997) Geomicrobiology of sulfide mineral oxidation. In, Banfield,J.F. and Nealson,K.H. (eds), *Geomicrobiology Interactions between Microbes and Minerals*. Reviews in mineralogy, pp. 361–390.

Orcutt, B., Wheat, C.G., and Edwards, K.J. (2010) Subseafloor Ocean Crust Microbial Observatories: Development of FLOCS (FLow-through Osmo Colonization System) and Evaluation of Borehole Construction Materials. *Geomicrobiology Journal* **27**: 143–157.

Orcutt, B.N., Bach, W., Becker, K., Fisher, A.T., Hentscher, M., Toner, B.M., et al. (2011) Colonization of subsurface microbial observatories deployed in young ocean crust. *ISME J* **5**: 692–703.

Rickard, D. and Luther, G.W. (2007) Chemistry of Iron Sulfides. *Chem. Rev.* **107**: 514–562.

Roine, A., HSC Chemistry Database 5.11, Outokumpu Research, Finland (2002)

Schrenk, M.O., Kelley, D.S., Delaney, J.R., and Baross, J.A. (2003) Incidence and Diversity of Microorganisms within the Walls of an Active Deep-Sea Sulfide Chimney. *Applied and Environmental Microbiology* **69**: 3580–3592.

Sidhu, P.S., Gilkes, R.J., Cornell, R.M., and Posner, A.M. (1981) Dissolution of iron oxides and oxyhydroxides in hydrochloric and perchloric acids. *Clays and Clay Minerals* **29**: 269–276.

Smith, A., Popa, R., Fisk, M., Nielsen, M., Wheat, C.G., Jannasch, H.W., et al. (2011) In situ enrichment of ocean crust microbes on igneous minerals and glasses using an osmotic flow-through device. *Geochem. Geophys. Geosyst.* **12**: n/a–n/a.

Smith, A.R., Fisk, M.R., Thurber, A.R., Flores, G.E., Mason, O.U., Popa, R., and Colwell, F.S. (2016) Deep Crustal Communities of the Juan de Fuca Ridge Are Governed by Mineralogy. *Geomicrobiology Journal* 00–00.

Suzuki, Y., Inagaki, F., Takai, K., Nealson, K.H., and Horikoshi, K. (2004) Microbial Diversity in Inactive Chimney Structures from Deep-Sea Hydrothermal Systems. *Microb Ecol* **47**: 186–196.

Sylvan, J.B., Sia, T.Y., Haddad, A.G., Briscoe, L.J., Toner, B.M., Girguis, P.R., and Edwards, K.J. (2013) Low Temperature Geomicrobiology Follows Host Rock Composition Along a Geochemical Gradient in Lau Basin. *Front. Microbio.* **4**: 1–18.

Toner, B.M., Lesniewski, R.A., Marlow, J.J., Briscoe, L.J., Santelli, C.M., Bach, W., et al. (2013) Mineralogy Drives Bacterial Biogeography of Hydrothermally Inactive Seafloor Sulfide Deposits. *Geomicrobiology Journal* **30**: 313–326.

Toner, B.M., Santelli, C.M., Marcus, M.A., Wirth, R., Chan, C.S., McCollom, T., et al. (2009) Biogenic iron oxyhydroxide formation at mid-ocean ridge hydrothermal vents: Juan de Fuca Ridge. *Geochimica et Cosmochimica Acta* **73**: 388–403.

Weber, K.A., Achenbach, L.A., and Coates, J.D. (2006) Microorganisms pumping iron: anaerobic microbial iron oxidation and reduction. *Nat Rev Micro* **4**: 752–764.

Chapter 5

Conclusions

One major unifying theme running through all of these chapters is that of heterogeneity and scale. In each chapter, initial hypotheses of clear correlations with geochemistry or variation by mineral substrate were not supported. Instead, the roles of chemistry or mineral substrate in structuring community composition or activity was overshadowed by the substantial heterogeneity inherent to these, and likely all, microbial communities. There is a fundamental unanswered question in microbial ecology that extends far beyond the scope of this work – over what scale to microbial communities vary, and how do we know if we are sampling them and collecting metadata appropriately? Answering these questions would enable us to more fully understand the broader relevance of any study such as the ones presented here.

This question of scale could be addressed in hydrothermal vent ecosystems through a systematic attempt to describe composition and structure of microbial communities (be it from fluids, sulfide chimneys, or sediments) at multiple spatial scales. For example by extracting DNA and sequencing the 16S gene from multiple sub-samples within a sample of a vent chimney sulfide, multiple samples from a single chimney, multiple chimneys from the same vent field, and multiple vent fields along the same tectonic plate boundary, we could begin to determine how much variability there is in microbial communities at these different scales. This would enable us to better understand how representative the single samples are of the chimneys (or diffuse flows) from which they were collected. In fact, many (if not all) of the samples necessary to perform this analysis already exist in lab freezers.

Despite the substantial heterogeneity of these communities, I was able to draw some broad conclusions through this work. Each of these chapters is related to

chemosynthesis at hydrothermal vents. By measuring rates directly (Chapter 2), investigating total microbial activity (Chapter 3), and examining the role of solid-state mineral substrates as electron donors and acceptors (Chapter 4), I have investigated diverse aspects of microbial chemosynthesis at vents. I have demonstrated the importance of low temperature habitats in vent fields for microbial activity overall, and for primary productivity specifically. By measuring higher rates of carbon fixation at low temperature (in Chapter 2) and subsequently identifying hydrothermally influenced microbial activity throughout the intra-field vent waters (in Chapter 3), this work highlights the need to study hydrothermal vent fields inclusively, rather than focusing solely on a specific vent habitat (e.g., chimney, diffuse flow, or plume).

Perhaps the broadest question related to chemosynthesis at hydrothermal vents is how far reaching is its extent. Most models of global carbon cycling depict the deep sea simply as a sink for carbon that escapes consumption as it sinks to the seafloor and eventually gets buried. However, at hydrothermal vents inorganic carbon is fixed and converted into biomass. This process is clearly relevant on local scales, but its relevance to the global carbon is unclear. While it is likely to be minimal, the carbon fixation rate measurements (Chapter 2) and discussion of activity throughout entire vent fields (Chapter 3) are steps towards being able to predict the overall scale of carbon fixation at vents globally. Before global estimates can be made, however, more rate measurements are needed from different types of hydrothermal structures. Similarly, the potential for and extent of microbial carbon fixation in intra-field fluids between and among chimney structures need to be evaluated in a variety of hydrothermal vent fields.

Finally, Chapter 4 provides a compelling hypothesis that Deltaproteobacteria (and likely other microbes) are taking advantage of electrochemical gradients between minerals. However, direct evidence from laboratory experiments is needed to confirm this. For example, various available strains of Deltaproteobacteria known to carry out extracellular electron transport could be grown in single and multiple mineral conditions where it would be possible to test the influence of mineral substrate on growth rate. It would also be possible to assess the influence of different combinations of minerals on growth, and determine if predictions of favorability based on calculated Standard Redox Potential would be supported by growth rate data.

Taken together, the work presented in this dissertation deepens our understanding of the influence that abiotic factors (specifically temperature, chemistry, and mineralogy) have on free-living chemosynthetic microbial communities in hydrothermal vent ecosystems. These data emphasize the importance of low temperature habitats in this environment characterized by high temperature, they also highlight the intra-field habitat as an often overlooked, but potentially important component of hydrothermal vent ecosystems, and they demonstrate the influence of different mineral substrates on these microbial communities.

Hydrothermal vent ecosystems regulate aspects of global ocean chemistry, are sources of valuable biological and mineral resources, and represent analogue environments for early Earth as well as potentially habitable extraterrestrial worlds. In the roughly 40 years since their discovery, these ecosystems have taught us a huge amount about life on Earth (and potentially beyond), but there are still vast areas of unexplored seafloor, and likely many vent fields containing species new to science with unique

adaptation to the extreme conditions of temperature and chemistry found at vents. As global pressure for mineral resources builds, it is important to continue to learn as much as possible about the nature of these communities in their undisturbed states, so that future impacts can be assessed once mining begins. Additionally, the prospect of visits to planetary bodies such as Europa within our lifetime underscore the importance of better understanding chemosynthesis, in particular carbon fixation, at hydrothermal vents.

Appendix A

Supplemental Material for Chapter 2

Tables for Supplemental Information

Table S1 Published rates of carbon fixation from hydrothermal vent chimneys

Sample Type	Location	Incubation Conditions	Reported Units	Converted units for comparison	Rates of Carbon Fixation	Reference
anhydrite-rich chimney sulfides	Middle Valley, JdFR	4°C, 25°C - shipboard	nmol C g chimney^{-1} d^{-1}	nmol C g chimney-1 d-1	0.03 - 33.63	this study
rusty, partially oxidized sulfide "scrapings"	26°N, MAR	20°C, 50°C - shipboard	umol CO2 fixed ml suspension^{-1}	nmol C g chimney-1 d-1	3 - 50	Wirsen et al., 1993[a]
sulfide surface "scrapings"	26°N, MAR	20°C, 80°C - shipboard	umol CO2 fixed ml suspension^{-1}	nmol C g chimney-1 d-1	13 - 130	Wirsen et al., 1993[a]
sulfide 1.4 cm below surface "scrapings"	26°N, MAR	80°C - shipboard	umol CO2 fixed ml suspension^{-1}	nmol C g chimney-1 d-1	1	Wirsen et al., 1993[a]
incubated scrapings from sulfide surfaces	Snake pit (23°N) & TAG (26°N) MAR	room temp - shipboard	nmol C fixed mg protein^{-1} 5hrs^{-1}	nmol C mg protein^{-1} d^{-1}	12, 72	Polz et al,. 1998
Scrapings from incubated chunks of sulfide	26°N, MAR – TAG	*in situ*, 30-35°C	umol C cm^{-2} (surface area)	nmol C cm^{-2} d^{-1}	63, 183	Eberbard et al 1995
Scrapings from incubated chunks of sulfide	26°N MAR - Snakepit	*in situ*, 12-25°C	umol C cm^{-2} (surface area)	nmol C cm^{-2} d^{-1}	35, 79	Eberbard et al 1995
sulfide in vent water	13°N, EPR	65, 80, 90, 100°C - shipboard	ng C cm-3 d-1	nmol C cm-3 d-1	0 – 02.5	Bonch-Osmolovskaya et al., 2011[b,c]
Hydrothermal Fluid	Galapagos Rift - "Mussel Bed"	in situ ~2500m	nmol C liter^{-1} day^{-1}	nmol C ml^{-1} d^{-1}	0.08 - 0.3	Tuttle et al., 1983
Hydrothermal Fluid	Galapagos Rift - "Rose Garden"	in situ ~2500m	nmol C liter^{-1} day^{-1}	nmol C ml^{-1} d^{-1}	0.003 - 0.4	Tuttle et al., 1983
Hydrothermal Fluid	EPR - "Holger's Hole" (23°C)	3°C	nmol C liter^{-1} day^{-1}	nmol C ml^{-1} d^{-1}	n.d. – 0.03	Tuttle et al., 1985
Hydrothermal Fluid	EPR - "Holger's Hole" (23°C)	23°C	nmol C liter^{-1} day^{-1}	nmol C ml^{-1} d^{-1}	0.04 - 0.14	Tuttle et al., 1985
Hydrothermal Fluid	EPR - White Smoker (160°C)	3°C	nmol C liter^{-1} day^{-1}	nmol C ml^{-1} d^{-1}	n.d. - 0.05	Tuttle et al., 1985
Hydrothermal Fluid	EPR - White Smoker (160°C)	23°C	nmol C liter^{-1} day^{-1}	nmol C ml^{-1} d^{-1}	0.21 - 0.52	Tuttle et al., 1985
Hydrothermal Fluid	JdFR - Axial	shipboard, temp not	mg C m^{-3} day^{-1}	nmol C ml^{-1} d^{-1}	201.5	Chase et al., 1985

Hydrothermal Fluid	EPR - 21°N	reported in situ, 2600m	mg C m^{-3} day^{-1}	nmol C ml^{-1} d^{-1}	1.2	Wirsen et al., 1986
Hydrothermal Fluid	EPR - 21°N	shipboard, 3°C	mg C m^{-3} day^{-1}	nmol C ml^{-1} d^{-1}	n.d. - 5.0	Wirsen et al., 1986
Hydrothermal Fluid	EPR - 21°N	shipboard, 23°C	mg C m^{-3} day^{-1}	nmol C ml^{-1} d^{-1}	41.1 - 517.7	Wirsen et al., 1986
Hydrothermal Fluid	MAR - 26°N	in situ, 13-17°C	mg C m^{-3} day^{-1}	nmol C ml^{-1} d^{-1}	57.7 - 183.2	Wirsen et al., 1993
Hydrothermal Fluid	Galapagos Rift - "Rose Garden"	in situ, 2°C	nmole $liter^{-1}$ day^{-1}	nmol C ml^{-1} d^{-1}	1.5 - 5	Mandernack & Tebo, 1999
Hydrothermal Fluid	JdFR - Endeavour	in situ, 2°C	nmole $liter^{-1}$ day^{-1}	nmol C ml^{-1} d^{-1}	n.d.	Mandernack & Tebo, 1999

Abbreviations: JdFR, Juan de Fuca Ridge; MAR, Mid-Atlantic Ridge; EPR, East Pacific Rise;

[a]Note that in Wirsen et al., 1993 reported rates for sulfide scrapings are reported as ml of slurry, however it is impossible to know the mass of sulfide per ml of slurry.

[b]In Bonch-Osmolovskaya there is very little detail reported for methods, additionally sulfides were not homogenized, so it is difficult to assess how comparable these rates are.

[c]Rates were converted under the assumption that chimney material has a density of 2.9 g per cm^3 (the density of anhydrite, and bulk oceanic crust)

Table S2 Primers and Conditions for qPCR Functional Gene Analysis.

Process	Target Gene	Forward Primer (nM)	Reverse Primer (nM)	Positive Control	Annealing Temp (°C)	Reference
Calvin Benton Bassham	*RuBisCO* form II	*cbbM591F* (200) TTC TGG CTG GGB GGH GAY TTY ATY AAR AAY GAC GA	*cbbM918R* (200) CCG TGR CCR GCV CGR TGG TAR TG	*Thermococcus profundis*	55	Campbell and Cary, 2004
rTCA	*ATP citrate lyase*	*aclB275F (200)* TAG AGG ATG CRG CTA AWT GGA TTG ATG A	*aclB1204R* (200) GTT GGG GCC RCC WCK KCK NAC	*Sulfurovum denitrificans*	*55*	*Takai et al., 2005*
Methano-genesis	*Methyl CoM reductase*	*qmcrA (150)* GAR GAC CAC TTY GGH GGT TC	*ML-R (200)* TTCATTGCRT AGTTWGGRTA GTT	*Methanosarcina acetovorans, Methanococcus jannaschii*	*55*	*J. Huber, unpublished; Luton et al., 2002*
Bacteria	16S rRNA	*Bact1369F* (1000) GTT GGG GCC RCC WCK KCK NAC	*Prok1541R* (1000) CGGTGAATAT GCCCCTGC	*Arcobacter nitrofigulis*	*59*	*Suzuki et al., 2001*
Archaea	16S rRNA	*Arch1-1369F* (500) CGGTGAATACG TCCCTGC + *Arch2-1369F* (500) *CGGTGAATATGC CCCTGC*	*Prok1541R* (1000) CGGTGAATAT GCCCCTGC	*Methanosarcina acetovorans*	*59*	*Suzuki et al., 2001*

Table S3 Diversity Metrics describing the communities in the three structures[a]

Diversity Metric	Needles		Dead Dog		Chowder Hill	
	Bacteria	**Archaea**	**Bacteria**	**Archaea**	**Bacteria**	**Archaea**
Number of OTUs (97% similarity)[b]	254	119	178	46	48	n/a
Chao OTU estimate[b]	544	254	273	96	52	n/a
Shannon diversity index[b]	4.04	4.36	4.15	2.69	2.81	n/a
Simpson diversity index[b]	0.06	0.04	0.04	0.14	0.11	n/a
% OTUs with >99 sequences	91.73	93.28	78.65	84.78	50.00	n/a
% OTUs with <10 sequences	70.87	27.51	53.37	8.88	29.17	n/a
% singleton & doubleton OTUs	71.00	27.51	53.00	8.88	29.00	n/a
% dominance most abundant OTU	15.60	17.46	10.70	36.09	27.40	n/a
% dominance 5 most abundant OTUs	46.70	70.00	35.10	36.00	58.30	n/a

[a]All values based on a random sub-sample of sequences from each sample to allow comparison among samples with equal number of sequences (n=1709 for bacterial, n=338 for archaea) using the Mother pipeline
[b]Calculated using the Mothur pipeline

Table S4 Percentage sequence abundance of 454 libraries by taxa corresponding to Figure 4

	Needles	Dead Dog	Chowder Hill
Bacteria			
Actinobacteria	0.35	0.41	1.64
Aquificae	0	0.12	0.47
Bacteroidetes	4.97	2.75	0.35
Chloroflexi	0	0.94	0
Firmicutes	0.12	0.41	4.10
Fusobacteria	0	0.18	0
GN02	0.06	0	0
Lentishaerae	0.47	0	0
MBMPE71	0.059	0	0
Nitrospirae	0.29	0	0
Planctomycetes	0.056	0	0
Alphaproteobacteria	1.29	1.46	0.76
Betaproteobacteria	2.63	0.82	8.89
Deltaproteobacteria	7.78	5.27	0.94
Epsilonproteobacteria	0.64	48.57	27.44
Gammaproteobacteria	41.43	7.43	49.91
Proteobacteria-unclassified	9.89	16.91	0.18
Oceanithermus	0	0.64	0
Thermodesulfovibrio	15.62	0	0
Unclassified bacteria	14.34	14.10	5.33
Archaea			
Archaeoglobus	0	36.10	n/a
Korarchaeota	0	0.30	n/a
Methanocaldococcaceae	0	0.30	n/a
pMC1	0.89	0	n/a
pMC2A384	0	0.30	n/a
Cenarchaeum	5.03	0	n/a
Thermococci	0	4.44	n/a
Marine group II	1.78	0	n/a
Aciduliprofundaceae	0	6.21	n/a
Desulfurococcus	0	0.59	n/a
Pyrodictiaceae	0	0.30	n/a
Pyrobaculum	0	0.30	n/a
unclassified Thermoprotei	0.30	12.13	n/a
unclassified Thermoplasmata	0	4.44	n/a
Unclassified archaea	92.01	34.62	n/a

Table S5 pH adjusted estimates of vent fluid CO_2

	CO_2 [mM][a]		
Assumed pH	**Needles**	**Dead Dog**	**Chowder Hill**
Non-compensated	4.05	10.14	17.18
4	4.14	10.37	17.58
4.5	4.43	11.09	18.81
5	5.36	13.40	22.73
5.5	8.29	20.72	35.14
6	17.60	43.99	74.61
6.5	47.63	118.97	201.86
7	913.51	2280.79	3870.65

[a]Mean of 10 highest values per site

Figures for Supplemental Information

Plate 1: Chowder Hill

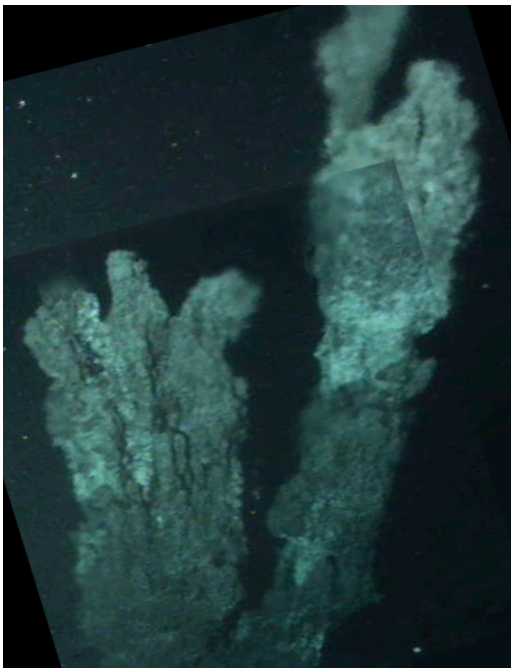

Plate 2: Needles (note red dots are laser sights representing 10 cm distance)

Plate 3: Dead Dog

For all 3 chimneys, see Table 1 for size estimation

References

Bonch-Osmolovskaya EA, Perevalova AA, Kolganova TV, Rusanov II, Jeanthon C, Pimenov NV (2011) Activity and Distribution of Thermophilic Prokaryotes in Hydrothermal Fluid, Sulfidic Structures, and Sheaths of Alvinellids (East Pacific Rise, 13 N). *Applied And Environmental Microbiology*, **77**(8), 2803–2806.

Campbell BJ, Cary SC (2004) Abundance of Reverse Tricarboxylic Acid Cycle Genes in Free-Living Microorganisms at Deep-Sea Hydrothermal Vents. *Applied And Environmental Microbiology*, **70**(10), 6282-6289.

Chase RL, Delaney JR, Karsten JL, Johnson HP, Juniper SK, Lupton JE, Scott SD, Tunnicliffe V, Hammond SR (1985) Hydrothermal vents on an axis seamount of the Juan de Fuca ridge. *Nature*, **313**(17), 212–214.

Eberhard C, Wirsen C, Jannasch H (1995) Oxidation of polymetal sulfides by chemolithoautotrophic bacteria from deep-sea hydrothermal vents. *Geomicrobiology Journal*, **13**(3), 145–164.

Luton PE, Wayne JM, Sharp RJ, Riley PW (2002) The mcrA gene as an alternative to 16S rRNA in the phylogenetic analysis of methanogen populations in landfill. *Microbiology*, **148**(11), 3521–3530.

Mandernack KW, Tebo BM (1999) In situ sulfide removal and CO2 fixation rates at deep-sea hydrothermal vents and the oxicranoxic interface in Framvaren Fjord, Norway. *Marine Chemistry*, **66**, 201–213.

Polz M, Robinson J, Cavanaugh C, van Dover C (1998) Trophic ecology of massive shrimp aggregations at a Mid-Atlantic Ridge hydrothermal vent site. *Limnology and Oceanography*, **43**(7), 1631–1638.

Suzuki MT, Beja O, Taylor LT, DeLong EF (2001) Phylogenetic analysis of ribosomal RNA operons from uncultivated coastal marine bacterioplankton. *Environmental Microbiology*, **3**, 323-331.

Takai K, Campbell BJ, Cary SC, Suzuki M, Oida H, Nunoura T, Hirayama H, Nakagawa S, Suzuki Y, Inagaki F (2005). Enzymatic and Genetic Characterization of Carbon and Energy Metabolisms by Deep-Sea Hydrothermal Chemolithoautotrophic Isolates of Epsilonproteobacteria. *Applied And Environmental Microbiology*, **71**(11), 7310-7320.

Tuttle J, Wirsen C, Jannasch H (1983) Microbial Activities in the Emitted Hydrothermal Waters of the Galapagos Rift Vents. *Marine Biology*, **73**(3), 293–299.

Tuttle JH (1985) The role of sulfur-oxidizing bacteria at deep-sea hydrothermal vents. *Bulletin of the Biological Society of Washington*, (6), 335–343.

Wirsen C, Tuttle J, Jannasch H (1986) Activities of Sulfur-Oxidizing Bacteria at the 21-Degrees-N East Pacific Rise Vent Site. *Marine Biology*, **92**(4), 449–456.

Wirsen C, Jannasch H, Molyneaux S (1993) Chemosynthetic Microbial Activity at Mid-Atlantic Ridge Hydrothermal Vent Sites. *Journal of Geophysical Research*, **98**(B6), 9693–9703.

Appendix B

Supplemental Material for Chapter 3

Methods

D-ESP sampling

For this and associated efforts, the D-ESP was fitted with an *in situ* mass spectrometer (ISMS; Wankel et al, 2011) for co-registered analyses of dissolved volatiles (data not shown). The ISMS and CTD shared a common in-let and were in series with ISMS first. Of the 5L samples collected, the decompressed sample was partitioned whereby 1L was archived in RNALater providing the samples used in this work. 2L went to real-time analyses using DNA probe arrays and quantitative PCR to detect a variety of ribosomal RNA and target gene sequences (data not presented in this work; Preston et al., 2009; Ussler et al., 2013).

Metatranscriptomic Sequencing

Library construction is performed using the Illumina TruSeq Stranded mRNA Sample NA Preparation Kit (cat# FC-122-2101, FC-122-2102 or FC-121-2103) using the following methods. Poly-A RNA is purified from total RNA (100 ng to 4 ug) using poly-T oligo-attached magnetic beads. The Poly-A RNA is eluted from the beads and fragmented with divalent cations under elevated temperature. RNA fragments are copied into first strand cDNA using random primers and Superscript II Reverse Transcriptase. Second strand cDNA synthesis is accomplished using DNA polymerase I and Rnase H under conditions in which dUTP is substituted for dTTP and yields blunt-ended cDNA in which the second strand is marked with dUTP. An A-base is added to the blunt ends as a means to prepare the cDNA fragments for adapter ligation and block concatamer formation during the ligation step. Adapters containing a T-base overhang are ligated to the A-tailed DNA

fragments. Ligated fragments are PCR-amplified (12-15 cycles). PCR enables amplification of the first strand cDNA product, whereas attempted amplifciation of the second strand product stalls at dUTP bases and therefore is not enriched. Follwoing amplificaiton, the library is purified by bead based methodologies.

The concentration of the lamplified ibrary is measured using the Invitrogen Qubit dsDNA HS Assay (Q32851) and an aliquot of the library is resolved on an Agilent 2200 Tape Station using a D1K (cat# 5067-5361 and 5067-5362) or a High Sensitivity D1K (cat# 5067-5363 and 5067-5364) assay to define the size range. Libraries are adjusted to a concentration of approximately 10 nM and quantitative PCR is performed using the KapaBiosystems Kapa Library Quant Kit (cat# KK4824) to quantitate adapter ligated library molecules. The concentration is further adjusted following qPCR to prepare the library for Illumina sequence analysis.

References

Preston C, Marin R III, Jenson S, Feldman J, Massion E, DeLong E, *et al.* (2009). Near real-time, autonomous detection of marine bacterioplankton on a coastal mooring in Monterey Bay, California, using rRNA-targeted DNA probes. *Environ Microbiol* B:1168-1180.

Ussler W III, Preston C, Tavormina P, Pargett D, Jensen S, Roman B, *et al.* (2013). Autonomous Application of Quantitative PCR in the Deep Sea: In Situ Surveys of Aerobic Methanotrophs Using the Deep-Sea Environmental Sample Processor. *Environ Sci Technol* **47**:9339–9346.

Wankel SD, Germanovich LN, Lilley MD, Genc G, DiPerna CJ, Bradley AS, *et al.* (2011). Influence of subsurface biosphere on geochemical fluxes from diffuse hydrothermal fluids. *Nature Geosci* **4**:1–8.

Figures

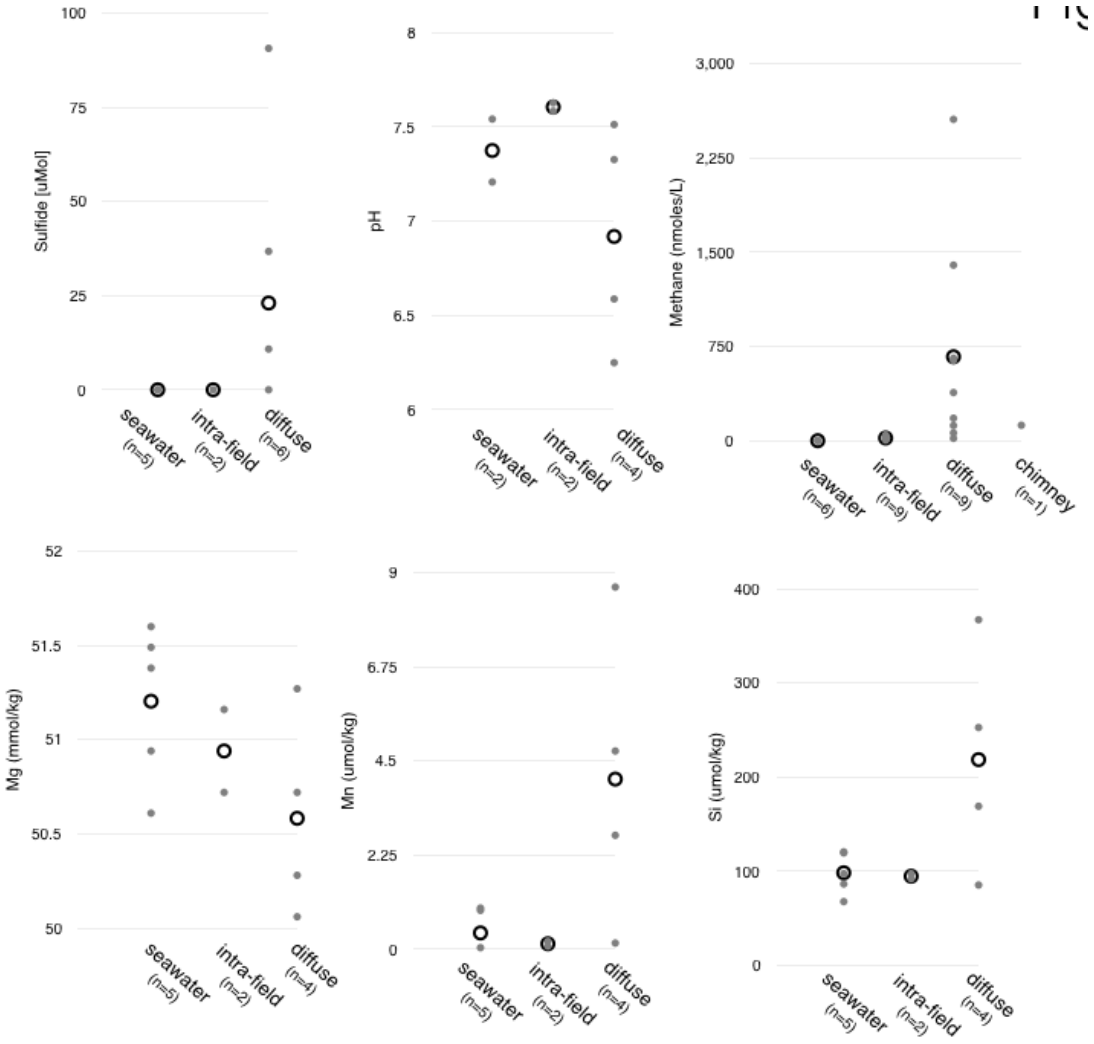

Supplemental Figure 3.1 All geochemical measurements, including from samples that were not sequenced. Mean values are represented by dark circles. Each grey dot represents one measurement.

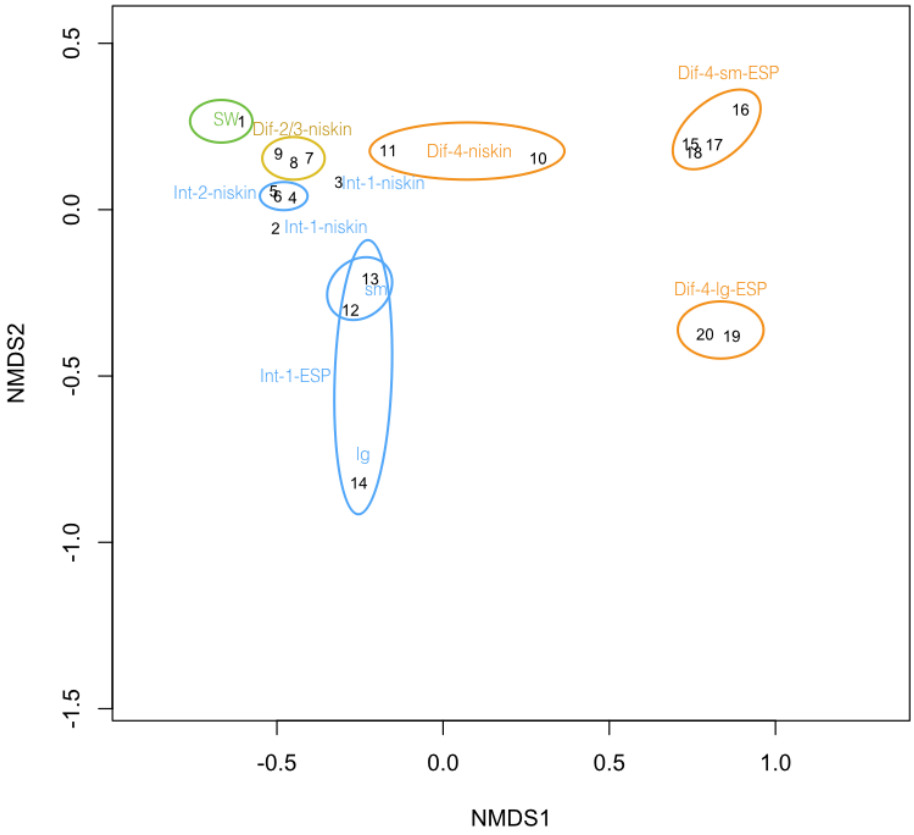

Supplemental Figure 3.2 NMDS plot of all samples (same date used for cluster diagram in Figure 4) showing similarity among active communities (as determined by rRNA reads).

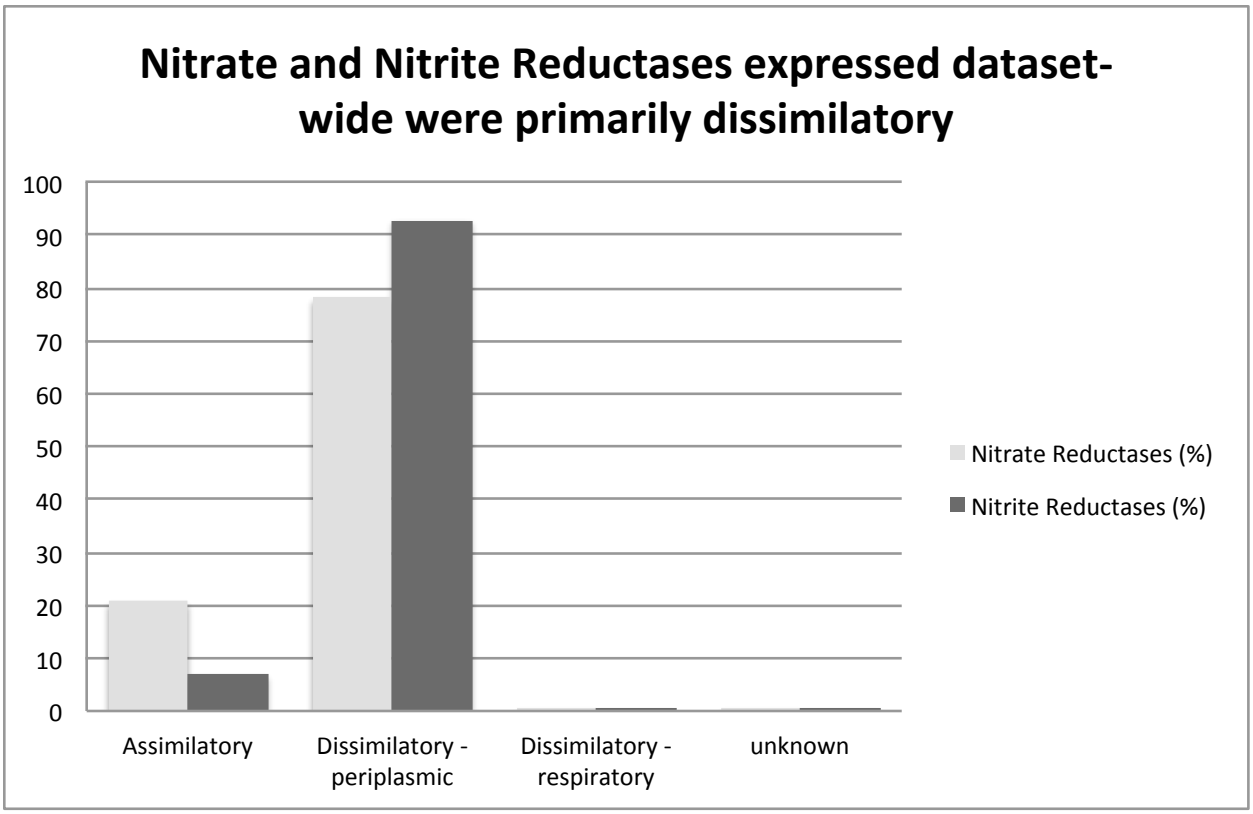

Supplemental Figure 3.3

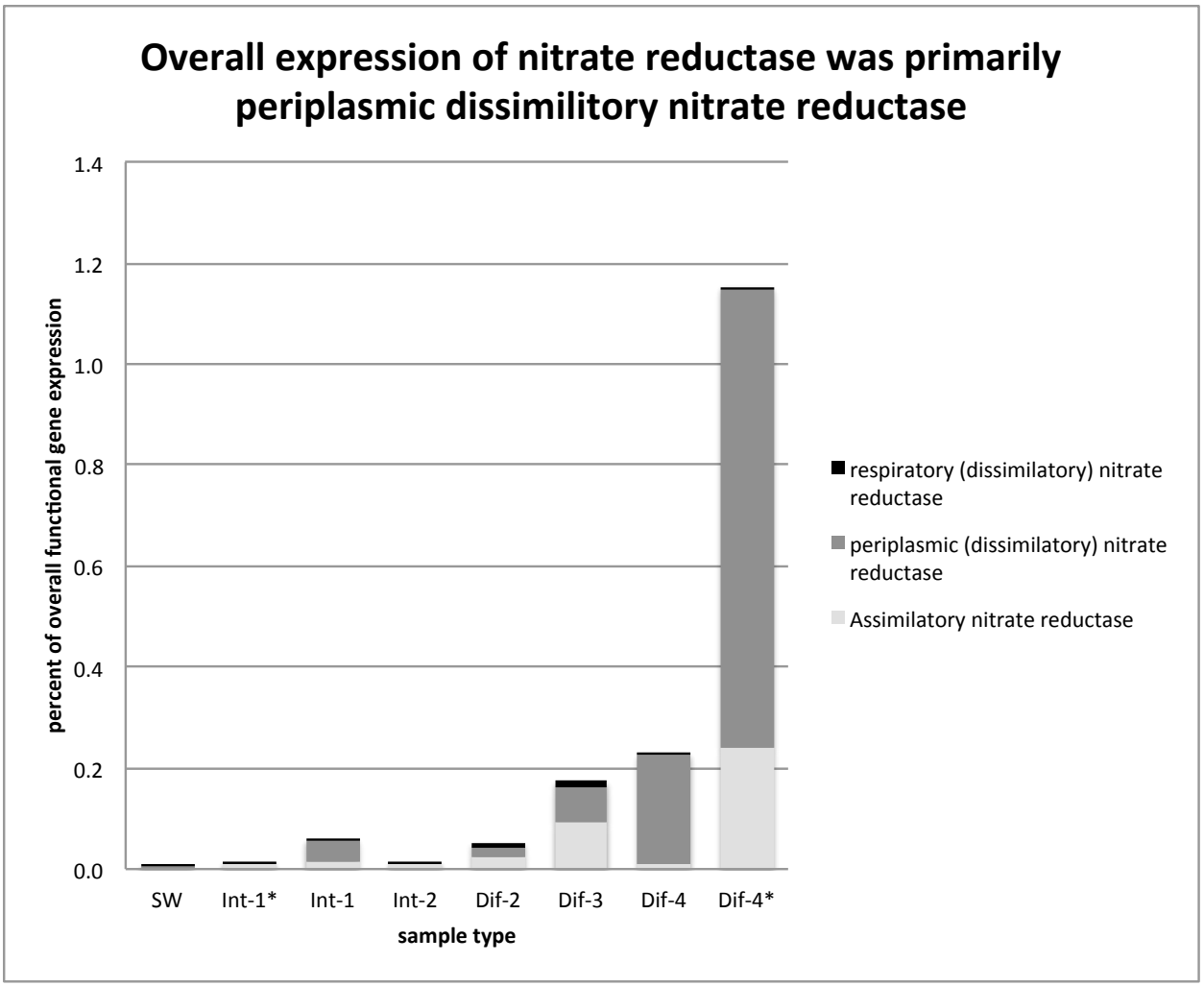

Supplemental Figure 3.4

a

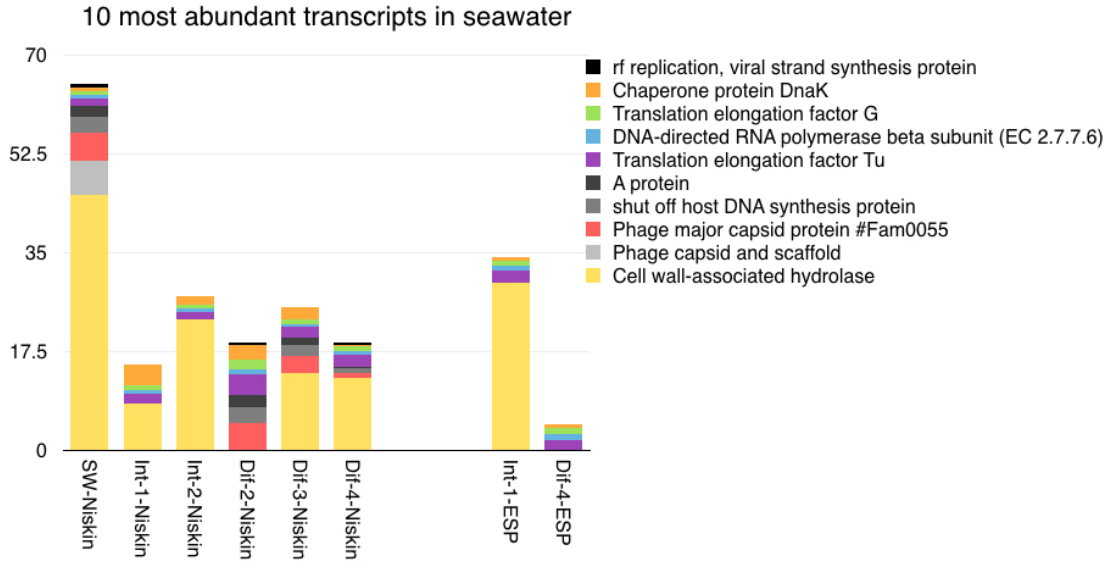
10 most abundant transcripts in seawater
70
52.5
35
17.5
0
SW-Niskin
Int-1-Niskin
Int-2-Niskin
Dif-2-Niskin
Dif-3-Niskin
Dif-4-Niskin
Int-1-ESP
Dif-4-ESP
rf replication, viral strand synthesis protein
Chaperone protein DnaK
Translation elongation factor G
DNA-directed RNA polymerase beta subunit (EC 2.7.7.6)
Translation elongation factor Tu
A protein
shut off host DNA synthesis protein
Phage major capsid protein #Fam0055
Phage capsid and scaffold
Cell wall-associated hydrolase

b

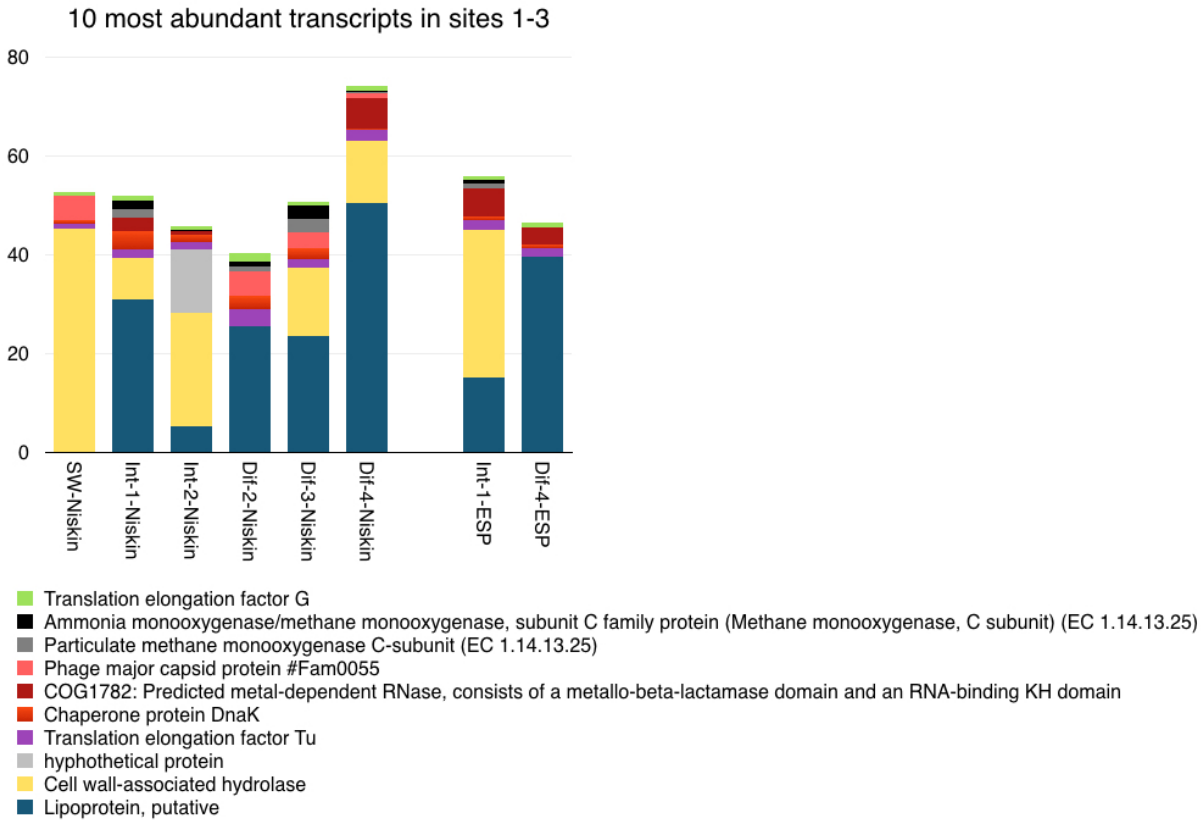
10 most abundant transcripts in sites 1-3
80
60
40
20
0
SW-Niskin
Int-1-Niskin
Int-2-Niskin
Dif-2-Niskin
Dif-3-Niskin
Dif-4-Niskin
Int-1-ESP
Dif-4-ESP
Translation elongation factor G
Ammonia monooxygenase/methane monooxygenase, subunit C family protein (Methane monooxygenase, C subunit) (EC 1.14.13.25)
Particulate methane monooxygenase C-subunit (EC 1.14.13.25)
Phage major capsid protein #Fam0055
COG1782: Predicted metal-dependent RNase, consists of a metallo-beta-lactamase domain and an RNA-binding KH domain
Chaperone protein DnaK
Translation elongation factor Tu
hyphothetical protein
Cell wall-associated hydrolase
Lipoprotein, putative

c

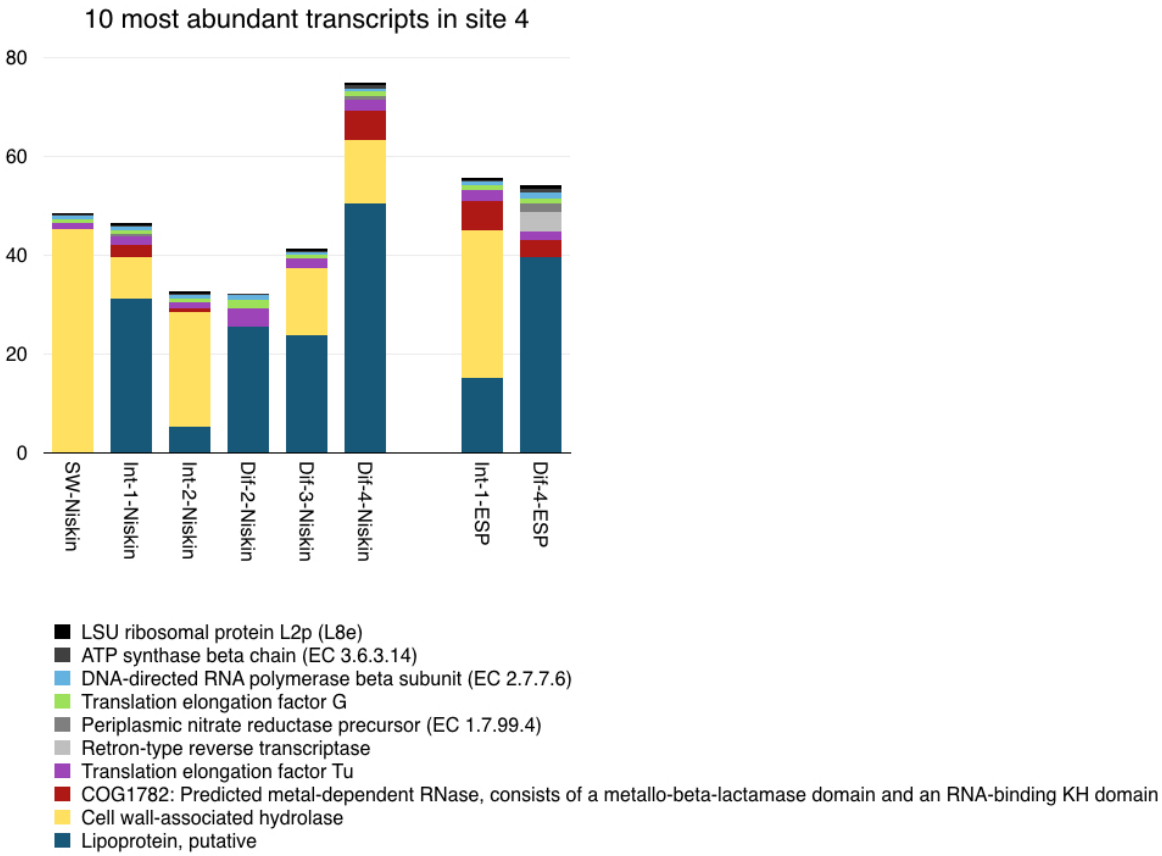

Supplemental Figure 3.5

Tables

Supplemental Table 3.1

ESP Sample Number	Corresponding MG-RAST ID	Sample Start time	Sample End Time	Int-1*	Dif-4*
1	4565284.3	7/13/11 19:09	7/13/11 19:25	*	
7	4565472.3	7/14/11 16:29	7/14/11 16:46	*	
23	4565473.3	7/17/11 1:08	7/17/11 1:23		*
29	4565474.3	7/18/11 0:34	7/18/11 0:49		*
30	4565475.3	7/18/11 3:24	7/18/11 3:39		*
31	4565464.3	7/18/11 6:12	7/18/11 6:26		*

Supplemental Table 3.2

Description	Sample name	MG-RAST ID	Upload: sequence count	Post QC: sequence count	Post QC: mean sequence length	Post QC: mean GC %	total M5RNA tax. IDs	total SEED functional IDs	Subsystem L1 IDs
SW-Niskin	3060	4551453.3	9,885,039	9,461,486	106 ± 26	51 ± 5	7,120,287	1,039,471	98,909
Int-1-Niskin	3007	4565465.3	15,015,234	14,526,420	112 ± 29	49 ± 5	16,593,713	1,922,098	212,005
Int-1-Niskin	3014	4565466.3	14,755,760	14,273,334	109 ± 28	48 ± 5	15,256,011	1,556,273	68,667
Int-2-Niskin	3237	4565468.3	17,876,264	17,235,158	110 ± 28	49 ± 5	20,986,145	2,470,522	453,647
Int-2-Niskin	3238	4565469.3	15,855,175	15,308,541	109 ± 28	50 ± 5	18,283,775	2,117,804	439,818
Int-2-Niskin	3239	4565470.3	15,605,206	15,077,545	111 ± 29	50 ± 5	18,299,932	2,239,360	413,146
Dif-2-Niskin	3234	4551455.3	10,887,331	10,435,245	107 ± 26	50 ± 5	8,287,205	1,292,912	107,999
Dif-3-Niskin	3495	4551443.3	10,368,683	9,968,436	115 ± 30	50 ± 5	7,775,902	1,114,581	93,698
Dif-3-Niskin	3494	4565467.3	21,472,651	20,759,160	109 ± 27	49 ± 5	22,264,145	2,244,846	152,401
Dif-4-Niskin	3471	4565471.3	16,567,419	16,074,027	112 ± 29	48 ± 5	17,395,616	2,449,093	358,446
Dif-4b-Niskin	3498	4551454.3	13,494,976	13,034,080	108 ± 27	48 ± 5	8,590,917	1,287,766	83,800
Int-1-lg-ESP	WCR 1	4620934.3	14,057,110	13,664,800	112 ± 29	46 ± 7	9,529,438	1,142,981	62,739
Int-1-sm-ESP	WCR 1	4565284.3	14,565,731	14,086,549	113 ± 30	50 ± 5	16,196,605	1,860,167	183,080
Int-1-sm-ESP	WCR 7	4565472.3	10,660,730	10,127,396	103 ± 21	49 ± 5	8,397,646	1,147,626	44,080
Dif-4-sm-ESP	WCR 23	4565473.3	14,053,708	13,609,944	109 ± 27	48 ± 5	9,464,190	1,413,252	313,728
Dif-4-lg-ESP	WCR 23	4620935.3	15,849,209	15,379,195	109 ± 27	48 ± 5	11,228,550	2,198,898	377,913
Dif-4-sm-ESP	WCR 29	4565474.3	19,944,458	19,313,650	104 ± 23	48 ± 5	18,516,154	1,906,272	336,112
Dif-4-sm-ESP	WCR 30	4565475.3	16,013,080	15,518,719	109 ± 27	47 ± 6	14,340,278	1,708,959	554,398
Dif-4-lg-ESP	WCR 31	4620933.3	14,888,091	14,452,517	109 ± 28	48 ± 6	10,497,031	2,261,309	519,431
Dif-4-sm-ESP	WCR 31	4565464.3	15,453,393	14,995,631	109 ± 28	47 ± 6	13,392,976	1,751,585	644,363

Supplemental Table 3.3

Selected Functional Genes: Figure 8				
	Kruskal	Wilcox	Wilcox	Wilcox
graph label	by site	by envi	by altenvi	by method
all Rubisco	**0.0092**	0.0328	**0.0002**	0.0350
all Citrate Lyase	**0.0028**	**0.0091**	**0.0003**	0.2428
all sox	**0.0208**	**0.0012**	**0.0121**	0.3562
all sqr	0.1459	0.3817	0.5882	0.5367
all apr	**0.0067**	**0.0068**	**0.0001**	0.0653
all dsr	**0.0041**	**0.0025**	**0.0001**	0.0279
all ammonia monooxygenase	**0.0059**	0.1259	**0.0014**	**0.0079**
all nitrite reductase	0.0363	0.1266	**0.0164**	0.0521
all nitrate reductase	**0.0069**	**0.0003**	**0.0002**	0.0653
all nitric oxide reductase	**0.0150**	**0.0050**	**0.0012**	0.6038
ferric transporters	0.2411	0.7547	0.1290	0.1120
ferrous	**0.0055**	0.0826	**0.0059**	0.0491
mcr	0.3173	0.8362	0.9013	0.5396
hydrogenases	**0.0095**	0.0506	**0.0008**	0.1128
# of tests	56.0000			
bonferroni	0.0009	**highly sig**		
Benjamini-Hochberg	0.0254	**sig**		
SEED L1 Subsystems: Figure 7				
test	Kruskal	Wilcox	Wilcox	Wilcox
	site	envi	altenvi	method
protein_metabolism	0.4666	0.9039	0.2060	0.1128
clustering_based_subsystems	0.2559	0.7168	0.3511	0.1564
respiration	0.1512	0.5999	0.2060	0.1128
carbohydrates	**0.0103**	0.3511	**0.0018**	**0.0010**
RNA_metabolism	0.4493	0.2060	0.9678	**0.0006**
amino_acids_and_derivatives	0.0765	0.3950	0.7780	0.2775
miscellaneous	0.5779	0.7780	0.2723	0.0279

cofactors_vitamins_prosthetic_groups_and_pigments	**0.0040**	**0.0025**	**0.0000**	0.4002
N_metabolism	**0.0053**	**0.0036**	**0.0001**	0.1823
S_metabolism	0.1078	0.0620	0.0328	0.0789
stress_response	**0.0091**	0.0620	**0.0003**	**0.0006**
phages_prophates_transposable_elements_and_plasmids	**0.0228**	0.3100	**0.0025**	**0.0101**
membrate_transport	**0.0154**	0.1087	**0.0018**	**0.0133**
nucleosides_and_nucleotides	**0.0224**	0.0259	**0.0018**	0.0279
cell_wall_and_capsule	**0.0248**	0.0506	0.0908	0.4002
DNA_metabolism	0.4798	0.0754	0.0409	0.4002
fatty_acids_lipids_and_isoprenoids	**0.0071**	0.9039	0.1288	**0.0000**
cell_division_and_cell_cycle	0.0884	0.9039	0.1288	0.4002
virulence_disease_and_defense	0.0275	0.1518	**0.0121**	0.1823
regulation_and_cell_signalling	0.6638	0.5448	0.5448	0.1128
motility_and_chemotaxis	0.4042	0.3511	0.7780	0.0947
P_metabolism	**0.0134**	**0.0018**	**0.0005**	0.7197
metabolism_of_aromatic_compounds	**0.0055**	0.0754	**0.0018**	0.0947
Fe_acquisition_and_metabolism	0.0377	0.2304	0.1998	0.0936
secondary_metabolism	**0.0031**	**0.0050**	**0.0000**	0.3562
K_metabolism	**0.0252**	0.0746	**0.0114**	0.0927
dormancy_and_sporulation	0.2488	0.4759	0.3348	0.7716
photosynthesis	0.4747	0.2403	0.1311	0.0513
# of tests	112.0000			
bonferroni	0.0004	**highly sig**		
Benjamini-Hochberg	0.0252	**sig**		
Taxonomic IDs: Figure 6				
	Kruskal	Wilcox	Wilcox	Wilcox
csv label	by site	by envi	by altenvi	by method
Archaea	0.0287	0.2723	**0.0050**	**0.0004**
Eukaryota	**0.0032**	**0.0204**	**0.0001**	0.0435

Bacteria	**0.0047**	**0.0012**	**0.0001**	0.0535
other	**0.0052**	**0.0121**	**0.0003**	**0.0101**
Actinobacteria	**0.0038**	0.0328	**0.0001**	**0.0010**
Firmicutes	0.0530	0.4920	0.0259	**0.0220**
Bacteroidetes	**0.0031**	**0.0008**	**0.0000**	**0.0076**
unclassified bacteria	**0.0073**	**0.0204**	**0.0005**	0.0435
Proteobacteria	0.1573	0.3100	0.1288	0.7802
Zetaproteobacteria	**0.0198**	0.1288	**0.0025**	0.0435
Deltaproteobacteria	0.0763	0.1774	0.0259	0.0350
unclassified proteobacteria	**0.0038**	**0.0008**	**0.0000**	0.2775
Alphaproteobacteria	**0.0045**	**0.0018**	**0.0001**	0.0653
Betaproteobacteria	**0.0034**	**0.0204**	**0.0000**	0.0535
Epsilonproteobacteria	**0.0028**	**0.0003**	**0.0000**	0.0535
Gammaproteobacteria	**0.0042**	**0.0018**	**0.0000**	**0.0172**
# of tests	64.0000		64.0000	
bonferroni	0.0008	**highly sig**		
Benjamini-Hochberg	0.0254	**sig**		

Appendix C

Supplemental Material for Chapter 4

Supplemental Table 4.1

Unit	Days deployed	Observed OTUs	Chao1	Shannon	Simpson_e
12a	2	1011	2481	5.398	0.015
3	2	982	2379	5.452	0.014
10	3	1074	2673	5.761	0.015
6a	3	1032	2657	5.867	0.018
2	3	961	2420	5.205	0.010
9a	4	873	2278	5.231	0.016
5	4	985	2397	5.419	0.015
11	40	1139	2823	6.136	0.019
1	40	1004	2480	5.536	0.015
4	40	1211	3088	5.857	0.015
12b	685	1246	3175	6.220	0.018
6b	685	994	2566	5.208	0.012
9b	685	863	1926	5.399	0.014

Supplemental Table 4.2

wra	High Temp Time Series						Low Temp Time Series							
#OTU ID	**2 day (#3 ave)**	**40 day (#4 ave)**	**st. err #3**	**st. err #4**	**high T ave**	**high T rank**	**2 day (#12)**	**40 day (#11)**	**685 day (#12b)**	**st err #12**	**st err #11**	**st err #12b**	**low T ave**	**low T rank**
k__Bacteria;p__Proteobacteria;c__Epsilonproteobacteria;o__Campylobacterales;f__Helicobacteraceae;g__Sulfurimonas	0.2357	0.3112	0.0707	0.0779	0.2750	1	0.4221	0.2573	0.1455	0.1070	0.0738	0.0489	0.2735	1
k__Bacteria;p__Proteobacteria;c__Epsilonproteobacteria;o__Campylobacterales;f__Helicobacteraceae;g__	0.1841	0.1803	0.0657	0.0652	0.1882	2	0.0776	0.2541	0.2330	0.0156	0.0478	0.0498	0.1822	2
k__Bacteria;p__Proteobacteria;c__Epsilonproteobacteria;o__;f__;g__	0.1233	0.1708	0.0451	0.0662	0.0764	3	0.1522	0.0478	0.0293	0.0483	0.0160	0.0164	0.1471	3
k__Bacteria;p__Bacteroidetes;c__Bacteroidia;o__Bacteroidales;f__VC21_Bac22;g__	0.0152	0.0399	0.0079	0.0238	0.0459	4	0.0093	0.0552	0.0731	0.0075	0.0314	0.0396	0.0276	6
k__Bacteria;p__Proteobacteria;c__Epsilonproteobacteria;o__Campylobacterales;f__Campylobacteraceae;g__Arcobacter	0.0236	0.0203	0.0123	0.0115	0.0365	5	0.0536	0.0403	0.0157	0.0231	0.0213	0.0084	0.0220	10
k__Archaea;p__Euryarchaeota;c__Thermoplasmata;o__Thermoplasmatales;f__[Aciduliprofundaceae];g__	0.0623	0.0011	0.0401	0.0008	0.0151	11	0.0448	0.0002	0.0003	0.0422	0.0001	0.0001	0.0317	4
k__Bacteria;p__Proteobacteria;c__Deltaproteobacteria;o__;f__;g__	0.0297	0.0222	0.0283	0.0150	0.0156	10	0.0020	0.0371	0.0076	0.0006	0.0267	0.0025	0.0259	7
k__Bacteria;p__Proteobacteria;c__Epsilonproteobacteria;o__Nautiliales;f__Nautiliaceae;g__	0.0301	0.0190	0.0159	0.0130	0.0110	16	0.0280	0.0020	0.0030	0.0167	0.0006	0.0022	0.0245	8
k__Bacteria;p__Bacteroidetes;c__Bacteroidia;o__Bacteroidales;f__;g__	0.0143	0.0185	0.0116	0.0085	0.0185	8	0.0033	0.0227	0.0294	0.0023	0.0080	0.0052	0.0164	11
k__Bacteria;p__Proteobacteria;c__Epsilonproteobacteria;o__Campylobacterales;f__Campylobacteraceae;g__	0.0054	0.0108	0.0021	0.0059	0.0258	6	0.0049	0.0307	0.0418	0.0017	0.0112	0.0137	0.0081	17
k__Bacteria;p__Aquificae;c__Aquificae;o__Aquificales;f__Desulfurobacteriaceae;Other	0.0247	0.0317	0.0235	0.0316	0.0047	na	0.0136	0.0001	0.0005	0.0131	0.0000	0.0005	0.0282	5
Unassigned;Other;Other;Other;Other;Other	0.0181	0.0143	0.0076	0.0063	0.0160	9	0.0137	0.0138	0.0205	0.0071	0.0038	0.0058	0.0162	12
k__Bacteria;p__Proteobacteria;c__Deltaproteobacteria;o__AF420338;f__;g__	0.0442	0.0001	0.0440	0.0001	0.0001	na	0.0001	0.0001	0.0001	0.0001	0.0000	0.0000	0.0222	9
k__Bacteria;p__Proteobacteria;c__Alphaproteobacteria;o__Rhizobiales;f__;g__	0.0001	0.0014	0.0000	0.0012	0.0205	7	0.0001	0.0196	0.0419	0.0000	0.0195	0.0146	0.0007	na

k__Bacteria;p__Proteobacteria;c__Deltaproteobacteria;o__Desulfobacterales;f__Desulfobacteraceae;g__	0.0003	0.0091	0.0002	0.0067	0.0147	12	0.0039	0.0119	0.0285	0.0038	0.0055	0.0148	0.0047	23
k__Bacteria;p__Proteobacteria;c__Deltaproteobacteria;o__Desulfurellales;f__Desulfurellaceae;g__	0.0225	0.0007	0.0156	0.0004	0.0062	20	0.0185	0.0002	0.0001	0.0169	0.0001	0.0000	0.0116	13
k__Bacteria;p__Proteobacteria;c__Deltaproteobacteria;o__Desulfobacterales;f__Desulfobulbaceae;g__Desulfocapsa	0.0003	0.0053	0.0002	0.0034	0.0142	13	0.0012	0.0124	0.0290	0.0009	0.0107	0.0080	0.0028	na
k__Bacteria;p__Proteobacteria;c__Gammaproteobacteria;o__;f__;g__	0.0032	0.0037	0.0016	0.0023	0.0129	15	0.0024	0.0186	0.0177	0.0008	0.0102	0.0059	0.0035	na
k__Bacteria;p__Proteobacteria;c__Deltaproteobacteria;o__Desulfobacterales;f__Desulfobulbaceae;g__	0.0003	0.0053	0.0002	0.0034	0.0130	14	0.0016	0.0112	0.0261	0.0011	0.0059	0.0099	0.0028	na
k__Bacteria;p__Bacteroidetes;c__Flavobacteriia;o__Flavobacteriales;f__Flavobacteriaceae;g__	0.0006	0.0084	0.0002	0.0073	0.0100	18	0.0008	0.0038	0.0256	0.0002	0.0015	0.0090	0.0045	24
k__Bacteria;p__Proteobacteria;c__Epsilonproteobacteria;o__Nautiliales;f__Nautiliaceae;g__Caminibacter	0.0095	0.0089	0.0054	0.0057	0.0051	na	0.0121	0.0010	0.0021	0.0090	0.0003	0.0017	0.0092	15
k__Archaea;p__Crenarchaeota;c__Thermoprotei;o__;f__;g__	0.0212	0.0018	0.0123	0.0018	0.0024	na	0.0070	0.0000	0.0000	0.0047	0.0000	0.0000	0.0115	14
k__Bacteria;p__Bacteroidetes;c__Bacteroidia;o__Bacteroidales;f__SB-1;g__	0.0001	0.0063	0.0000	0.0043	0.0101	17	0.0033	0.0081	0.0188	0.0033	0.0047	0.0061	0.0032	na
k__Bacteria;p__Proteobacteria;c__Gammaproteobacteria;o__Oceanospirillales;f__SUP05;g__	0.0065	0.0063	0.0037	0.0035	0.0060	23	0.0105	0.0023	0.0051	0.0040	0.0009	0.0028	0.0064	19
k__Bacteria;p__Thermotogae;c__MS9;o__;f__;g__	0.0174	0.0000	0.0138	0.0000	0.0029	na	0.0086	0.0001	0.0001	0.0085	0.0000	0.0001	0.0087	16
k__Bacteria;p__WWE1;c__[Cloacamonae];o__[Cloacamonales];f__MSBL8;g__	0.0071	0.0043	0.0070	0.0036	0.0058	25	0.0047	0.0064	0.0064	0.0046	0.0058	0.0058	0.0057	20
k__Bacteria;p__Spirochaetes;c__Spirochaetes;o__Spirochaetales;f__Spirochaetaceae;g__	0.0009	0.0045	0.0006	0.0029	0.0070	19	0.0018	0.0131	0.0061	0.0017	0.0060	0.0032	0.0027	na
k__Bacteria;p__Caldiserica;c__Caldisericia;o__Caldisericales;f__;g__	0.0135	0.0001	0.0087	0.0000	0.0025	na	0.0075	0.0000	0.0000	0.0074	0.0000	0.0000	0.0068	18
k__Bacteria;p__Proteobacteria;c__Deltaproteobacteria;o__Desulfuromonadales;f__Desulfuromonadaceae;g__	0.0009	0.0047	0.0005	0.0034	0.0061	21	0.0006	0.0037	0.0140	0.0003	0.0018	0.0044	0.0028	na
k__Bacteria;p__Proteobacteria;c__Gammaproteobacteria;o__Chromatiales;f__;g__	0.0024	0.0029	0.0010	0.0016	0.0059	24	0.0015	0.0054	0.0109	0.0004	0.0020	0.0047	0.0026	na
k__Bacteria;p__Proteobacteria;c__Deltaproteobacteria;o__Desulfuromonadales;f__Desulfuromonadaceae;g__Desulfuromonas	0.0005	0.0025	0.0004	0.0020	0.0061	22	0.0066	0.0023	0.0095	0.0065	0.0016	0.0057	0.0015	na

k__Archaea;p__Crenarchaeota;c__Thermoprotei;o__Desulfurococcales;f__Desulfurococcaceae;Other	0.0103	0.0001	0.0091	0.0001	0.0009	na	0.0028	0.0000	0.0000	0.0026	0.0000	0.0000	0.0052	21
k__Archaea;p__Crenarchaeota;c__Thermoprotei;o__Desulfurococcales;f__Pyrodictiaceae;Other	0.0081	0.0015	0.0077	0.0015	0.0009	na	0.0028	0.0000	0.0000	0.0024	0.0000	0.0000	0.0048	22
k__Bacteria;p__Aquificae;c__Aquificae;o__Aquificales;f__Desulfurobacteriaceae;g__	0.0042	0.0038	0.0031	0.0035	0.0016	na	0.0040	0.0001	0.0007	0.0035	0.0001	0.0006	0.0040	25

Supplemental Figure 4.1

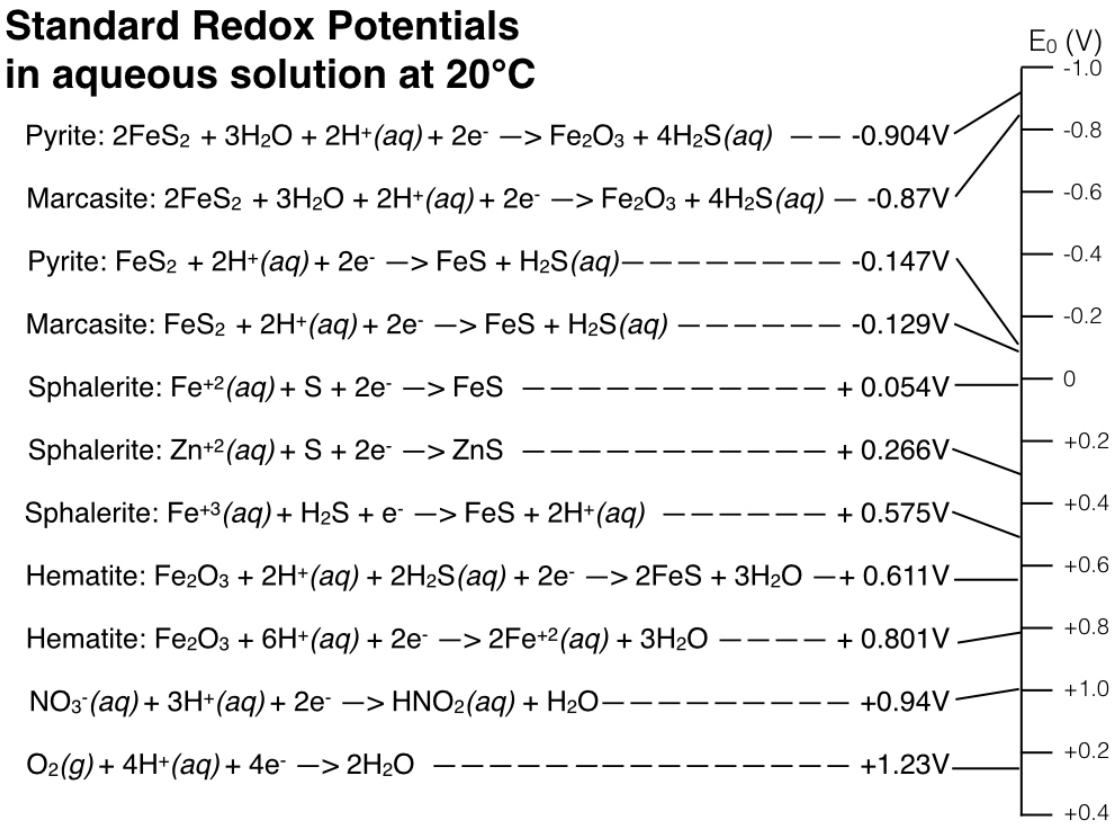

Supplemental Figure 4.2

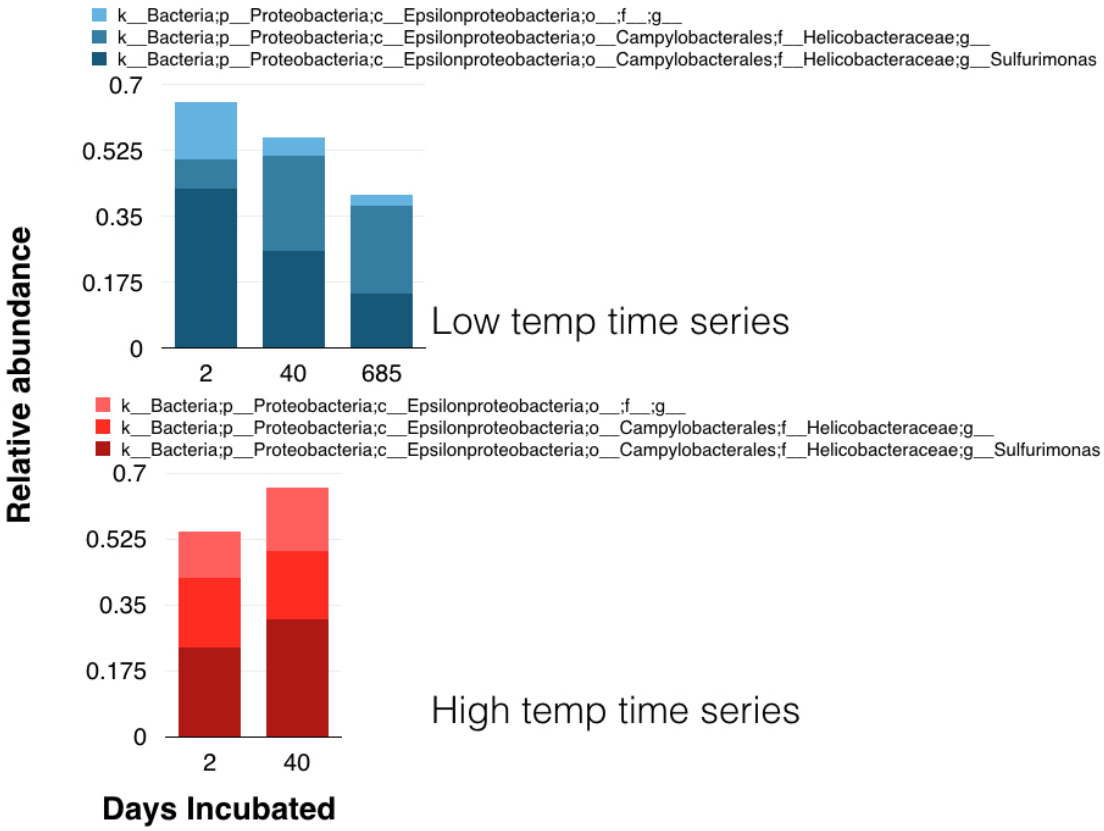

Supplemental Figure 4.3

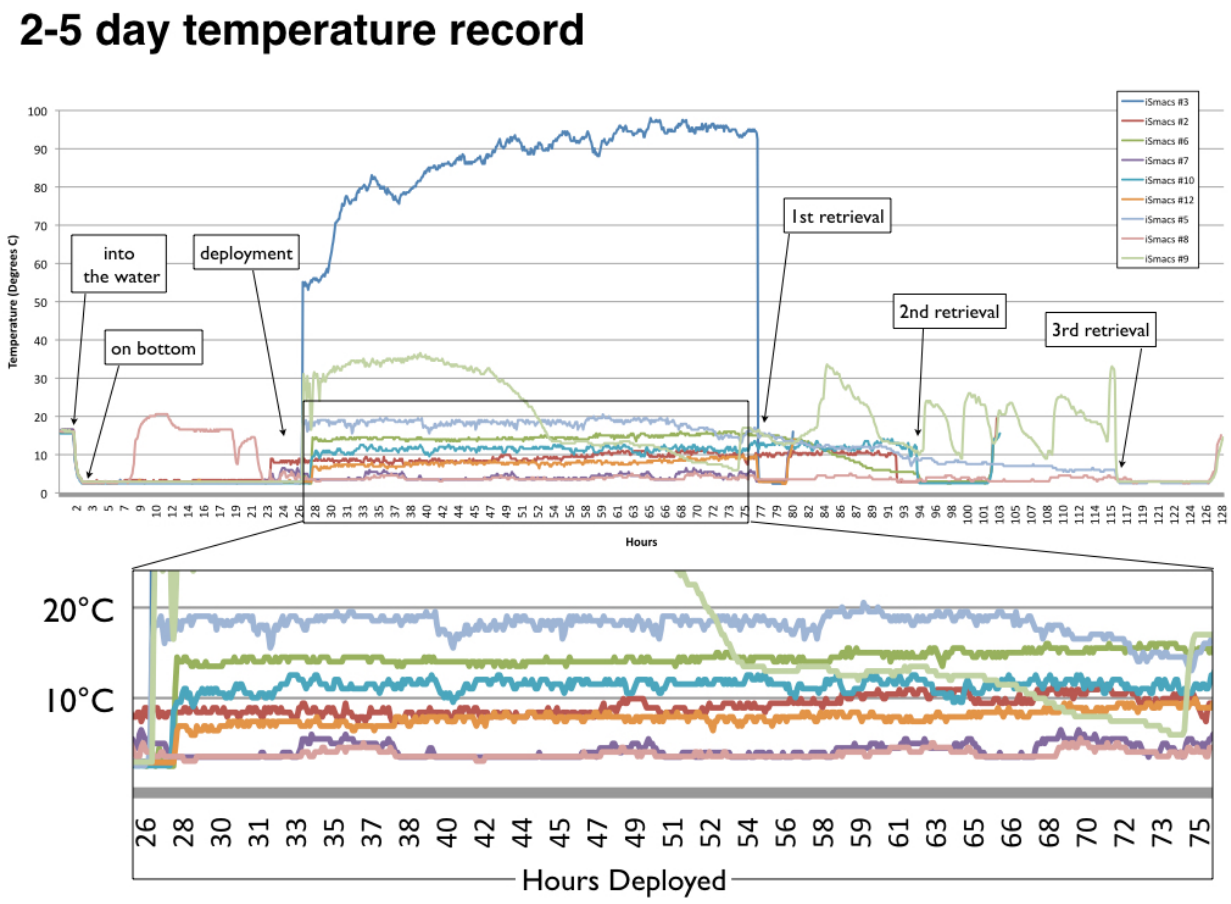

Supplemental Figure 4.4

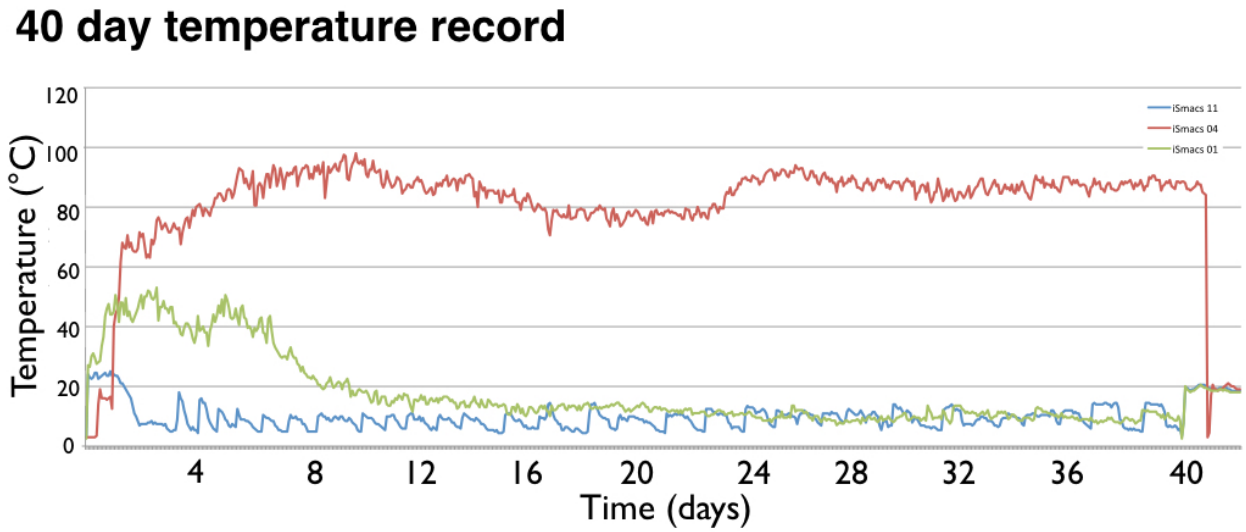

Supplemental Figure 4.5

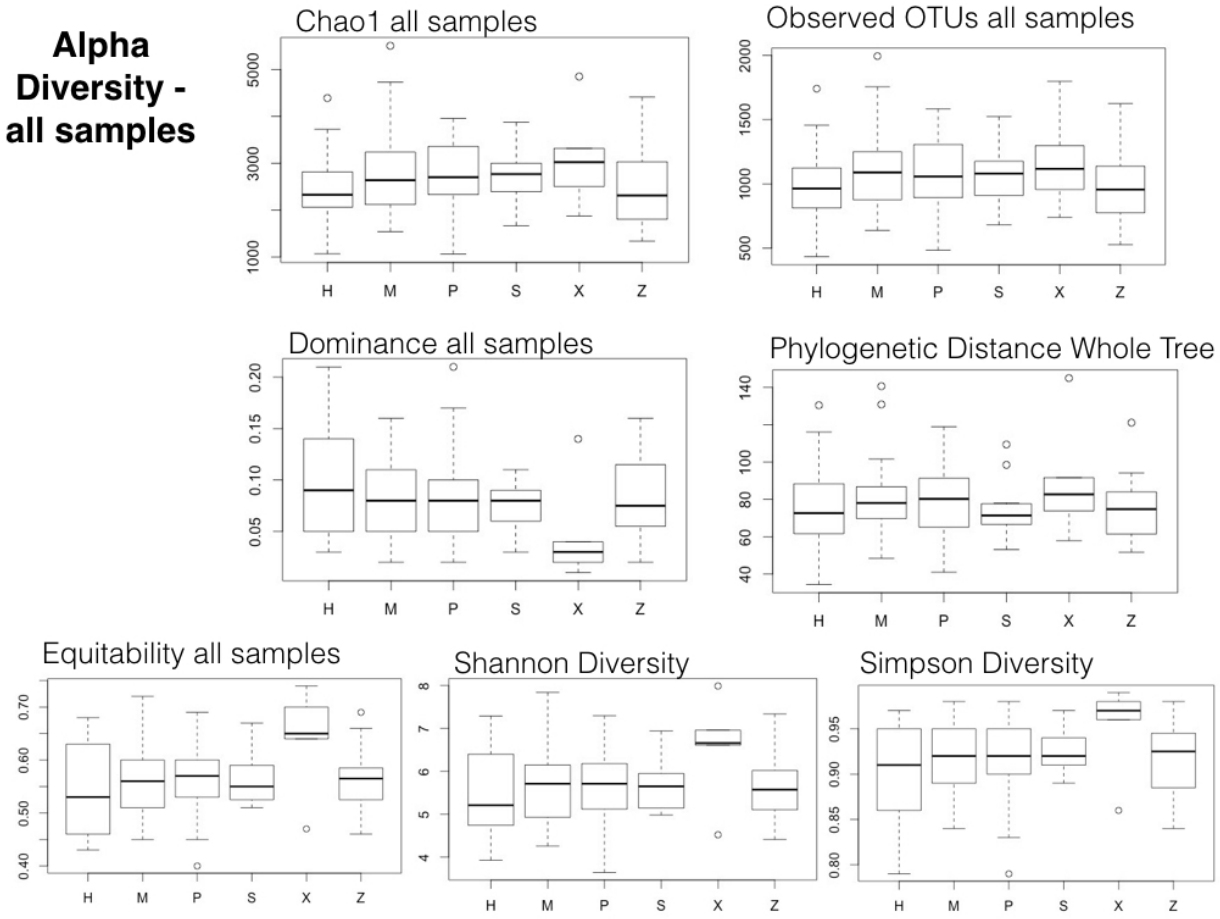

Appendix D

SEM images and evidence of Iron Oxidation on certain minerals from the ISMACS incubations

In addition to the ISMACS analyses described in Chapter 4 and Appendix C, SEM imaging of mineral grains from the two-year incubations showed twisted stalk formations characteristic of Iron oxidizers only on the iron sulfide minerals Pyrite and Marcasite, indicating ecologically relevant metabolic differences among colonizing communities.

Scanning Electron Microscopy & Energy dispersive X-ray spectroscopy

Mineral samples were stored in ethanol or 50% ethanol/ 50% glutaraldehyde, or paraformaldehyde, and frozen until the time of analysis. Samples were ethanol dehydrated via sequential ethanol exchange using 30, 50, 70, 90, 95 and 100% ethanol solutions. Once dehydrated, samples were stored in 100% ethanol until analysis. Following ethanol dehydration, samples were critical point dried using a Tousimis 931 GL critical point dryer and CO_2. The samples were affixed to aluminum SEM stubs using conductive carbon tape, and sputter coated with Au/Pd using a EMS 300T dual head sputter coater. SEM/EDS was performed using a Zeiss Supra 55Vp field emission SEM. High resolution imaging was performed using an accelerating voltage of 3kV. An accelerating voltage of 20kV was used when performing EDS.

Images

Figure D1. Hematite surface showing microbial attachment, pitting, and long sheaths.

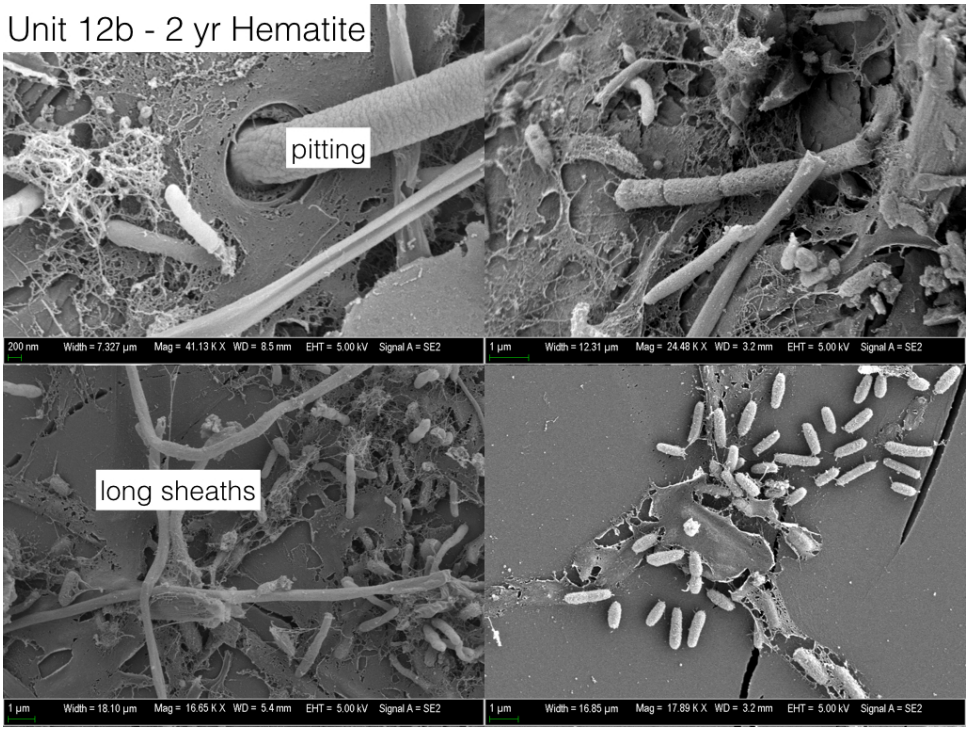

Figure D2. Marcasite surfaces showing twisted stalk formations

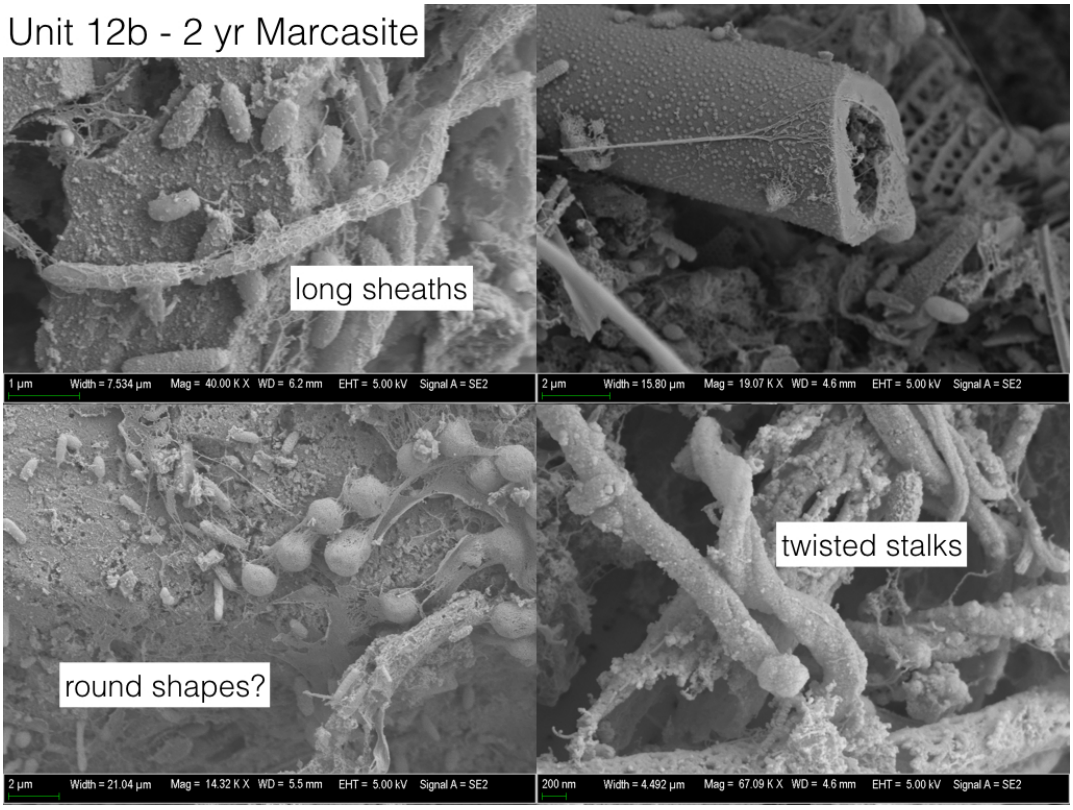

Figure D3. Pyrite surfaces showing twisted stalk formations and sheaths.

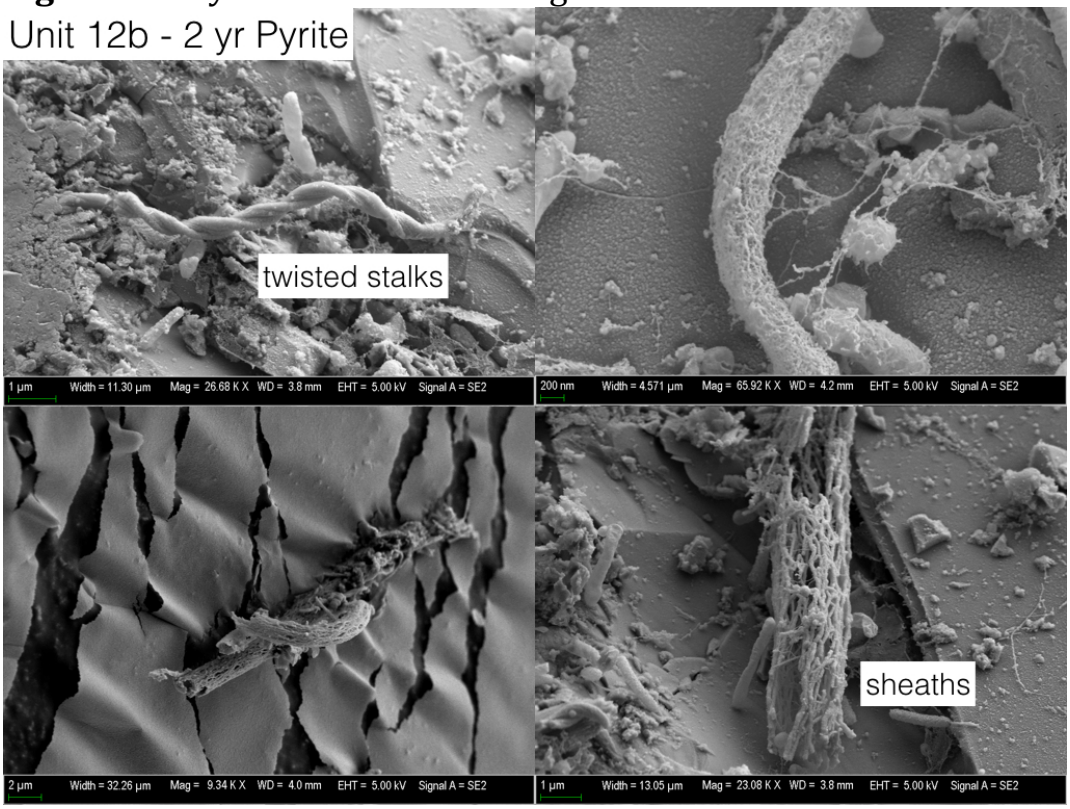

Figure D4. Sphalerite surfaces with attached microbes.

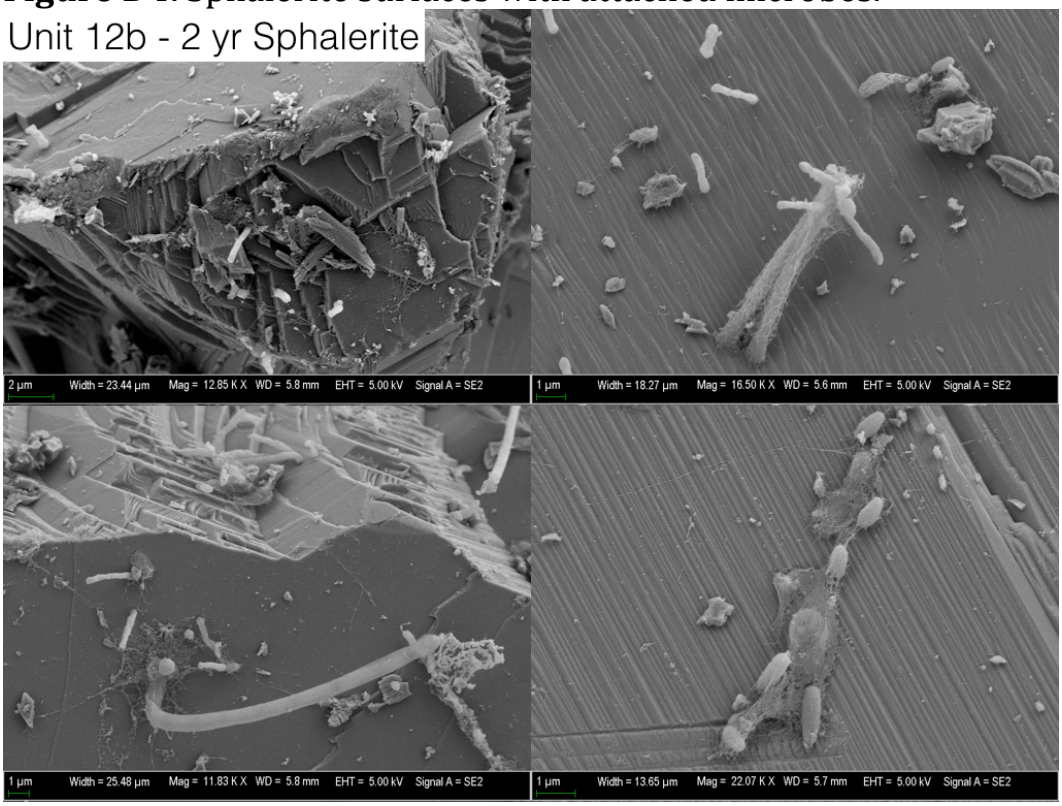

Figure D5. Zironia bead surfaces showing microbial attachment.